TRANSFERS BETWEEN THE EARTH-MOON AND SUN-EARTH SYSTEMS

USING MANIFOLDS AND TRANSIT ORBITS

A Thesis

Submitted to the Faculty

of

Purdue University

by

Masaki Kakoi

In Partial Fulfillment of the

Requirements for the Degree

of

Master of Science in Aeronautics and Astronautics

December 2005

[Peace]

ACKNOWLEDGMENTS

It is amazing where I stand right now considering all the changes I have been through in my life. I would like to thank my father, Masahiro, and mother, Kayoko, from the bottom of my heart. This thesis could not have been accomplished without their support. They have always respected my decisions in my life. I think it has not been easy because I have come up with some crazy ideas. I am very lucky to have such supportive parents. Of course, my brother, Hiroki, and sisters, Mayumi and Fukumi, have been a great support. Probably, I am not the best big brother in the world. I appreciate their patience.

I am also very lucky to have my adviser, Professor Howell. It is not easy to meet a "right" adviser. Fortunately, it happened to me in the very first semester at Purdue University. I knew she would be a great adviser for me even though I was just taking AAE 203. Of course, I did not have the slightest idea about her research, but her teaching style was enough to convince me that I would learn a lot from her. Years later, I still feel the same. My three and half years of graduate study have been very fruitful. My greatest respect surely goes to her.

I would like to thank the department of Aeronautics and Astronautics. Without the department's support, I could not have completed my degree. All the faculty and staff members are friendly and eager to help students. I am very fortunate to be able to learn from great professors in the department.

My life in West Lafayette has been a great fun because of the wonderful people I have met. Our research group members are friendly, fun, diverse, and, of course, smart. I am grateful to be a part of this group. All of my friends, regardless of what they study, bring me a great joy to my life. Also, I would like to thank all the friends outside West Lafayette, all over the world. Their friendship means a lot to me. Thank you very much.

TABLE OF CONTENTS

Page

LIST OF TABLES

LIST OF FIGURES

ABBREVIATIONS

CR3BP   Circular Restricted 3 Body Problem

STM   State Transition Matrix

EM   Earth-Moon

SE   Sun-Earth

BKE   Kinematic Basic Equation

ISEE-3   International Sun-Earth Explorer-3

GMAS   Goddard Mission Analysis System

ABSTRACT

Kakoi, Masaki. M.S.A.A., Purdue University, December, 2005. Transfers Between the Earth-Moon and Sun-Earth Systems Using Manifolds and Transit Orbits. Major Professor: Kathleen C. Howell.

The L_1 and L_2 libration points have been proposed as gateways granting inexpensive access to interplanetary space. The lunar libration points, in conjunction with the collinear libration points in the Sun-Earth system, may also become primary hubs for future human activities in the Earth's neighborhood. The associated manifold tubes have been introduced by a number of researchers as the basis for design strategies to produce trajectories that shift between different systems. Intersections may ultimately be sought between many tubes from many different libration point orbits in each system; the complexity forces a new look at the computations. Individual transfers between three-body systems have been the focus of some recent investigations. This study presents an approach to solve the general problem for transfers between the Earth-Moon system (lunar orbits and/or lunar libration point orbits) and Sun-Earth/Moon L_2 libration point orbits. The solutions are transitioned to the full ephemeris models with additional perturbations and the transfers can be determined for various lunar phases. The solution process also seeks the particular Lissajous trajectory in each system to accomplish the transfer at a low cost. Some results are presented for various types of transfer problems.

1. Introduction

In 2005, spacecraft and the ability to launch them successfully to any orbit - near Earth, in the Earth's neighborhood, or throughout the solar system - influence many aspects of life. For example, it is common to check the weather every day, and weather prediction cannot be accomplished without weather satellites. Also, telecommunications and the Global Positioning System rely on constellations of satellites. Scientists have discovered fascinating facts about the Earth and its neighborhood from numerous scientific missions including the Apollo missions, Voyager to Mars, Galileo to Jupiter, and more recently spacecraft to libration point orbits such as GENESIS, WIND, and others. Launch, orbit design, maneuvers, station keeping, constellation design, navigation, tracking, etc. are all based on a fundamental knowledge of orbital mechanics. For some applications, the current knowledge base is sufficient. However, as humans move away from the Earth, both human and robotic missions become more complex, and further understanding of orbital mechanics and astrodynamics is required.

1.1 Problem Definition

Based on Newton's fundamental Laws of Motion, as well as the Law of Gravity, mathematicians have been able to model the planetary motions in terms of differential equations for at least 300 years. However, the greatest challenge is to actually solve the equations of motion for a system involving n bodies. Newton developed his solution for the differential equations governing a system consisting of only two bodies. However, it became extremely difficult to solve the equations when even just one more body is added to the system. The three-body problem has defied closed-form solution for the last 200 years by any of the great mathematicians. For example, for the problem

of 3 bodies, 18 integrals of the motion are required for solution. Thus, to solve this problem, it requires 18 constants. With judicious assumptions and a reformulation of the problem, Euler first simplified the problem sufficiently for detailed investigation.

It has long been known that analytical solution of the multi-body problem is hindered by a lack of sufficient integrals. A reformulation of the problem was required for progress. Euler first introduced the synodic (rotating) coordinate system and, with various assumptions, simplified the three-body problem to the Circular Restricted Three-Body Problem (CR3BP) [2, 3]. Both Euler and Lagrange then sought equilibrium solutions in this restricted problem. In 1772, Euler determined three collinear solutions, now denoted the L_1, L_2, and L_3 equilibrium points. Lagrange verified Euler's results and subsequently identified two triangular solutions currently labelled L_4 and L_5 [2]. These solutions are called Lagrange points or libration points. However, Euler and Lagrange still did not determine a closed-form solution to the problem. In 1887, Bruns proved that there exist only ten classical integrals of motion for a rectangular coordinate system and this particular solution approach [2]. However, this conclusion did not discourage mathematicians from studying the three-body problem. In fact, mathematicians have continuously studied this problem over the last two centuries, but not until the mid-20th century did understanding of the problem increase sufficiently to consider spacecraft applications. Any recent advances are greatly due to the development of computers.

As the computational power increases due to technological developments, it becomes faster and more efficient to integrate differential equations numerically. Since there is no closed-form solution, numerical simulations play a large role in the study of the multi-body problem. Therefore, the vast improvement of computational capabilities has influenced research significantly. However, the Circular Restricted Three-Body Problem (CR3BP) remains a challenge because of the complexity of the problem. Further investigation of the problem is required. Computation in the three-body problem is also complicated by sensitivity to the initial conditions. This is a property of chaotic systems [4, 5]. Henri Poincaré first described the chaotic behavior of

a dynamical system mathematically by identification of homoclinic points [2]. It is inherent in the nonlinear dynamics associated with the three-body problem. Even though the numerical integration is easily accomplished, the problem sensitivity implies a very difficult design process. Without knowledge of the underlying dynamical structure, the design process is extremely time consuming and inefficient.

The gravity force of the Sun can have a significant influence on the vehicles in the vicinity of the Earth. Any Sun-planet system can be modelled as a three-body problem: Sun-Mars, Sun-Earth, Sun-Jupiter. It is also possible to model some planet-moon combinations as three-body systems: Earth-Moon, Jupiter-Europa, Saturn-Titan. The Earth-Moon case is unique because of the relatively larger mass of the Moon, as well as the influence of the Sun. Including the gravity force of the Sun, Earth and the Moon, the problem becomes a four-body problem. This special four-body problem is of increasing interest as new mission scenarios seek the capability to move freely in the Sun-Earth-Moon space.

It is not trivial to design effectively in a four-body regime, however. Of course, time-consuming shooting techniques can be employed, but more sophisticated techniques are sought. If it is possible to combine the Sun-Earth and Earth-Moon three-body systems, perhaps more effective design tools can be developed. To accomplish such a task, insight into both the three- and four-body problems, as well as their overlap, is required. The specific challenge in this work is to develop a methodology to not only design a trajectory in this four-body regime, but to compute one that shifts between regions that are dominated by one three-body system or the other. Of course, any such result must be shown to exist in the full ephemeris model as well.

1.2   Previous Work

Henri Poincaré's strong interest in the three-body problem resulted in significant contributions. Poincaré introduced the Poincaré map in 1881 [6]. Perko [6] notes that the Poincaré map is "probably the most basic tool for studying the stability and

bifurcations of periodic orbits." Poincaré's contributions extend to a wide range of topics. Poincaré's discovery of homoclinic points "embodied the first mathematical description of chaotic motion in a dynamical system" [2].

Near the end of 1960's, Robert Farquhar began to publish studies of the three-body problem in association with John Breakwell [7]. A unique challenge existed for NASA's proposed Apollo 18 mission. The Moon always maintains the same face directed toward the Earth; the Apollo 18 vehicle would land on the back side of the Moon. Farquhar suggested the use of a periodic orbit in the vicinity of the Earth-Moon L_2 point with in-plane and out-of-plane frequencies that were nearly commensurate for a communications satellite to maintain a link with astronauts on the lunar surface [7]. This is the origin of the basic concept of a halo orbit. Unfortunately, the mission was cancelled. The opportunity to test Farquhar's idea was postponed. However, Breakwell and Farquhar saw great potential in halo orbits and proceeded with further study. Many of the libration-point missions accomplished in the 1990's were based on the ideas that Breakwell and Farquhar suggested at the time [7].

To calculate halo orbits in the vicinity of the translunar L_2 libration point, the out-of-plane amplitude must be sufficient to make the orbit visible from Earth. However, the linearized model is no longer valid when the amplitude becomes large. Breakwell [8] observed that the effect of the nonlinear terms becomes significant if the orbit size is comparable with the distance of L_2 from the Moon in the Earth-Moon system. (Also notable, the in-plane and out-of-plane frequencies are commensurate only if the nonlinear terms are included.) Farquhar and Kamel [9] used a truncated Lindstedt-Poincaré series to calculate these orbits. This nonlinear method included the Solar gravity [9]. Breakwell and Brown [8] established a numerical method to calculate orbits with large amplitudes by using the fact that the periodic orbits are symmetric. From the structure of the mathematical model, the plane of symmetry is apparent. They computed families of halo orbits near L_1 and L_2 in the Earth-Moon system [8]. Halo orbits are known to generally be unstable. However, Breakwell and Brown [8]

located a narrow band of stable orbits. Later, Howell [10] extended the search for halo families and the stable region to different mass ratios.

An historic moment for the application of the three-body problem to spacecraft design occurred on November 20, 1978. The International Sun-Earth Explorer-3 (ISEE-3) spacecraft was placed into a halo orbit associated with the Sun-Earth L_1 libration point [11]. This was the first such libration point mission and the goal was to complete a number of particles and fields investigations in the interplanetary medium [11, 12]. The halo obit near L_1 was well-suited as a location from which to observe the characteristics of the solar wind and other solar-induced phenomena, such as solar flares, without disturbance from Earth [11, 12]. The halo orbit concept truly gained credibility by the success of the ISEE-3 [7].

As the halo orbit concept gained credibility, interest in missions to libration points increased. Without an analytical solution to the three-body problem, mission designers required improved design techniques for more complex and numerous missions. Prior to the 1980's, as one of a number of such developments, Goddard Space Flight Center developed a trajectory design software package called Goddard Mission Analysis System (GMAS) for mainframe computers [13]. Then, during the late 1990's, Goddard Space Flight Center developed a operational program called Swingby for personal computers [13]. Swingby is capable of calculating trajectories with gravity assists for lunar, planetary, libration, and deep space missions [13]. The Swingby software was also a significant step by introducing new graphics capabilities. The complete mission analysis and operations support for the WIND, SOHO, and ACE missions was provided by the Swingby [13]. The Swingby software was developed, in part, to address the computational difficulties apparent in a problem with no analytical solution. However, Swingby, as well as other more conventional tools, does not incorporate any new theoretical understanding of the multi-body problem. True for all problems in this regime, very good initial conditions are required for these programs. Without a good preliminary design process, it requires a significant amount of time to design a mission.

In the 1990's, with the improvement in the computational capabilities, the numerical techniques were further developed to update the mission design process. The most recent steps forward have been accomplished by close study of the dynamical structure of the CR3BP. The focus of the recent studies is the set of special solutions, such as libration points, periodic orbits, quasi-periodic trajectories, and invariant manifolds. An invariant manifold is a surface such that "orbits starting on the surface remain on the surface throughout the course of their dynamical evolution" [14].

At Purdue University, a design software package called Generator was also developed by Howell et al. Besides some traditional approaches, Generator is also capable of producing different types of solution arcs based on dynamical systems theory; other conventional software, including Swingby, does not currently exploit this dynamical structure [13, 15]. Generator does reduce the time for design and/or analysis for certain applications [15]. The Generator software was used for analysis in support of actual missions, such as MAP; Generator was also used to produce the original trajectories for GENESIS. Even though Generator reduces the time to design and/or analyze trajectories in the multi-body problem, a good initial guess for the initial conditions is still required. This indicates the necessity of an accurate preliminary design technique.

In the vicinity of the Earth, but sufficiently beyond the Earth's sphere of influence, mission designers consider the Sun, the Earth, and the Moon as the major gravitational bodies. The implication is that the CR3BP is not a sufficient model in this case; a model that includes at least four bodies is necessary. By combining the three-body Sun-Earth and Earth-Moon systems, a simplified model can be built. It is possible to exploit the knowledge of the CR3BP in this way. The result must, of course, be transitioned to the full ephemeris model. To design a mission in the simplified model first, transfers or overlapping trajectories between the Sun-Earth and Earth-Moon systems must be available. Thus, a methodology to accomplish such a design is the next step. Techniques involving transfers between two CR3BPs have been studied recently by a few mathematicians and engineers. One useful technique suggested by Koon et al. is

the use of transit orbits [16]. Transit orbits exist inside the closed surface of invariant manifolds, sometimes called a manifold tube. In this technique, transfers are achieved by connecting transit orbits inside two manifold tubes. For example, in the system including the Sun, Earth, and Moon, a manifold tube is obtained in each system. If these two manifold tubes intersect, it might be possible to connect transit orbits near the intersection point. Koon et al. introduce a method to obtain transit orbits inside the manifold tubes. This method is not limited to the Sun-Earth-Moon system. It has also been applied to interplanetary transfers [17]. Topputo et al. investigate the problem further, [18], i.e., transfers that can be determined even when there is no intersection between two manifold tubes by using a two-body Lambert arc to connect the tubes, Topputo et al. create acceptable transfers.

1.3   Current Work

Although previous researchers have published remarkable results, the analysis is limited to specific sets of initial conditions. The methodology to seek the best possible transfer under arbitrary conditions is not developed. The difficulty in completing such a search follows from the complexity of the problem dynamics. The purpose of this study is to establish a preliminary design strategy to compute the best possible transfer between a Sun-Earth L_2 halo orbit and an Earth-Moon L_2 halo orbit or the vicinity of the Moon. The "best" transfer is defined as one corresponding to the lowest required velocity difference. Similar to other researchers, the Sun-Earth-Moon system is modelled as a combination of two CR3BPs. In this study, the establishment of the methodology is based on the dynamics of transit orbits and invariant manifold tubes.

The development of this design process and representative examples are detailed in the following chapters:

- Chapter 2

Any study of this problem requires a basic understanding of the Circular Restricted Three-Body Problem. The detailed definition of the problem is presented with all appropriate notation. First, a brief introduction to the n-Body Problem is presented; subsequently, the problem is reduced to the Circular Restricted Three-Body Problem. Basic properties, such as the existence of the libration points and Jacobi Constant are derived. Unique orbits and/or trajectory arcs in the CR3BP, such as halo orbits and invariant manifolds, are introduced.

- Chapter 3

  Application of the basic knowledge introduced in the previous chapter yields some unique tools for use in the system-to-system transfer problem. The steps in the computation of invariant manifold tubes and transit orbits in two dimensions are outlined. Computational procedures to produce a transit orbit passing through two manifold tubes in the same three-body system are presented. Transit orbits that pass through manifold tubes in two different three-body systems are examined. An example is also discussed.

- Chapter 4

  This chapter initiates an investigation of the three-dimensional problem. A transit orbit in three dimensions increases the computational complexity significantly. Of course, a single transit orbit is not the ultimate goal. Thus, the basic technique to design a transfer trajectory using a transit orbit is presented. It is noted that the Earth-Moon to Sun-Earth transfers as well as the Sun-Earth to Earth-Moon transfers each have unique requirements. Also, the transfer design process is integrated into a single procedure. Transfers from the Sun-Earth system to the Earth-Moon system are completed. The validity of the methodology is tested via the complete models in the Generator software. A brief explanation concerning Generator is included. Results from application of the new strategy and the final design from Generator are compared.The differences are discussed.

- Chapter 5

  Results from the technique establised in the previous chapter are analyzed in this chapter. A new more efficient technique is developed by analyzing the results. The validity of the methodology is tested via the complete models in the Generator software. The Results from the new technique and the previous technique are compared. Also, the technique developed in the previous chapter is compared with the cell estimation technique. This chapter also includes examples of transfers to the Moon.

2. Background

A successful outcome to a challenge is accomplished by a persistent attack with the proper strategies based on the correct knowledge of the problem. The study of the three-body problem is not an exception. The most general model of the n-body problem under Newton's Law of Gravity is not solvable in closed-form and must be reduced to make progress. Here, it is reduced to the CR3BP under certain assumptions. The fundamental mathematics and properties of the CR3BP are later seen to be the fundamental elements that are required for strategies to attack the n-body problem.

2.1 n-Body Problem

Assume that n particles are given and that they are spherically symmetric. Each particle is of mass m_i. Newton's Law of Gravity models the attraction among the masses as an inverse square gravitational force between each pair of particles. Let the subscript i identify the particle. Then the mass of particle i is represented as m_i. The total force, $\bar{F}_t$, on the mass, m_i, can be expressed by assuming that gravity is the only force acting as follows,

$$\bar{F}_t = -Gm_i \sum_{j=1, j\neq i}^{n} \frac{m_j}{r_{ji}^3} \bar{r}_{ji} \,, \tag{2.1}$$

where

$$\bar{r}_{ji} = \bar{r}_i - \bar{r}_j \,. \tag{2.2}$$

The position vectors $\bar{r}_i$ and $\bar{r}_j$ represent the position of particles i and j, respectively. (Overbars indicate vectors.) The constant G is the universal gravitational constant. In Figure 2.1, the total force on m_1, $\bar{F}_t$, appears. The total gravity force is due to the existence of m_2, m_3, ..., m_i where $i = 1, 2, ...n$. The position vectors $\bar{r}_1$ and $\bar{r}_2$

are measured from the origin in the inertial frame $[\hat{\xi}, \hat{\eta}, \hat{\zeta}]^T$. (The carets above the vectors indicate unit vectors and the superscript T indicates the transpose.) The set of unit vectors comprises a right-handed orthonormal triad. The position vector $\bar{r}_{21}$ represents the position of m_1 relative to m_2 as noted in Figure 2.1. The force model in Equation (2.1) is substituted into Newton's law of motion, that is,

$$m_i \frac{d^2 \bar{r}_i}{dt^2} = -G \sum_{j=1, j\neq i}^{n} \frac{m_i m_j}{r_{ji}^3} \bar{r}_{ji} . \tag{2.3}$$

This vector second-order differential equation is written in terms of dimensional quantities.
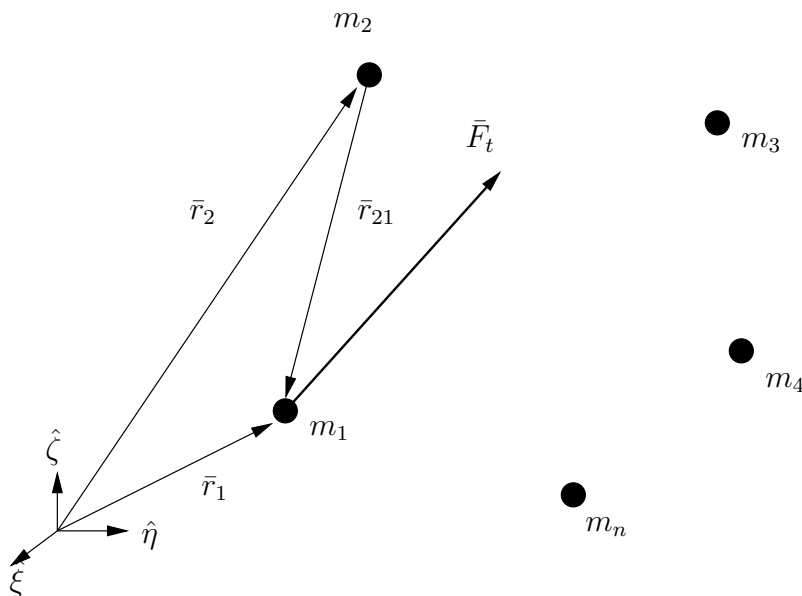
Figure 2.1. n-Body Problem: Total Force on m_1

Equation (2.3) applies in the most general case with an arbitrary number, n, of particles in the system. Since there are n number of bodies in this problem, it is called n-body problem. Of course, Equation (2.3) represents six first-order, scalar differential equations. Thus, $6n$ constants are required to solve the problem. However, the known integrals are limited to ten. In 1887, Bruns proved that the ten classical integrals are the only independent algebraic integrals in the problem when the rectangular coordinates are selected as dependent variables [2].

2.2 Circular Restricted Three Body Problem

A system with just two particles requires 12 constants for a closed-form analytical solution. However, the two-body problem is analytically solvable if it is formulated in terms of relative motion. Without an analytical solution, a relative formulation might also yield results in the three-body problem. Euler first assumed that two of the bodies rotate in a circle about the center of the mass, and that the third body, of infinitesimal mass, moves under the influence of the gravitational forces of the other two, but without influencing them [2]. Significantly, Euler also formulated the problem relative to the rotating coordinate frame [2]. This problem is called the Circular Restricted Three-Body Problem (CR3BP). The schematics of the problem appear in Figure 2.2. The first two masses P_1 and P_2 are called the primary bodies. Arbitrarily, let P_1 be more massive than P_2, then the center of the mass is closer to P_1. The center of the mass is called the barycenter and labelled B. The barycenter is assumed to be fixed in the inertial frame $[\hat{\xi}, \hat{\eta}, \hat{\zeta}]^T$. Under these assumptions, Equation (2.3) can be reduced to the following,

$$\frac{d^2 \bar{R}}{dt^2} = -G \sum_{j \neq i}^{2} \frac{m_j}{r_{j3}^3} \bar{r}_{j3} \,, \tag{2.4}$$

where

$$\bar{R} = \bar{r}_3 - \bar{r}_B \,. \tag{2.5}$$

The position vector $\bar{R}$ indicates the position of the third body with respect to the barycenter. The position of the barycenter and P_3 with respect to the origin, O, of the inertial frame are $\bar{r}_B$ and $\bar{r}_3$, respectively. Also $\bar{r}_{j3}$ is the distance between the primary body j and the particle of interest, P_3.

2.3 Characteristic Quantities

One way to simplify the problem without losing the generality of the mathematical model is nondimensionalization. It can be accomplished by defining parameters that are characteristic in the problem, i.e., the characteristic quantities. In the CR3BP,
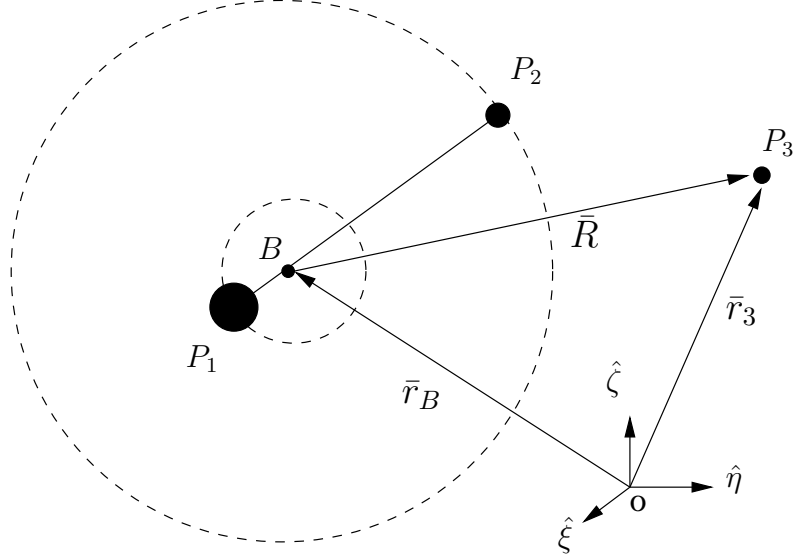
Figure 2.2. Circular Restricted 3-Body Problem

the distance between primary bodies is defined to be the reference distance, L_{ref}. The sum of the masses of the primary bodies is defined to be the reference mass, M_{ref}. The time taken by the primaries to rotate through exactly one radian is defined to be the reference time, t_{ref}. The mean motion of the primaries is evaluated as follows,

$$n = \sqrt{\frac{GM_{ref}}{L_{ref}^3}} \, . \tag{2.6}$$

Define θ to be the angle of rotation of a frame moving with the primaries relative to the inertial frame, then, $\frac{\theta}{n}$ is the time taken to rotate through θ. This is true because primaries rotate in a circle about the center of the mass in this model at a constant rate. Therefore, the reference time, t_{ref}, is expressed as follows,

$$t_{ref} = \sqrt{\frac{L_{ref}^3}{GM_{ref}}} \, . \tag{2.7}$$

Dividing Equation (2.4) by GM_{ref} and multiplying it by L_{ref}^2, will nondimensionalize the equation, and it appears in the following form,

$$\frac{d^2 \bar{R}}{dt^2} \frac{L_{ref}^2}{GM_{ref}} = -\frac{m_1 L_{ref}^2}{M_{ref} r_{13}^3} \bar{r}_{13} - \frac{m_2 L_{ref}^2}{M_{ref} r_{23}^3} \bar{r}_{23} \, . \tag{2.8}$$

Nondimensional position vectors are defined as follows,

$$\bar{r}_{13nd} = \frac{\bar{r}_{13}}{L_{ref}}\,, \tag{2.9}$$

$$\bar{r}_{23nd} = \frac{\bar{r}_{23}}{L_{ref}}\,. \tag{2.10}$$

The subscript 'nd' indicates a nondimensional quantity. The nondimensional mass of the secondary primary is $\frac{m_2}{M_{ref}} = \mu$. Therefore $\frac{m_1}{M_{ref}}$ can be expressed as $1 - \mu$. Also, the nondimensional time is defined as follows,

$$t_{nd} = \frac{t}{t_{ref}}\,. \tag{2.11}$$

where t is the dimensional time. Thus, Equation (2.8) can be simplified as follows,

$$\frac{d^2 \bar{R}_{nd}}{dt_{nd}^2} = -\frac{1 - \mu}{r_{13nd}^3}\bar{r}_{13nd} - \frac{\mu}{r_{23nd}^3}\bar{r}_{23nd}\,. \tag{2.12}$$

Define the dimensional distance between the barycenter and larger primary body to be r_{B1}, that can, then, be expressed in the following form by using the relationship that defines the center of mass,

$$r_{B1} = \frac{m_2}{m_1 + m_2}L_{ref}\,. \tag{2.13}$$

This equation can be rewritten as follows,

$$\frac{r_{B1}}{L_{ref}} = \frac{m_2}{M_{ref}}\,. \tag{2.14}$$

Therefore, the nondimensional distance between the barycenter and larger primary body, r_{B1nd}, is the following,

$$r_{B1nd} = \frac{m_2}{M_{ref}} = \mu\,. \tag{2.15}$$

The nondimensional distance between the barycenter and the smaller primary body, r_{B2nd}, can be obtained in the same process and expressed as follows,

$$r_{B2nd} = \frac{m_1}{M_{ref}} = 1 - \mu\,. \tag{2.16}$$

These nondimensional variables are used in the derivation of the equation of motion in the next section.

2.4   Equations of Motion

Let ξ, η, ζ be defined as the nondimensional position components of the third body with respect to the barycenter written in terms of in the inertial frame, i.e., $\bar{R}_{nd} = \xi\hat{\xi} + \eta\hat{\eta} + \zeta\hat{\zeta}$. Then, Equation (2.12) can be rewritten as the following set of second order scalar differential equations,

$$\ddot{\xi} = (1 - \mu)\frac{\xi_1 - \xi}{r_{13nd}^2} + \mu\frac{\xi_2 - \xi}{r_{23nd}^2}, \tag{2.17}$$

$$\ddot{\eta} = (1 - \mu)\frac{\eta_1 - \eta}{r_{13nd}^2} + \mu\frac{\eta_2 - \eta}{r_{23nd}^2}, \tag{2.18}$$

$$\ddot{\zeta} = (1 - \mu)\frac{\zeta_1 - \zeta}{r_{13nd}^2} + \mu\frac{\zeta_2 - \zeta}{r_{23nd}^2}, \tag{2.19}$$

where

$$r_{13nd}^2 = (\xi_1 - \xi)^2 + \eta^2 + \zeta^2,$$

$$r_{23nd}^2 = (\xi_2 - \xi)^2 + \eta^2 + \zeta^2.$$

Dots indicate the derivatives with respect to the nondimensional time and relative to the inertial frame. The subscript 1 and 2 refer the first primary and second primary bodies respectively. Now define Euler's synodic frame, s, such that $\hat{x}$ is always directed from P_1 towards P_2, $\hat{y}$ is perpendicular to $\hat{x}$ and in the plane of motion of the primaries and in the general direction of primary velocity. Then, $\hat{z}$ is a right-handed cross product of $\hat{x} \times \hat{y}$ and is equal to $\hat{\zeta}$. Recall that the angular velocity, $^{I}\bar{\omega}^{s}$, is constant in magnitude and direction since $^{I}\bar{\omega}^{s} = n\hat{\zeta} = n\hat{z}$. Define the position coordinates of the particle P_3 relative to B, in terms of the rotational frame, to be x, y, and z respectively, i.e.,

$$\bar{r}_{3nd} = x\hat{x} + y\hat{y} + z\hat{z}. \tag{2.20}$$

The x-y projection of the system appears in Figure 2.3. In terms of the rotaing frame, the position of P_1 is written $[x_1, 0, 0]^T$, and the position of P_2 is expressed $[x_2, 0, 0]^T$. Hence, r_{13nd} and r_{23nd} can be expressed in the following form,

$$r_{13nd}^2 = (x_1 - x)^2 + y^2 + z^2, \tag{2.21}$$
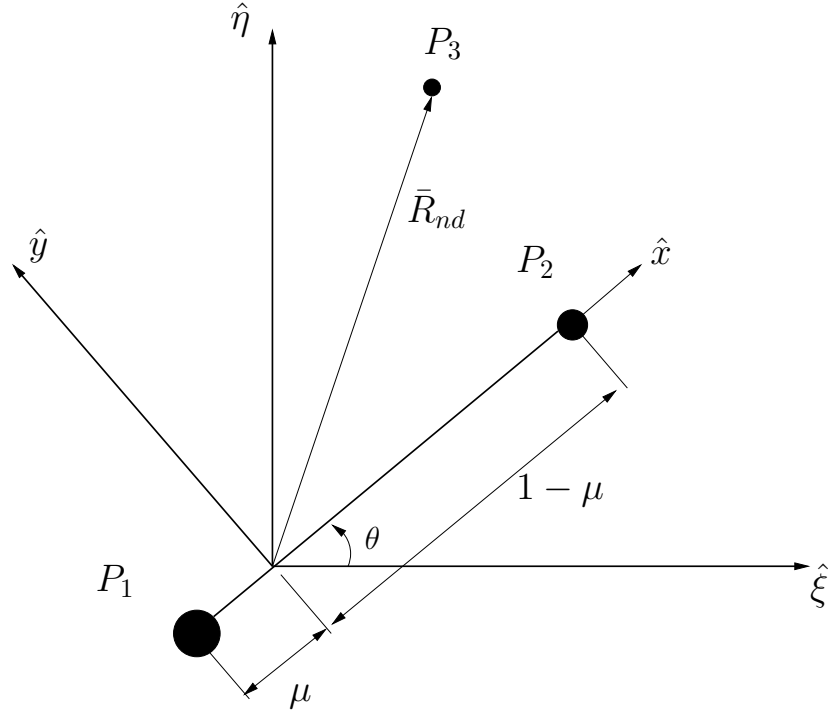
Figure 2.3. Formulation of Circular Restricted 3-Body Problem

$$r_{23nd}^2 = (x_2 - x)^2 + y^2 + z^2 \, . \tag{2.22}$$

The rotating and inertial coordinates can be related by using the following transformation,

$$\xi = x \cos t_{nd} - y \sin t_{nd} \, , \tag{2.23}$$

$$\eta = x \sin t_{nd} + y \cos t_{nd} \, , \tag{2.24}$$

$$\zeta = z \, . \tag{2.25}$$

Differentiating the scalar equations twice with respect to nondimensional time yields the following,

$$\ddot{\xi} = \ddot{x} \cos t_{nd} - 2\dot{x} \sin t_{nd} - x \cos t_{nd} - \ddot{y} \sin t_{nd} - 2\dot{y} \cos t_{nd} + y \sin t_{nd} \, , \tag{2.26}$$

$$\ddot{\eta} = \ddot{x} \sin t_{nd} + 2\dot{x} \cos t_{nd} - x \sin t_{nd} + \ddot{y} \cos t_{nd} - 2\dot{y} \sin t_{nd} - y \cos t_{nd} \, , \tag{2.27}$$

$$\ddot{\zeta} = \ddot{z} \, . \tag{2.28}$$

After substituting Equations (2.26), (2.27), and (2.28) into Equations (2.17), (2.18), and (2.19), the algebraic process yields,

$$\ddot{x} - 2\dot{y} - x = -(1-\mu)\frac{x-x_1}{r_{13}^3} - \mu\frac{x-x_2}{r_{23}^3}, \tag{2.29}$$

$$\ddot{y} + 2\dot{x} - y = -\left(\frac{1-\mu}{r_{13}^3} + \frac{\mu}{r_{23}^3}\right)y, \tag{2.30}$$

$$\ddot{z} = -\left(\frac{1-\mu}{r_{13}^3} + \frac{\mu}{r_{23}^3}\right)z. \tag{2.31}$$

Define a pseudo potential function as the following,

$$U^* = \frac{1}{2}(x^2 + y^2) + \frac{1-\mu}{r_{13}} + \frac{\mu}{r_{23}}. \tag{2.32}$$

Then,

$$\frac{\partial U^*}{\partial x} = x + \frac{(1-\mu)(x_1 - x)}{r_{13}^3} + \frac{\mu(x_2 - x)}{r_{23}^3}, \tag{2.33}$$

$$\frac{\partial U^*}{\partial y} = y - \frac{(1-\mu)y}{r_{13}^3} - \frac{\mu y}{r_{23}^3}, \tag{2.34}$$

$$\frac{\partial U^*}{\partial z} = -\left(\frac{1-\mu}{r_{13}^3} + \frac{\mu}{r_{23}^3}\right)z. \tag{2.35}$$

Therefore, Equations (2.29), (2.30), and (2.31) can also be written in the form,

$$\ddot{x} - 2\dot{y} = \frac{\partial U^*}{\partial x}, \tag{2.36}$$

$$\ddot{y} + 2\dot{x} = \frac{\partial U^*}{\partial y}, \tag{2.37}$$

$$\ddot{z} = \frac{\partial U^*}{\partial z}. \tag{2.38}$$

These are the standard, nondimensional, scalar equations of motion in the CR3BP. They can be numerically integrated to compute trajectories.

2.5   Jacobi's Integral

As mentioned previously, only ten integrals of motion are known to exist in the CR3BP. One of the integrals can be derived from the equations of motion [19], as

discussed by A.E. Roy. Multiplying Equation (2.36) by $\dot{x}$, Equation (2.37) by $\dot{y}$, and Equation (2.38) by $\dot{z}$ and adding, yields

$$\dot{x}\ddot{x} + \dot{y}\ddot{y} + \dot{z}\ddot{z} = \frac{\partial U^*}{\partial x}\dot{x} + \frac{\partial U^*}{\partial y}\dot{y} + \frac{\partial U^*}{\partial z}\dot{z} \,. \tag{2.39}$$

Integrating this equation results in the expression

$$\dot{x}^2 + \dot{y}^2 + \dot{z}^2 = 2U^* - C \,, \tag{2.40}$$

where C is the integration constant. With the substitution of the definition for the pseudo potential, U^* in Equation (2.32), the equation can be expressed as the following,

$$\dot{x}^2 + \dot{y}^2 + \dot{z}^2 = (x^2 + y^2) + 2\left(\frac{1-\mu}{r_{13}}\right) + \frac{2\mu}{r_{23}} - C. \tag{2.41}$$

This is the only integral of motion that can be obtained in the CR3BP and is denoted as Jacobi's Integral [19]. The constant C is usually labelled the Jacobi Constant [3].

2.6 Libration Points

In 1772, Euler sought equilibrium points and identified three such collinear points along the x-axis. Lagrange confirmed this result and added two triangular equilibrium points [2]. These five equilibrium points are called Lagrange or libration points [2,19]. The relative location of each libration point appears in Figure 2.4. Libration points L_1, L_2, L_3 are termed the collinear points and are linearly unstable [19]. A particle placed at any of these libration points leaves the vicinity of the point if perturbed slightly. Libration points L_4 and L_5 complete equilateral triangles with the primary bodies, and are linearly stable for certain values of mu [19]. Thus, motion in the vicinity of L_4 or L_5 is bounded even under perturbation. The labels in Figure 2.4 are consistent with those defined by NASA. Without a general analytical solution to Equations (2.36)-(2.38) and only one integral, equilibrium solutions offer insight and greater understanding of the problem.
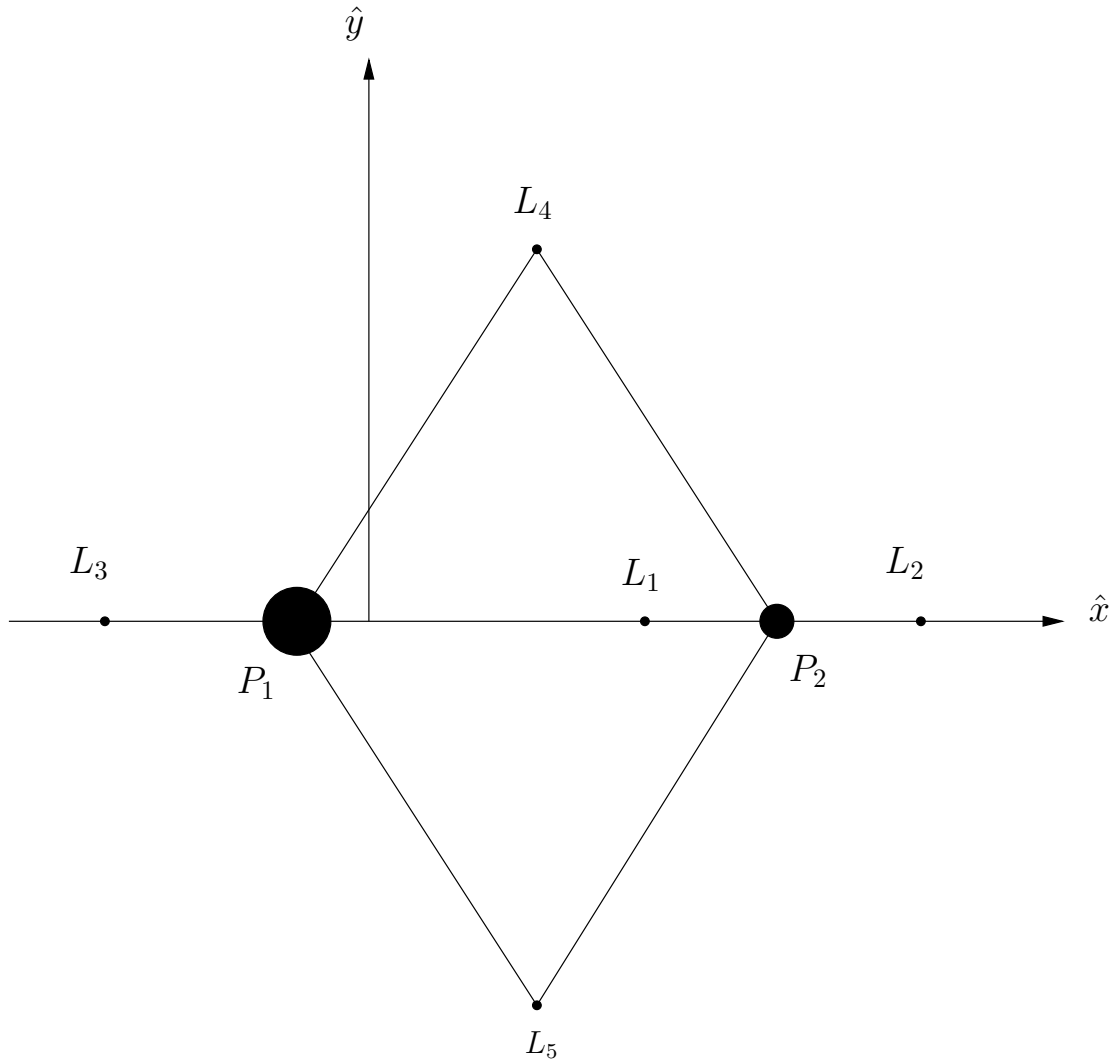
Figure 2.4. Libration Points

2.7   Linear Analysis

Let $\bar{x}$ be a state vector in three-dimensional space, i.e., $\bar{x} = [x, y, z, \dot{x}, \dot{y}, \dot{z}]^T$. Then, a nonlinear dynamical system can be described by a differential equation of the form

$$\dot{\bar{x}} = f(\bar{x}) \,. \tag{2.42}$$

In the CR3BP, the equations of interest are Equations (2.36), (2.37), and (2.38). Various types of particular solutions to the nonlinear differential equations are known to exist, for example, the constant equilibrium points as well as an infinite number of

periodic orbits. To linearize Equation (2.42) about an equilibrium point or a periodic orbit, expand the reference solution in a Taylor series. To model the behavior near the reference solution, ignore the hight order terms in the expansion. Define the perturbation relative to the reference as $\delta\bar{x}$ such that $\delta\bar{x} = [\delta x, \delta y, \delta z, \delta\dot{x}, \delta\dot{y}, \delta\dot{z}]^T$. Then, the variational equations can be rewritten as a linear homogeneous equation, i.e.,

$$\delta\dot{\bar{x}} = A(t)\delta\bar{x} \,, \tag{2.43}$$

where, in general, $A(t)$ is a 6×6 time-varying square matrix. The $A(t)$ matrix is evaluated on the reference solution. Generally, the reference solution changes with time. Thus, $A(t)$ is not constant. However, the $A(t)$ matrix is constant when the reference solution is constant, e.g., an equilibrium point.

2.7.1 Stable and Unstable Manifolds: Equilibrium Points

The variational differential equations relative to an equilibrium point, such as a libration point, results in a constant A matrix and, thus, appear in the following form.

$$\delta\dot{\bar{x}} = A\delta\bar{x} \,. \tag{2.44}$$

Consider a nonlinear system as represented in Equation (2.42) and a constant equilibrium solution $\bar{x}_{eq}$. Suppose an A matrix is computed by linearizing Equation (2.42) about $\bar{x}_{eq}$. If the eigenvalues, λ, of A possess negative and positive real parts, stable and unstable subspaces exist, i.e., E^s and E^u respectively, and they are spanned by stable and unstable eigenvectors, i.e., $\bar{v}_s$ and $\bar{v}_u$ respectively. Consider the neighborhood of $\bar{x}_{eq}$. Then, the local stable manifold, $W^s_{loc}(\bar{x}_{eq})$, is the local flow approaching $\bar{x}_{eq}$ as the time goes to ∞. Also, the local unstable manifold, $W^u_{loc}(\bar{x}_{eq})$, is the local flow approaching $\bar{x}_{eq}$ as the time goes to -∞. Guckenheimer and Holmes [20] state the following theorem.

Theorem 2.7.1 (Stable Manifold Theorem for a Fixed Point) *Suppose that $\dot{x}$ = $f(x)$ has a hyperbolic fixed point $\bar{x}$. Then there exist local stable and unstable manifolds $W^s_{loc}(\bar{x})$, $W^u_{loc}(\bar{x})$, of the same dimensions n_s, n_u as those of the eigenspaces*

E^s, E^u of the linearized system, and tangent to E^s, E^u at $\bar{x}$. $W^s_{loc}(\bar{x})$, $W^u_{loc}(\bar{x})$ are as smooth as the function f.

At a hyperbolic point, the eigenvalues of A possess no zero real parts or pure imaginary parts. An example of stable and unstable manifolds that correspond to a hyperbolic equilibrium point appears in Figure 2.5. Arrows indicate the direction of the flow. Stable manifolds approach $\bar{x}_{eq}$, and unstable manifolds move away from $\bar{x}_{eq}$. The global stable and unstable manifolds, W^s and W^u, respectively can be "obtained by letting points in W^s_{loc} flow backwards in time and those in W^u_{loc} flow forwards" [20]. For the collinear libration points, there exist six eigenvalues of A, and four are pure imaginary. Thus, the collinear points are not hyperbolic points. Guckenheimer and Holmes [20] state the following theorem for a non-hyperbolic equilibrium point, $\bar{x}_{eq} = \bar{0}$.

Theorem 2.7.2 (Center Manifold Theorem for Flows) *Let $\bar{f}$ be a C^r vector field on $\mathbb{R}^n$ vanishhing at the origin ($\bar{f}(\bar{0}) = \bar{0}$) and let $A = Df(\bar{0})$. Divide the spectrum of A into three parts, σ_s, σ_c, σ_u with*

$$Re(\lambda) = \begin{cases} < 0 & if \quad \lambda \in \sigma_s \,, \\ = 0 & if \quad \lambda \in \sigma_c \,, \\ > 0 & if \quad \lambda \in \sigma_u \,. \end{cases}$$

Let the (generalized) eigenspaces of σ_s, σ_c, and σ_u be E^s, E^c, and E^u, respectively. Then there exist C^r stable and unstable invariant manifolds W^u and W^s tangent to E^u and E^s at 0 and a C^{r-1} center manifold W^c tangent to E^c at 0. The manifolds W^u, W^s, W^c are all invariant for the flow of $\bar{f}$. The stable and unstable manifolds are unique, but W^c need not be.

For the collinear points, two of the eigenvalues of A are real; one is negative and the other is positive. Thus, stable and unstable modes can be identified to compute stable and unstable manifolds, W^s and W^u, respectively. Recall that the libration points are equilibrium points. For example, to place a satellite at the L_2 point, manifolds represent potential transfer trajectories to deliver a vehicle into the L_2 point or to

depart the L_2 for another location. However, the existence of a positive real part in the eigenvalues indicates that the collinear libration points are unstable. The libration point L_2 has often been proposed as a location for an astrophysical observatory. Even though it's not practical to place a satellite at L_2, it might be possible to stay at the vicinity.
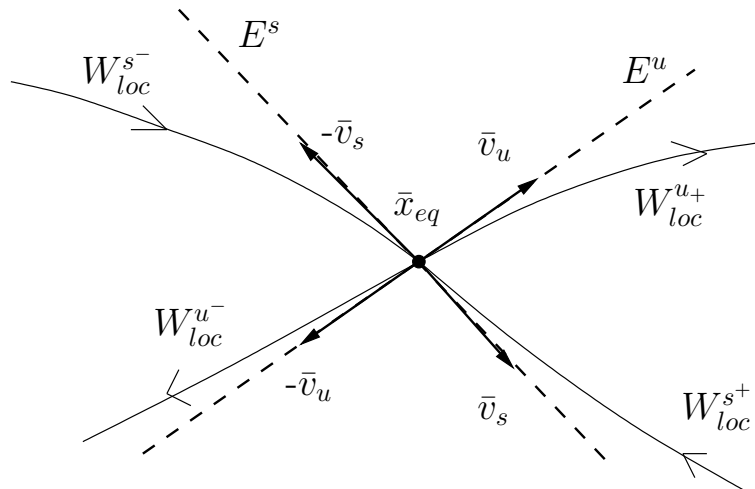
Figure 2.5. Stable and Unstable Manifolds Near a Hyperbolic Equilibrium Point

2.8   Periodic Orbits

Near the beginning of the 20th century, a number of researchers studied the three-body problem and developed approximation methods to compute periodic orbits. Most worked in the two-dimensional problem. The determination of three-dimensional orbits was the focus of fewer studies because of the computational challenges. In his early analysis in the 1920's, F.R. Moulton determined three types of finite, precisely periodic solutions at collinear points in the CR3BP [21]. He included three-dimensional orbits in the study. K.C. Howell [21] discusses each type of solutions and offers earlier references on the analytical and numerous developments. One type of solution is the Lyapunov, planar, periodic orbit for motion in the x-y plane. One of the Lyapunov orbits near L_2 in the Earth-Moon system appears in Figure

2.6. The orbit possesses a large in-plane excursion in the direction of the y-axis, i.e., $Ay =$ 58,850 km. Note that any three-dimensional trajectory is presented as an orthographic projection. The origin of the plot is the barycenter of the Earth-Moon system. The upper left plot is the x-y projection; the lower left is the x-z view; and, the projection in the lower right is onto the y-z plane, that is, the view from the negative $\hat{x}$-direction. Although a Lyapunov orbit is symmetric about the x-axis, it is not circular or elliptic. The shape is very unique to the CR3BP. As seen in the figure, there is no out-of-plane component in a Lyapunov orbit. The second type of solution is the nearly vertical orbit, also symmetric about x-axis. This type of orbit is dominated by the out-of-plane component, but not exclusively in the z-direction. The third type is the halo orbit. The halo orbit is actually a combination of the Lyapunov and nearly vertical orbits. It is three-dimensional and an example appears in Figure 2.7. This particular halo orbit is computed in the Earth-Moon system and possesses an out-of-plane amplitude $Az =$ 15,100 km, an in-plane excursion $Ay =$ 38,850 km. The x-y projection of the orbit appears in the upper left, and looks identical to a Lyapunov orbit. However, in the x-z and y-z projections, the out-of-plane component is clearly evident. Note that a halo orbit is <u>not</u> planar.

Computing a periodic orbit in the CR3BP is not an easy task. Not only is there no analytical solution, but this is also a region of space that is chaotic. Thus, most computational methods are burdened by a sensitivity to initial conditions. However, numerical tools and mathematical results not available to Moulton, now offer insight, such as certain characteristics of periodic orbits. With a good initial guess for the initial conditions, linear analysis can be used to numerically compute a periodic orbit.

2.8.1 State Transition Matrix (STM)

Instead of placing a satellite at a collinear libration point, using a periodic orbit near a libration point is a more practical option. As such, it is necessary to compute periodic orbits efficiently. However, numerical computation of periodic orbits
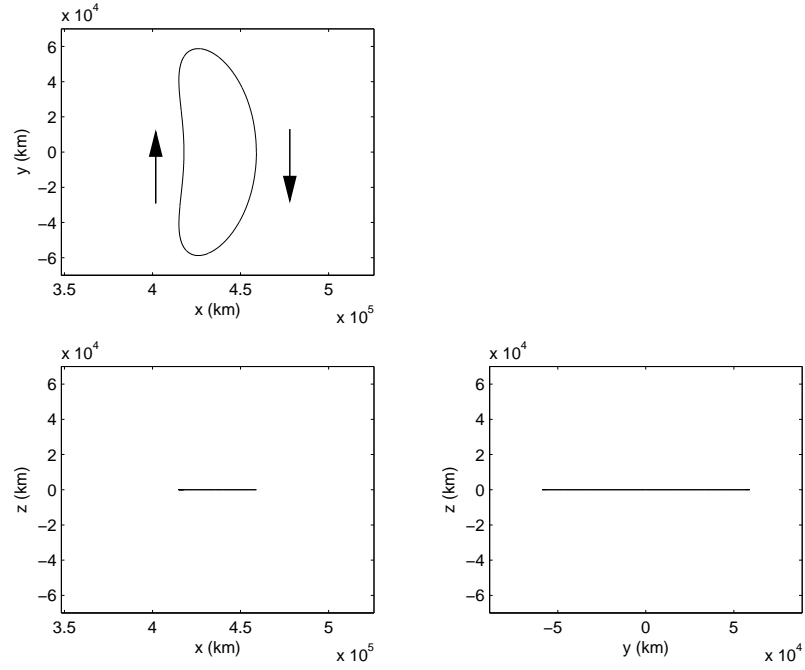
Figure 2.6. Lyapunov Orbit: Earth-Moon System, $Ay = 58{,}800$ km
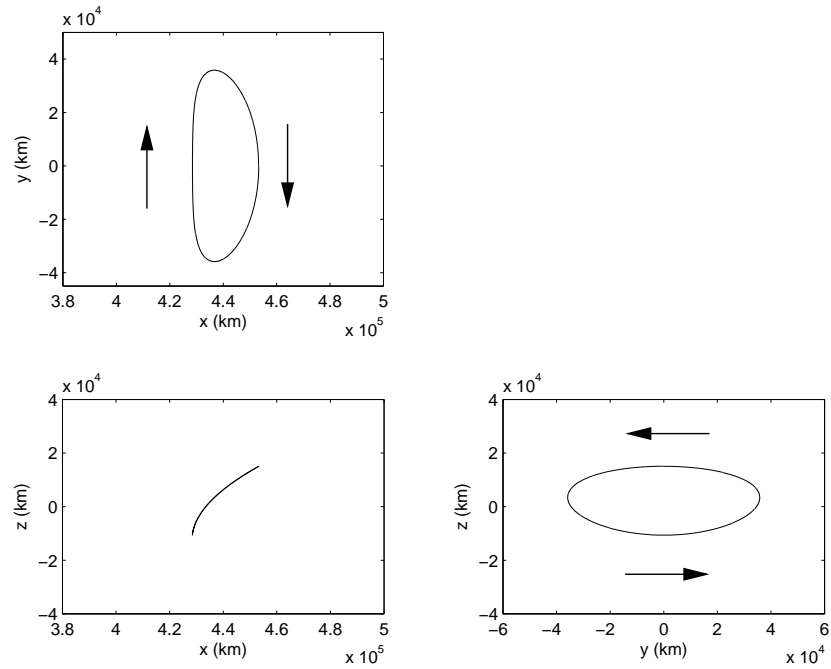
Figure 2.7. Halo Orbit: Earth-Moon System, $Az = 15{,}100$ km, $Ay = 38{,}850$ km

is generally time consuming unless a good initial guess is already available. A trial-and-error process is an option to obtain a good initial guess, but it is not always effective. Thus, development of a numerical method to improve an initial guess by predicting behavior near the reference solution is desirable. Such a method requires the information concerning sensitivity of the state to changes in the initial guess, i.e., state transition matrix.

Recall the nonlinear equation, $\dot{\bar{x}} = f(\bar{x})$. If a periodic orbit exists, it is possible to linearize about the periodic orbit. Then, again, Equation (2.43), $\delta\dot{\bar{x}} = A(t)\delta\bar{x}$, is obtained. The 6×6 Jacobian matrix, $A(t)$, appears in the form as follows [22],

$$A(t) = \begin{bmatrix} I_3 & 0_3 \\ U_{ij}^* & 2\Omega_3 \end{bmatrix}, \tag{2.45}$$

where the submatrices I_3 and 0_3 correspond to the 3×3 identity matrix and null matrix, respectively. Also the elements of the submatrix, U_{ij}^* appear as follows,

$$U_{ij}^* = \begin{bmatrix} U_{xx}^* & U_{xy}^* & U_{xz}^* \\ U_{yx}^* & U_{yy}^* & U_{yz}^* \\ U_{zx}^* & U_{zy}^* & U_{zz}^* \end{bmatrix}, \tag{2.46}$$

where U^* is the pseudo-potential defined in Equation (2.32) and each element is the second partial derivative with respect to the position states that are indicated by the subscript. Also, the constant 3×3 submatrix Ω_3 is evaluated as follows,

$$\Omega_3 = \begin{bmatrix} 0 & 1 & 0 \\ -1 & 0 & 0 \\ 0 & 0 & 0 \end{bmatrix}. \tag{2.47}$$

Let $\psi(t)$ be any nonsingular 6×6 matrix that satisfies the following,

$$\dot{\psi}(t) = A(t)\psi(t). \tag{2.48}$$

Then, the general solution of Equation (2.43) can be expressed in the form [23],

$$\delta\bar{x}(t) = \psi(t)\bar{c}, \tag{2.49}$$

where $\bar{c}$ is a constant vector. At the initial time, t_0, Equation (2.49) is the following,

$$\delta\bar{x}(t_0) = \psi(t_0)\bar{c}. \tag{2.50}$$

This equation can be solved for $\bar{c}$ as follows,

$$\bar{c} = \psi(t_0)^{-1}\delta\bar{x}(t_0). \tag{2.51}$$

Then, substitute this equation into Equation (2.49),

$$\delta\bar{x}(t) = \psi(t)\psi(t_0)^{-1}\delta\bar{x}(t_0). \tag{2.52}$$

The state transition matrix (STM), $\Phi(t, t_0)$, is defined as follows,

$$\Phi(t, t_0) = \psi(t)\psi(t_0)^{-1}. \tag{2.53}$$

Now, the general solution can be expressed in the following form,

$$\delta\bar{x}(t) = \Phi(t, t_0)\delta\bar{x}(t_0). \tag{2.54}$$

Since Equation (2.54) must also be true if evaluated at the initial time,

$$\Phi(t_0, t_0) = I, \tag{2.55}$$

where I is the identity matrix. The STM relates its initial state and the state at some future time, t. In other words, the STM indicates the sensitivity of subsequent behavior of the system to its initial state. Therefore, the STM is sometimes called the sensitivity matrix. Also, the state transition matrix after one complete cycle, $\Phi(T, t_0)$, is labelled the monodromy matrix.

2.8.2 Poincaré and Stroboscopic Maps

Consider a system described by Equation (2.42), $\dot{\bar{x}}=f(\bar{x})$. If a periodic orbit Γ exists, a hyperplane Σ that is perpendicular to Γ at a point, $\bar{x}_0$, exists such that an orbit departing from any point $\bar{x} \in \Sigma$ near $\bar{x}_0$, crosses Σ again at a point $P(\bar{x})$ near

$\bar{x}_0$ [6]. This concept is illustrated in Figure 2.8 for a lower-dimensional system. This mapping technique yields the Poincaré map [5,6,20]. The Poincaré map is constructed by defining a Poincaré Section. In Figure 2.8, a periodic orbit is seen to exist in a three-dimensional system. A Poincaré Section essentially "slices" through the phase space to reduce the dimension by one [24]. Thus, in Figure 2.8, the two-dimensional, plane Σ is the Poincaré Section. The system in Equation (2.42) is six-dimensional. Thus, the Poincaré Section is higher dimensional in this case. The concept behind a Poincaré map was introduced by Henri Poincaré in 1881 [6]. When the Poincaré Section is used, the crossing time, t_{ps}, i.e., when an orbit crosses the Σ, is not fixed. Thus, the general solution can be expressed in the following form,

$$\delta\bar{x}(t_0 + t_{ps}) = \Phi(t_{ps}, t_0)\delta\bar{x}(t_0) \,. \tag{2.56}$$

The Poincaré map is also used to study the stability of the periodic orbit. When the state representing a periodic orbit Γ on Σ is disturbed slightly from $\bar{x}_0$, the next crossing of the orbit on Σ occurs at a different point. If the point on the Σ is closer to $\bar{x}_0$ than the initial point, the periodic orbit is stable. If the periodic orbit is not stable, it is unstable.

A special case of the Poincaré map is a stroboscopic map. A stroboscopic map maps a trajectory onto a hyperplane Σ at a constant time interval [5,25]. The general solution in this case can be represented as follows,

$$\bar{x}(t_0 + T) = \Phi(t_0 + T, t_0)\bar{x}(t_0) \,, \tag{2.57}$$

where T is a certain time period. If T is the period of a periodic orbit, the form of the solution after l revolutions is,

$$\bar{x}(t_0 + lT) = \Phi(t_0 + lT, t_0)\bar{x}(t_0) \,, l = 1, 2, ... \tag{2.58}$$

Of course, T can be any other constant time. Then, this equation represents the solution after l iterations of the stroboscopic map.

In this study, the Poincaré map is used because it allows free movement of a Poincaré section.
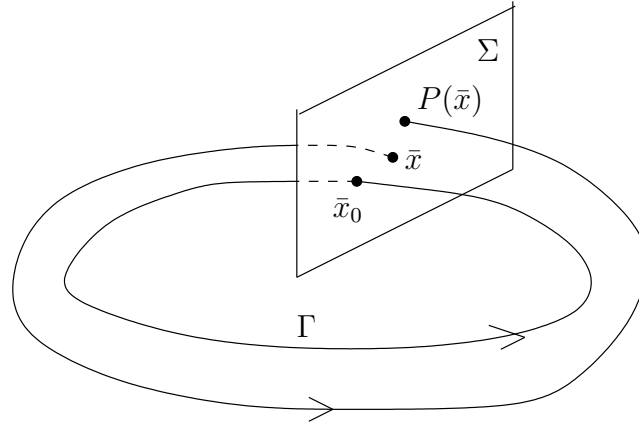
Figure 2.8. Poincaré Map

2.8.3   Differential Corrections

To compute a periodic orbit, specific initial conditions for the orbit are required. However, since there is no closed-form solution and this region of space is very sensitive to initial conditions, a search for such conditions can be time consuming. Thus, an efficient technique is necessary.

The characteristics of a periodic orbit offer useful information. As mentioned previously, the Lyapunov orbit and the x-y projection of a halo orbit near the collinear points are symmetric about the x-axis. Therefore, they possess perpendicular crossings on the x-axis. By locating the initial conditions on the x-axis, a periodic orbit re-crosses the x-axis, perpendicularly, at the half period of the orbit. If it is possible to determine such initial conditions, a periodic orbit can be computed. Two trajectory arcs appear in Figure 2.9. The thicker arc is a target arc that is a half periodic orbit; this is apparent from the perpendicular crossings of the x-axis. Another, thinner arc is the initial arc that is perturbed slightly from the target arc. By correcting the initial difference $\delta\bar{x}_0$, the final variation relative to the reference, $\delta\bar{x}_f$, is modified. Thus, when the correction is successful, the thinner arc converges onto the target arc.
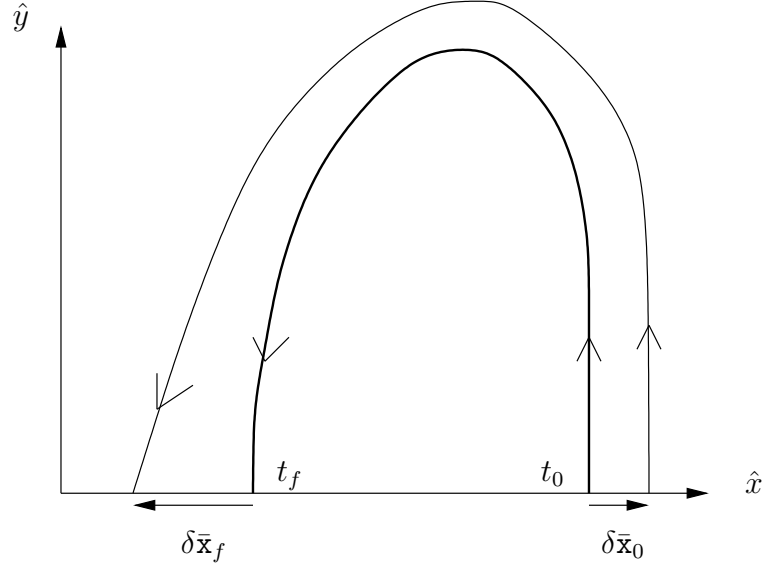
Figure 2.9. Differential Corrections

To determine a specific relationship between $\delta \bar{x}_0$ and $\delta \bar{x}_f$, exploit the STM. The final state of a trajectory can be computed by integrating the initial conditions until t_f, the final time. Thus, the final state can be expressed in the following form,

$$\bar{x}(t_f) = f(x_0, y_0, z_0, \dot{x}_0, \dot{y}_0, \dot{z}_0, t_f) \,, \tag{2.59}$$

where x_0, y_0, z_0, $\dot{x}_0$, $\dot{y}_0$, and $\dot{z}_0$ are initial values corresponding to each component. The variation of the final x component via a change in the initial conditions and final time can be expressed as follows,

$$\delta x_f = \frac{\partial x}{\partial x_0}\delta x_0 + \frac{\partial x}{\partial y_0}\delta y_0 + \frac{\partial x}{\partial z_0}\delta z_0 + \frac{\partial x}{\partial \dot{x}_0}\delta \dot{x}_0 + \frac{\partial x}{\partial \dot{y}_0}\delta \dot{y}_0 + \frac{\partial x}{\partial \dot{z}_0}\delta \dot{z}_0 + \frac{\partial x}{\partial t}\delta t_f \,, \tag{2.60}$$

where the partial derivatives are all evaluated at t_f. The variation in the other components can be expressed in the similar form. Since there is only one independent variable,

$$\frac{\partial}{\partial t} = \frac{d}{dt} \,. \tag{2.61}$$

Thus, $\frac{\partial x}{\partial t}$ becomes $\frac{dx}{dt} = \dot{x}$. Also, partial derivatives with respect to the components of state vector are just elements of the STM at t_f, i.e., $\Phi(t_f, t_0)$. Then, the linear variational equations can be written as follows,

$$\delta\bar{x}_f = \Phi(t_f, 0)\delta\bar{x}_0 + \dot{\bar{x}}|_{t_f}\delta t_f , \tag{2.62}$$

where $\dot{\bar{x}}|_{t_f}$ is the vector time derivative of the state vector, evaluated at t_f. In matrix form, Equation (2.62) can be expressed as follows,

$$\begin{bmatrix} \delta x \\ \delta y \\ \delta z \\ \delta\dot{x} \\ \delta\dot{y} \\ \delta\dot{z} \end{bmatrix}_{t_f} = \begin{bmatrix} \Phi_{11} & \Phi_{12} & \Phi_{13} & \Phi_{14} & \Phi_{15} & \Phi_{16} \\ \Phi_{21} & \Phi_{22} & \Phi_{23} & \Phi_{24} & \Phi_{25} & \Phi_{26} \\ \Phi_{31} & \Phi_{32} & \Phi_{33} & \Phi_{34} & \Phi_{35} & \Phi_{36} \\ \Phi_{41} & \Phi_{42} & \Phi_{43} & \Phi_{44} & \Phi_{45} & \Phi_{46} \\ \Phi_{51} & \Phi_{52} & \Phi_{53} & \Phi_{54} & \Phi_{55} & \Phi_{56} \\ \Phi_{61} & \Phi_{62} & \Phi_{63} & \Phi_{64} & \Phi_{65} & \Phi_{66} \end{bmatrix}_{t_f} \begin{bmatrix} \delta x_0 \\ \delta y_0 \\ \delta z_0 \\ \delta\dot{x}_0 \\ \delta\dot{y}_0 \\ \delta\dot{z}_0 \end{bmatrix} + \begin{bmatrix} \dot{x} \\ \dot{y} \\ \dot{z} \\ \ddot{x} \\ \ddot{y} \\ \ddot{z} \end{bmatrix}_{t_f} \delta t_f , \tag{2.63}$$

where Φ_{ij} indicates the element of STM at ith row and jth column. Also, the subscript, t_f, indicates that the vectors and matrix are evaluated at t_f. Now, let the vector of initial conditions be the following,

$$\bar{x}(t_0) = [x_0, y_0, z_0, \dot{x}_0, \dot{y}_0, \dot{z}_0]^T . \tag{2.64}$$

From Figure 2.9, it is obvious that y_0 is zero. Since the target arc has a perpendicular crossing on the x-axis, $\dot{x}_0$ is zero. Also, $\dot{z}_0$ is zero. Thus, the variational vector corresponding to the initial state under perturbation can be expressed as follows,

$$\delta\bar{x}(t_0) = [\delta x_0, 0, \delta z_0, 0, \delta\dot{y}_0, 0]^T . \tag{2.65}$$

Similarly, the final variation conditions can be written as follows,

$$\delta\bar{x}(t_f) = [\delta x_f, 0, \delta z_f, 0, \delta\dot{y}_f, 0]^T , \tag{2.66}$$

where δx_f, δz_f, and $\delta \dot{y}_f$ are final values of each component. Therefore, Equation (2.63) can be reduced to the following,

$$\delta y_f = \Phi_{21}\delta x_0 + \Phi_{23}\delta z_0 + \Phi_{25}\delta \dot{y}_0 + \dot{y}_f \delta t_f, \tag{2.67}$$

$$\delta \dot{x}_f = \Phi_{41}\delta x_0 + \Phi_{43}\delta z_0 + \Phi_{45}\delta \dot{y}_0 + \ddot{x}_f \delta t_f, \tag{2.68}$$

$$\delta \dot{z}_f = \Phi_{61}\delta x_0 + \Phi_{63}\delta z_0 + \Phi_{65}\delta \dot{y}_0 + \ddot{z}_f \delta t_f, \tag{2.69}$$

where Φ_{ij} indicates the element of the STM at i^{th} row and j^{th} column. Since a crossing at x-axis is observed, δy_f is always zero. Thus, Equation (2.67) can be solved for δt_f as follows,

$$\delta y_f = 0 = \Phi_{21}\delta x_0 + \Phi_{23}\delta z_0 + \Phi_{25}\delta \dot{y}_0 + \dot{y}_f \delta t_f. \tag{2.70}$$

This equation can be solved for δt_f, which is substituted it into Equations (2.68) and (2.69). Then, they become,

$$\delta \dot{x}_f = \Phi_{41}\delta x_0 + \Phi_{43}\delta z_0 + \Phi_{45}\delta \dot{y}_0 - \frac{\ddot{x}_f}{\dot{y}_f}(\Phi_{23}\delta z_0 + \Phi_{25}\delta \dot{y}_0), \tag{2.71}$$

$$\delta \dot{z}_f = \Phi_{61}\delta x_0 + \Phi_{63}\delta z_0 + \Phi_{65}\delta \dot{y}_0 - \frac{\ddot{z}_f}{\dot{y}_f}(\Phi_{23}\delta z_0 + \Phi_{25}\delta \dot{y}_0), \tag{2.72}$$

where $\ddot{x}_f$ and $\ddot{z}_f$ are the fourth and sixth components of $\dot{\bar{x}}|_{t_f}$. Assume x_0 is fixed, i.e., $\delta x_0 = 0$, then, by substitution into Equations (2.71) and (2.72), these expressions can be rewritten as follows,

$$\begin{bmatrix} \delta \dot{x}_f \\ \delta \dot{z}_f \end{bmatrix} = \left[\begin{bmatrix} \Phi_{43} & \Phi_{45} \\ \Phi_{63} & \Phi_{65} \end{bmatrix} - \frac{1}{\dot{y}_f} \begin{bmatrix} \ddot{x}_f \\ \ddot{z}_f \end{bmatrix} \begin{bmatrix} \Phi_{23} & \Phi_{25} \end{bmatrix} \right] \begin{bmatrix} \delta z_0 \\ \delta \dot{y}_0 \end{bmatrix}. \tag{2.73}$$

It is desired to offset the error in the final state, so the follwoing corrections are assumed,

$$\delta \dot{x}_f = -\dot{x}_f, \tag{2.74}$$

$$\delta \dot{z}_f = -\dot{z}_f. \tag{2.75}$$

The states at the perpendicular crossing can be computed by numerically integrating Equations (2.29), (2.30), and (2.31). The initial conditions for the simulation is required. Also, elements of the variable $A(t)$ matrix in Equation (2.43) can be

computed as required. Substitution of Equation (2.54), $\delta \bar{x}(t) = \Phi(t, t_0)\delta \bar{x}(t_0)$, into Equation (2.43), $\delta \dot{\bar{x}} = A(t)\delta \bar{x}$, yields,

$$\dot{\Phi}(t, t_0) = A(t)\Phi(t, t_0) \,. \tag{2.76}$$

Given $\Phi(t, t_0)$, sufficient information is available to compute δz_0 and $\delta \dot{y}_0$ in Equation (2.73). The computed δz_0 and $\delta \dot{y}_0$ are the necessary change to the current initial conditions. Assume the desired initial condition as follows,

$$\bar{x}_d = [x_d, 0, z_d, 0, \dot{y}_d, 0]^T \,. \tag{2.77}$$

Then, the current initial conditions can be expressed as follows,

$$\bar{x}_0 = \bar{x}_d + \delta \bar{x}_0 \,. \tag{2.78}$$

Thus, new initial conditions, $\bar{x}_{new}$ are,

$$\bar{x}_{new} = \bar{x}_0 - \delta \bar{x}_0 \,. \tag{2.79}$$

The new initial conditions can be evaluated by an iterative process. It may require several iterations till the new δz_0 and $\delta \dot{y}_0$ satisfy the desired tolerance.

2.8.4 Stable and Unstable Manifolds: Periodic Orbits

Even though the collinear libration points are linearly unstable, periodic orbits in their vicinity are well-suited as options for certain missions. However, designing a transfer trajectory from some primary body to a three-dimensional periodic orbit near an L_i point is a challenging task. An understanding of the natural dynamics of a periodic orbit is essential. A key property of a periodic orbit that has proven to be very useful is the existence of manifolds.

As for equilibrium points, stable and unstable manifolds offer much insight into the flow near a periodic orbit. Let $N(\Gamma)$ be the neighborhood of the periodic orbit Γ. Perko [6] states the following theorem.

Theorem 2.8.1 (The Stable Manifold Theorem for Periodic Orbits) *Let $f \in C^1(E)$ where E is an open subset of R^n containing a periodic orbit,*

$$\Gamma : \bar{x} = \gamma(t),$$

of $\dot{\bar{x}} = f(\bar{x})$ of period T. Let ϕ_t be the flow of $\dot{\bar{x}} = f(\bar{x})$ and $\gamma(t) = \phi_t(\bar{x}_0)$. If k of the characteristic exponents of $\gamma(t)$ have negative real part where $0 \leq k \leq n-1$ and $n-k-1$ of them have positive real part then there is a $\delta > 0$ such that the stable manifold of Γ,

$$S(\Gamma) = \{\bar{x} \in N_\delta(\Gamma) \,|\, d(\phi_t(\bar{x}), \Gamma) \to 0 \ as \ t \to \infty$$
$$and \ \phi_t(\bar{x}) \in N_\delta(\Gamma) \ for \ t \geq 0\},$$

is a $(k+1)$ - dimensional, differentiable manifold which is positively invariant under the flow ϕ_t and the unstable manifold of Γ,

$$U(\Gamma) = \{\bar{x} \in N_\delta(\Gamma) \,|\, d(\phi_t(\bar{x}), \Gamma) \to 0 \ as \ t \to -\infty$$
$$and \ \phi_t(\bar{x}) \in N_\delta(\Gamma) \ for \ t \leq 0\},$$

is an $(n-k)$ - dimensional, differentiable manifold which is negatively invariant under the flow ϕ_t. Furthermore, the stable and unstable manifolds of Γ intersect transversally in Γ.

Thus, stable (unstable) manifolds approach (leave) a periodic orbit asymptotically. Thus, it is not possible to obtain an exact point where a stable (unstable) manifold approaches (leaves) the periodic orbit. However, initial conditions are required to compute a manifold numerically. This indicates that it is necessary to approximate the manifolds for their use to estimate the initial conditions. Since the global manifolds in the nonlinear problem are tangent to the eigenspace near the periodic orbit, eigenvectors from the monodromy matrix can be exploited to approximate the manifolds. Guckenheimer [20] states the relationships between the subspaces and eigenvalues of the state transition matrix.

$$E^s = span\{eigenvectors \ whose \ eigenvalues \ have \ modulus < 1\},$$
$$E^u = span\{eigenvectors \ whose \ eigenvalues \ have \ modules > 1\}.$$

To obtain stable (unstable) eigenvectors that span the stable (unstable) subspace, a point on the periodic orbit is selected. Then, eigenvalues are computed from the monodromy matrix, $\Phi(T, t_0)$ at the point. The structure of the eigenvalues of the monodromy matrix is established by the following theorem [22, 23],

Theorem 2.8.2 (Lyapunov's Theorem) *If λ is an eigenvalue of the monodromy matrix $\Phi(T, 0)$ of a t-invariant system, then λ^{-1} is also an eigenvalue, with the same structure of elementary divisors.*

One of the eigenvalues must be one for a periodic orbit to exist; the structure of the system also results in eigenvalues that are always in reciprocals pairs. So, consistent with the theorem, at least two of eigenvalues are one. If one of the eigenvalues is real and not unity, its reciprocal eigenvalue must exist. Thus, if the magnitude of one of the real eigenvalues is smaller than one, the magnitude of another real eigenvalue must be larger than one due to the reciprocal structure. This indicates that stable and unstable manifolds must co-exist. If one of the eigenvalues is imaginary, its reciprocal imaginary eigenvalue must exist. To satisfy this condition, imaginary eigenvalues are all on the unit circle.

Once eigenvectors are computed from the eigenvalues, initial conditions to compute stable (unstable) manifolds numerically can be estimated. Let $\bar{V}^{W_s}$ and $\bar{V}^{W_u}$ be stable and unstable eigenvectors, respectively. Also, suppose $\bar{V}^{W_s} = [x_s, y_s, z_s, \dot{x}_s, \dot{y}_s, \dot{z}_s]^T$ and $\bar{V}^{W_u} = [x_u, y_u, z_u, \dot{x}_u, \dot{y}_u, \dot{z}_u]^T$. Then, let $\bar{Y}^{W_s}$ and $\bar{Y}^{W_u}$ be defined as follows [25],

$$\bar{Y}^{W_s} = \frac{\bar{V}^{W_s}}{\sqrt{x_s^2 + y_s^2 + z_s^2}}, \tag{2.80}$$

$$\bar{Y}^{W_u} = \frac{\bar{V}^{W_u}}{\sqrt{x_u^2 + y_u^2 + z_u^2}}. \tag{2.81}$$

The initial state vectors for a stable and unstable manifold are $\bar{X}_0^{W_s}$ and $\bar{X}_0^{W_u}$, respectively. These vectors are evaluated as follows,

$$\bar{X}_0^{W_s} = \bar{x}^* + d\bar{Y}^{W_s} \tag{2.82}$$

$$\bar{X}_0^{W_u} = \bar{x}^* + d\bar{Y}^{W_u}, \tag{2.83}$$

where $\bar{x}^*$ is the fixed point on the halo orbit and d is a scalar distance. The value of d depends on the system. Also, it should be sufficiently small to satisfy the range of validity for the linear assumption. However, if d is too small, "the time of flight becomes too large due to the asymptotic nature" of manifolds [25]. A subspace is spanned by any multiple of its eigenvector [26]. Thus, there are two directions for each $\bar{Y}^{W_s}$ and $\bar{Y}^{W_u}$. For each direction, half a manifold exists. An example of a single stable and a single unstable manifold corresponding to a fixed point along an L_2 halo orbit in the Sun-Earth system appears in Figure 2.10. The figure is in the Sun-Earth rotating frame. The Az of the halo orbit is 130,300 km. Blue indicates the stable manifold. Red indicates the unstable manifold. The blue circle represents the Earth. The black dot indicates the L_2 point. Note the symmetry apparent when the stable and unstable manifolds are compared. Since the initial conditions can be estimated by using any point along the periodic orbit, there exist infinitely many manifolds along a periodic orbit [14]. In configuration space, this result can be visualized as surfaces of stable and unstable flow arriving at or departing from the orbit. To identify specific manifolds along the orbit, "tag numbers" are defined for fixed points on the periodic orbit. An example of selected points along a halo orbit appears in Figure 2.11. The halo orbit is near the Sun-Earth L_2, and the Az value is 130,300 km. In the figure, 34 points are selected, and the time between each point is equal. The tag number "1" is indicated by a number one in the figure. It is on the x-axis and on the far side of the second primary, the Earth in this case. Then, the tag numbers increase clockwise. More points can be selected by decreasing the time between each point. However, the location of the tag number 1 is always the same. Theoretically, it is possible to compute infinitely many manifolds. However, it is not practical because it requires an infinite amount of computation time. However, it is possible to estimate the surface from the selected manifolds. A surface associated with the unstable Sun-Earth manifolds for a halo orbit near L_2 appears in Figure 2.12. This figure is also in the Sun-Earth rotating frame. The Az is 130,300 km. The surface forms a tube; trajectories corresponding to globalized manifolds comprise the surface. Hence, the

surface is sometimes labelled a "manifold tube". Manifold tubes are useful in the design of low cost transfer trajectories involving periodic orbits.

It is observed that stable and unstable manifold tubes also generally separate trajectories that are not actually on the tubes into two different types [17]. One type of orbits remains inside a manifold tube, and another type maintains a path beyond the manifold tube. Therefore, manifold tubes in the two-dimensional problem are also separatrices.
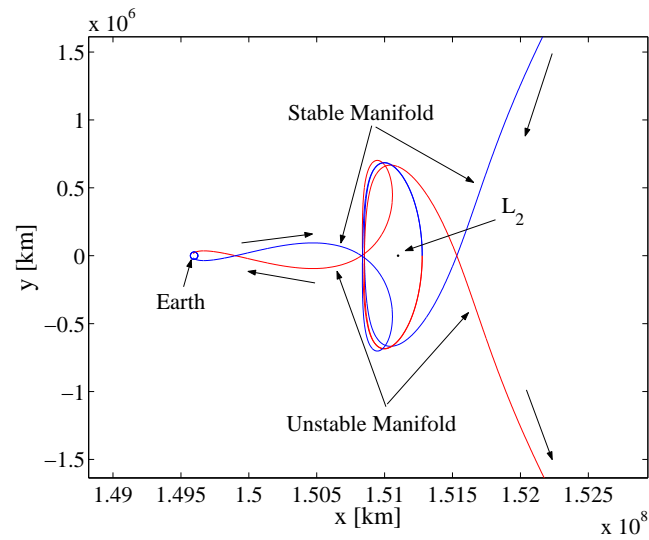

Figure 2.10. Sun-Earth Stable and Unstable Manifolds Near L_2; $Az = 130,300$ km
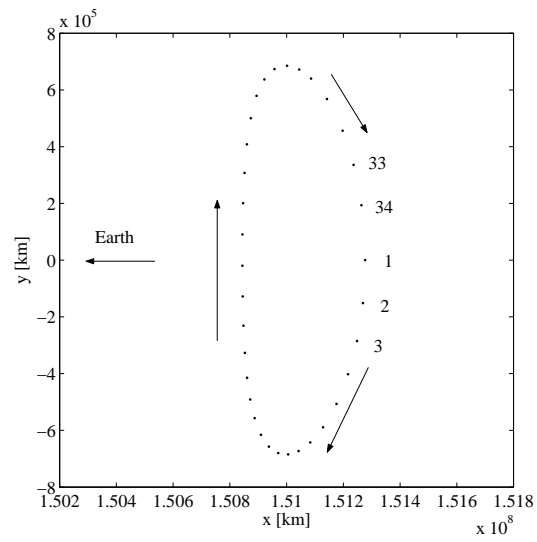
Figure 2.11. "Tag" Numbers for Selected Points on Sun-Earth Halo Orbit Near L_2; $Az = 130{,}300$ km
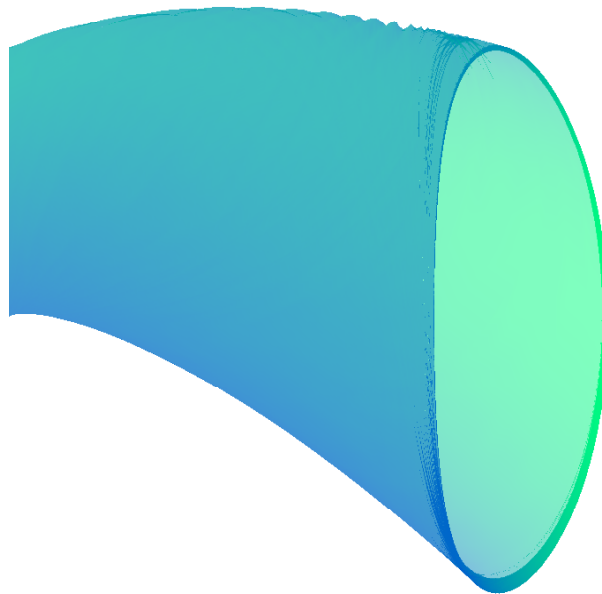
Figure 2.12. Sun-Earth Unstable Manifold Tube Near L_2; $Az = 130{,}300$ km

3. Two-Dimensional Transfers Between the Earth-Moon (EM) System and Sun-Earth (SE) System

Designing trajectories in a multi-body system is complicated and time consuming. The search for new, innovative techniques continues. Even though there is no closed-form solution in the CR3BP, knowledge of particular types of solutions generates part of a foundation for the design process. This is certainly critical in the system-to-system transfer problem.

3.1 Transit Orbits

Invariant manifolds offer unique insight into trajectories in the CR3BP. They indicate the existence of patterns in the dynamical structure. Understanding the dynamics associated with invariant manifolds might result in new ideas. One of the interesting manifestations of invariant manifolds is a manifold tube. A manifold tube, particularly as envisioned in configuration space, indicates the dynamical flow at a certain energy level. If there exists an orbit that passes through a manifold tube, it should yield a significant advantage in the trajectory design process and it is possible to compute such orbits. Under certain conditions, orbits called transit orbits, remain inside the manifold tube for all time [17]. One of the necessary conditions for computation of a transit orbit is that the corresponding Jacobi Constant is the same as that associated with the manifold tube of interest [17]. This property can be exploited to generate a transit orbit.

3.1.1 Generating Two-Dimensional Transit Orbits

Transit orbits exist in connection with either two- or three-dimensional manifold tubes. In the two-dimensional case, the manifold tube collapses to a plane. An example of a transit orbit passing through a manifold tube appears in Figure 3.1. The direction of the transit orbit is indicated by an arrow. The transit orbit passes through an unstable Sun-Earth manifold tube, red in this figure. The location of the Earth is indicated by a blue circle. To compute a transit orbit inside the tube, it is necessary to obtain the initial conditions corresponding the orbit. However, it is not trivial to obtain such an initial state vector. The Poincaré Section is particularly useful precisely because it reduces the dimension of the system by one. As discussed previously, the location of a Poincaré Section is flexible. The first step is to select a plane in configuration space to create a map. Let the plane be defined to be the "PS plane". Of course, such a plane can be selected at any orientation in the space, but a convenient choice appears in Figure 3.2. In the figure, the two-dimensional Sun-Earth manifold tube is terminated such that the "x" values of all the manifold trajectories equal that corresponding to the Earth location. This orientation is termed a "vertical Poincaré section". The location of the Poincaré Section is indicated by the PS plane in the figure. This manifold tube is the collection of unstable manifolds from the Lyapunov orbit near L_2. The Poincaré Section is defined along the y-axis where the manifold tube crosses the Earth's x-coordinate. Thus, x is fixed. In this two-dimensional tube, the free variables at the section are reduced to y, $\dot{y}$, and $\dot{x}$. To select y and $\dot{y}$, the phase plot y vs $\dot{y}$ at the Poincaré Section is useful. The phase plot appears in Figure 3.3. Note that this plot is a closed curve. Thus, this closed curve indicates the boundary conditions for transit orbits [17]. There exist two $\dot{y}$ values for each y value on the curve. The higher value is the upper boundary, and the lower value is the lower boundary. There also exist boundaries of y values for each $\dot{y}$ value. This means that the combination of y and $\dot{y}$ must remain inside the closed curve for a given transit orbit. By selecting a point inside the closed curve, y and $\dot{y}$

are determined. As a result, $\dot{x}$ is the only free variable. It is necessary for the transit orbit to possess the same value of Jacobi Constant as the value that corresponds to the manifold tube. Therefore, $\dot{x}$ is modified to satisfy this condition. The initial conditions are ready to be integrated when the desired Jacobi Constant is achieved.
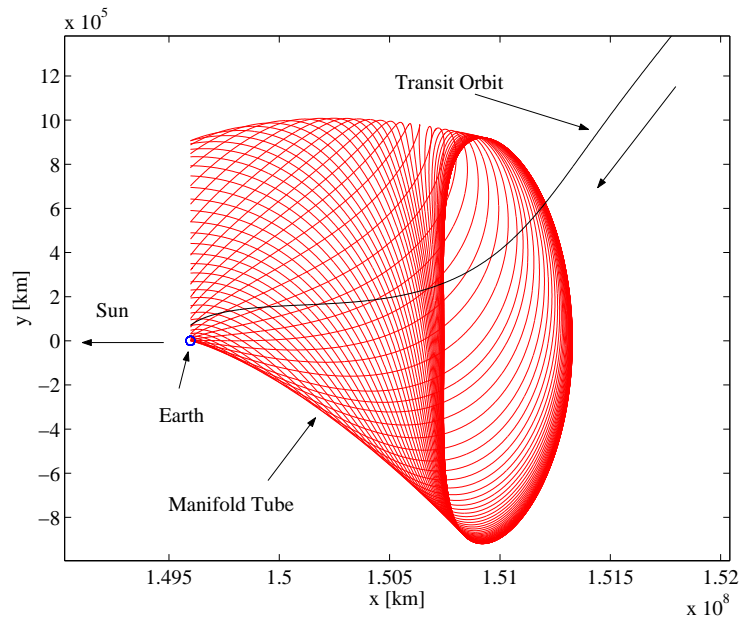
Figure 3.1. Two-Dimensional Transit Orbit Inside Unstable Sun-Earth Manifold Tube; $Ay = 920{,}000$ km

3.2 Transit Orbit through Two tubes

By using the transit orbit, it is possible to move from one manifold tube to another. An example appears in Figure 3.4. These manifolds are computed in the Earth-Moon system. The red manifold tube consists of unstable manifolds from the Lyapunov orbit associated with the Earth-Moon L_2 point and the Ay value is 49,100 km. The blue manifold tube is generated via a Lyapunov orbit in the L_1 family and is a stable manifold tube. The Ay amplitude is 46,200 km. The black orbit passing through the two manifold tubes is the transit orbit. Of course, these two manifold tubes must possess the same Jacobi Constant, about 3.129, for the transit orbit to pass through
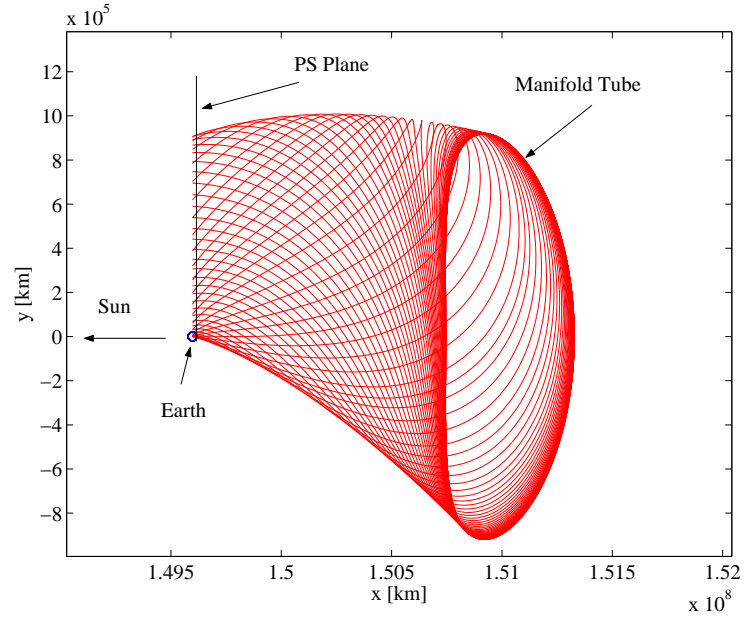
Figure 3.2. Sun-Earth L_2 Unstable Manifold Tube Terminated at a Vertical Poincaré Section; $Ay = 920,000$ km
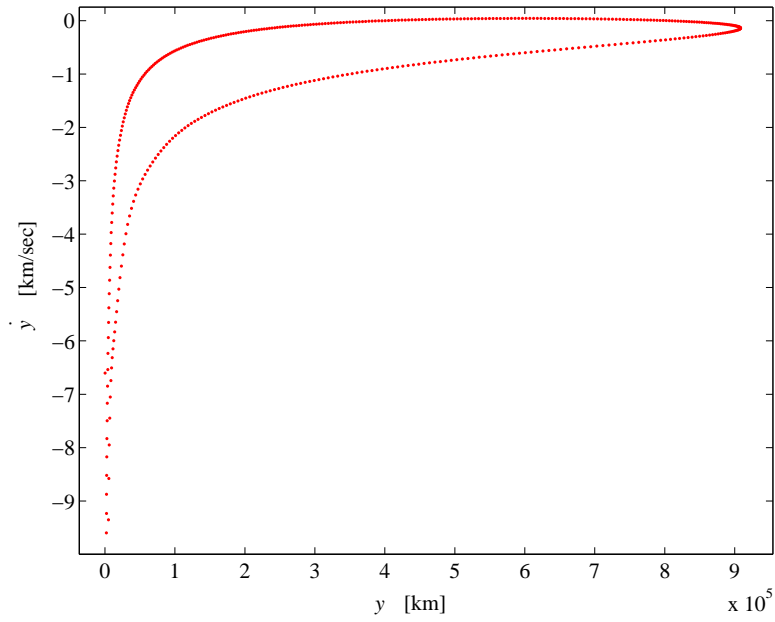
Figure 3.3. A Phase Plot of $\dot{y}$ vs y at the Poincaré Section

both tubes without a maneuver. So, the associated halo orbits are <u>not</u> exactly the same size. Once the two manifold tubes are computed, a PS plane is defined in configuration space where the tubes intersect. In this case, the plane is defined at the x-coordinate corresponding to the location of the Earth. In the previous section, only one closed curve appears in the phase plot of $\dot{y}$ vs y because only one manifold tube crosses the section. However, two manifold tubes intersect the plane in this case, one stable/one unstable. There are two closed curves in the phase plot. If a transit orbit exists inside both of the manifold tubes, then the two closed curves must intersect. The intersection serves to define the boundary conditions for the transit orbit. Any point inside the intersection can be selected to define $\dot{y}$ and y. The value of $\dot{x}$ is adjusted to produce the same value of Jacobi Constant as the manifold tubes. [In the three-dimensional transfer, z and $\dot{z}$ values must be determined. The value of z can be selected anywhere inside the tubes. Also, simply zero can be selected for the $\dot{z}$ value. However, the existence of a transit is not guaranteed.]

Figure 3.4. Two-Dimensional Transit Orbit Through Two Tubes in Earth-Moon System; Ay of halo orbit near $L_1 = 46{,}200$ km, Ay of halo orbit near $L_2 = 49{,}100$ km

3.3 Transfer between Earth-Moon System and Sun-Earth System in Two-Dimensions

The previous section presents a process to compute a transit orbit through two manifold tubes in a single system. However, it is possible to adapt the technique to transfer between two different systems. In 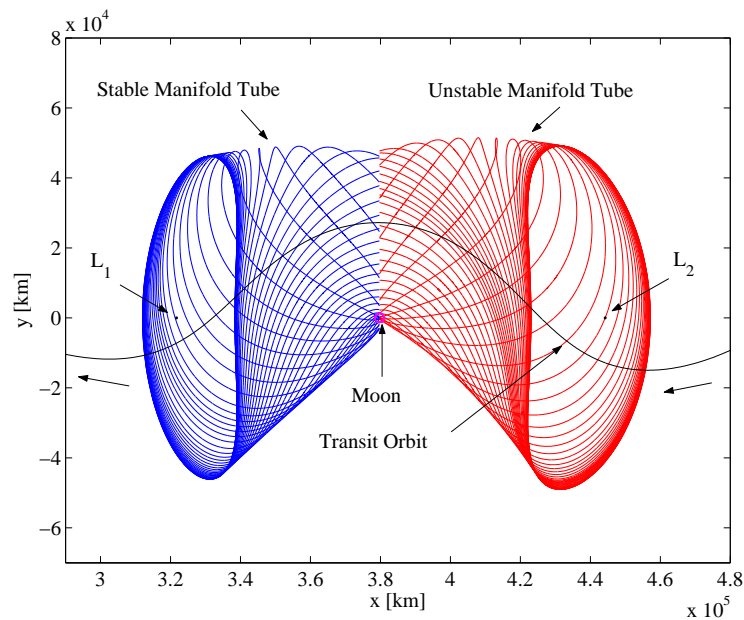the vicinity of the Earth and the Moon, it is necessary to consider the Sun-Earth-Moon system due to the significant influence of the solar gravity on spacecraft trajectories. Then, the model of the system can be constructed as overlapping three-body systems, i.e., the Earth-Moon system and the Sun-Earth system. Thus, it is possible to apply transit orbits to the trajectory design process in the vicinity of the Earth and the Moon. The goal is the determination of low cost transfer orbits between the Sun-Earth system and the Earth-Moon system. This step can be accomplished by applying the transit orbit technique. Transferring between systems does require multiple transformations and additional transformation matrices are required. Then, the transfer from the Earth-Moon to the Sun-Earth system is considered. Finally, a transfer in the opposite direction, i.e., from Sun-Earth to Earth-Moon system, is detailed.

3.3.1 Two-Dimensional Sun-Earth-Moon Model

The two-dimensional Sun-Earth-Moon system can be modelled by simply overlapping two CR3BP's, the Earth-Moon system and the Sun-Earth system, in the same plane, as it appears in Figure 3.5. The Earth-Moon and Sun-Earth rotating frames are defined by $[\hat{a}_1, \hat{a}_2]^T$ and $[\hat{b}_1, \hat{b}_2]^T$, respectively. The center of rotation of the Earth-Moon system is shifted from the barycenter to the Earth. Then, the modified Earth-Moon system is placed in the Sun-Earth system. Thus, the Moon is still assumed to move in a circular orbit.
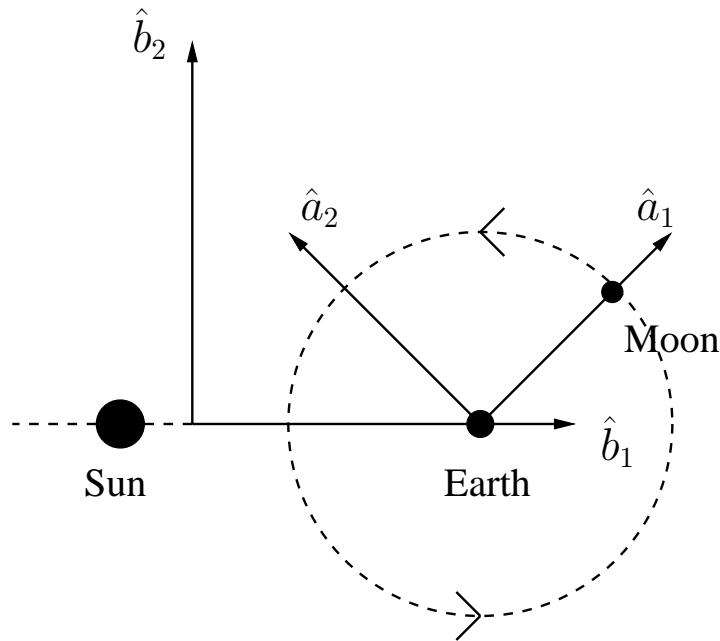
Figure 3.5. Two-Dimensional Model

3.3.2   Earth-Moon (EM) Manifold Tube

The first step to obtain a transit orbit is to compute the manifold tube. For a transfer from the Earth-Moon system to the Sun-Earth system, an unstable Earth-Moon manifold tube and a stable Sun-Earth manifold tube are required. The unstable manifold tube is the collection of unstable manifolds. Each unstable manifold is computed by the method discussed in the previous chapter. For this example, 58,800 km is selected arbitrarily for the Ay amplitude of a Lyapunov orbit. Then, the manifold tube must be transformed into the Sun-Earth system to compute an intersection with a Sun-Earth manifold tube.

The transformation is developed via the following steps. Recall that the Earth-Moon rotating frame is generally defined in terms of the unit vectors $[\hat{a}_1, \hat{a}_2, \hat{a}_3]^T$. Then, the coordinates of a position vector associated with the state along a trajectory in the Earth-Moon frame is defined as follows,

$$\bar{r}_{nd} = x\hat{a}_1 + y\hat{a}_2 + z\hat{a}_3 \,, \tag{3.1}$$

where x, y, and z are nondimensional position components in each direction. Thus, $\bar{r}_{nd}$ is a nondimensional position vector. The angle between the inertial frame and rotating frame is defined to be θ_{EM}. To transform the position from the Earth-Moon frame to Sun-Earth frame, the angle between the Earth-Moon rotating frame and Sun-Earth rotating frame, θ_{SE-EM}, is required. The angle between the Sun-Earth rotating frame and inertial frame, θ_{SE}, is defined to be,

$$\theta_{SE} = n_{SE} * t, \tag{3.2}$$

where n_{SE} is the mean motion of the Sun-Earth rotating frame with respect to the inertial frame, and t is the dimensional time. Then, the angle θ_{SE-EM} can be computed easily, since,

$$\theta_{SE-EM} = \theta_{EM} - \theta_{SE}. \tag{3.3}$$

Suppose that the Sun-Earth rotating frame is defined, in general via unit vectors, $[\hat{b}_1, \hat{b}_2, \hat{b}_3]^T$. Then, the direction cosine matrix from the Earth-Moon rotating frame to Sun-Earth rotating frame is written as follows,

$${}^{B}C^{A} = \begin{bmatrix} \cos\theta_{SE-EM} & -\sin\theta_{SE-EM} & 0 \\ \sin\theta_{SE-EM} & \cos\theta_{SE-EM} & 0 \\ 0 & 0 & 1 \end{bmatrix}. \tag{3.4}$$

In a more compact form, the Earth-Moon rotating frame and Sun-Earth rotating frame can be related as follows,

$$[\ \hat{b}_1, \ \ \hat{b}_2, \ \ \hat{b}_3 \ ]^T = {}^{B}C^{A}[\ \hat{a}_1, \ \ \hat{a}_2, \ \ \hat{a}_3 \ ]^T. \tag{3.5}$$

Therefore, the position vector in the Earth-Moon rotating frame can be transferred into the Sun-Earth rotating frame by using this matrix.

Transforming the velocity components can also be accomplished. Since the Earth-Moon rotating frame possesses constant angular velocity relative to the inertial frame, it is necessary to use the following equation,

$$\frac{{}^{i}d^{B}\bar{r}}{dt} = \frac{{}^{i}d^{A}\bar{r}}{dt} + {}^{A}\bar{\omega}^{B} \times {}^{A}\bar{r}, \tag{3.6}$$

to relate derivatives of vectors relative to different observers. Note that $^B\bar{r}$ is the position vector in the Sun-Earth rotating frame, $^A\bar{r}$ is the position vector in the Earth-Moon rotating frame, and $^A\bar{\omega}^B$ is the angular velocity of the Sun-Earth rotating frame with respect to the Earth-Moon rotating frame. Therefore, $\frac{^id^B\bar{r}}{dt}$ is the time derivative of $^B\bar{r}$ in the inertial frame, where the symbol 'i' in the upper left indicates that the derivative is relative to an inertial observer. Similarly, $\frac{^id^A\bar{r}}{dt}$ is the time derivative of $^A\bar{r}$ in the inertial frame. All the vectors are nondimensional, defined consistent with the characteristic quantities in the Earth-Moon system. Equation (3.6) is known as the Basic Kinematic Equation (BKE).

After the position and velocity components along a trajectory associated with the Earth-Moon manifold tube are transformed into the Sun-Earth rotating frame, these components must be dimensionalized by the same characteristic quantities that are used to nondimensionalize, i.e., characteristic quantities in the Earth-Moon system, to determine an intersection with a Sun-Earth tube. Of course, the Sun-Earth tube must be dimensionalized using the characteristic quantities in the Sun-Earth system. Then, a Poincaré Section is selected. It is possible to select the Poincaré Section anywhere in the system. A good intersection may vary depending on a number of parameters. A dimensionalized, Earth-Moon manifold tube in the Sun-Earth rotating frame appears in Figure 3.6. A vertical Poincaré Section is arbitrarily located at an x-coordinate equal to 1.494×10^8 km relative to the Sun-Earth rotating frame in this case. It is important to track the times that each trajectory reaches the section because they are all different. Unstable Earth-Moon manifolds are in red. The Ay excursion of the Lyapunov orbit corresponding to the manifolds is 58,800 km. The lunar circular orbit appears in blue. The Earth is represented by the small blue circle. The arrow indicates the direction to the Sun.

Once the intersection is determined in the Sun-Earth rotating frame, different approaches are available to accomplish the transfer to the Sun-Earth system. Of course, the approach is determined by the mission objective. There are four different types of mission scenarios considered. (1) One scenario is a transfer from an Earth-Moon Lya-

punov orbit to a Sun-Earth Lyapunov orbit. This type of transfer can be accomplished by shifting from an Earth-Moon manifold to a Sun-Earth manifold. The concept is to simply determine a transfer by identifying an Earth-Moon manifold that intersects a Sun-Earth manifold. However, this is not a trivial task when only numerical approaches are available. (2) The second scenario is a transfer from an Earth-Moon Lyapunov orbit to a transit orbit through a Sun-Earth tube. This approach is actually the simplest. (3) The third scenario is to transfer from a transit orbit inside an Earth-Moon tube to a Sun-Earth manifold. Then, the transfer trajectory arrives at a Lyapunov orbit. In this type, it is necessary to transform an intersecting point, determined in the Sun-Earth rotating frame, into the Earth-Moon rotating frame to compute a transit orbit inside an Earth-Moon tube. This simple transformation is challenging due to the unknown transfer time. (4) The fourth scenario is the transit transfer from an Earth-Moon tube to Sun-Earth tube. This transfer has the same challenge as type (3). Thus, the transfer types (2)-(4) are discussed here. The first type is discussed later.
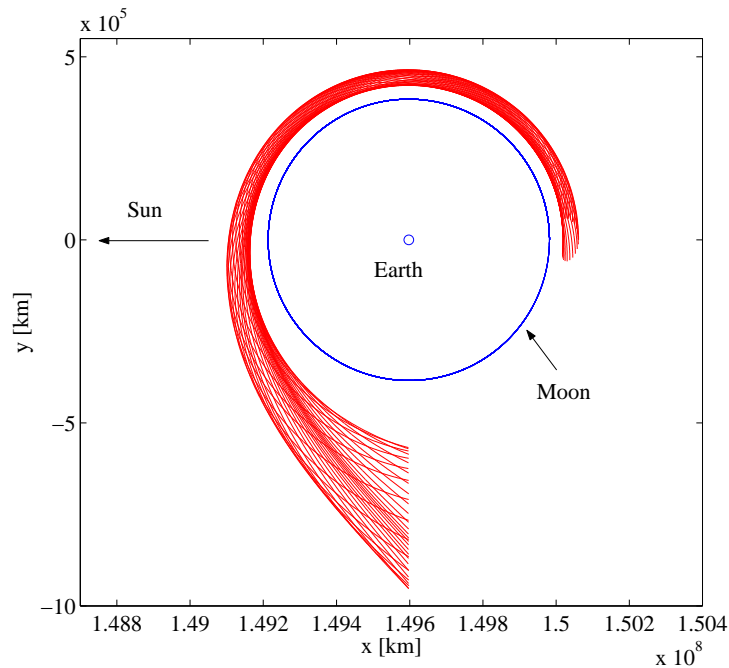
Figure 3.6. Unstable Earth-Moon Tube in Sun-Earth Frame; $Ay = 58{,}800$ km

3.3.3 Transit Transfers to Sun-Earth System

Once a Poincaré Section is determined, the intersection between the Earth-Moon tube and Sun-Earth tube can be obtained. An example of intersecting manifolds in the Sun-Earth rotating frame appears in Figure 3.7. The Earth-Moon manifolds are the same as those in Figure 3.6. Stable Sun-Earth manifolds appear in blue. These manifolds are associated with a Lyapunov orbit near L_2 point, and the Ay amplitude is 920,000 km. To obtain conditions for a transit orbit, the $\dot{y}$ vs y phase plot at this Poincaré Section is useful. The phase plot appears in Figure 3.8. The color in the plot corresponds to the color of the manifolds. Since the two closed curves intersect, it indicates the possibility of a free transit orbit inside the Sun-Earth tube or/and the Earth-Moon tube. Now, different types of transfers are considered.
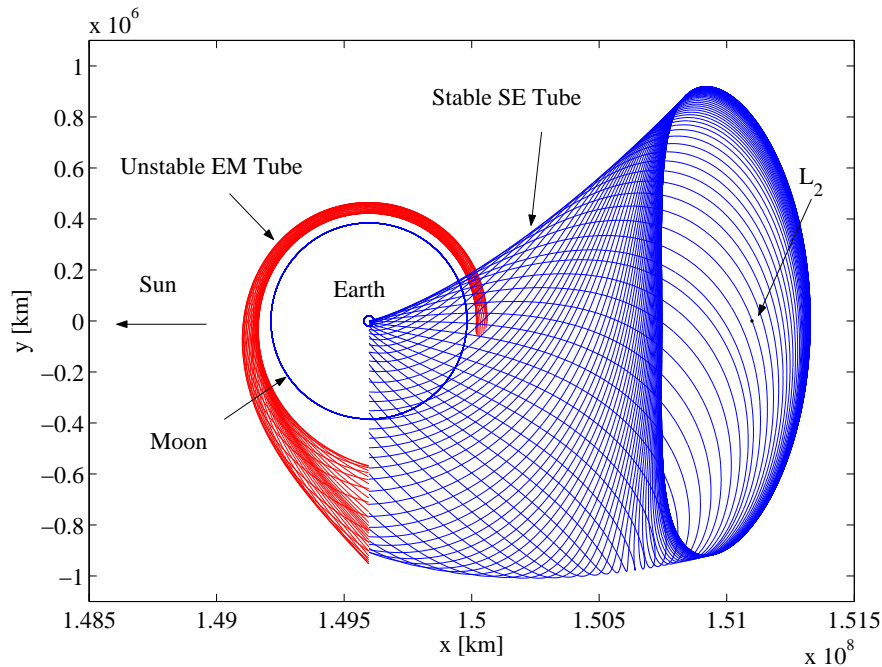
Figure 3.7. Unstable Earth-Moon Tube and Stable Sun-Earth Tube in Sun-Earth Rotating Frame; EM $Ay = 58,800$ km, SE $Ay = 920,000$ km
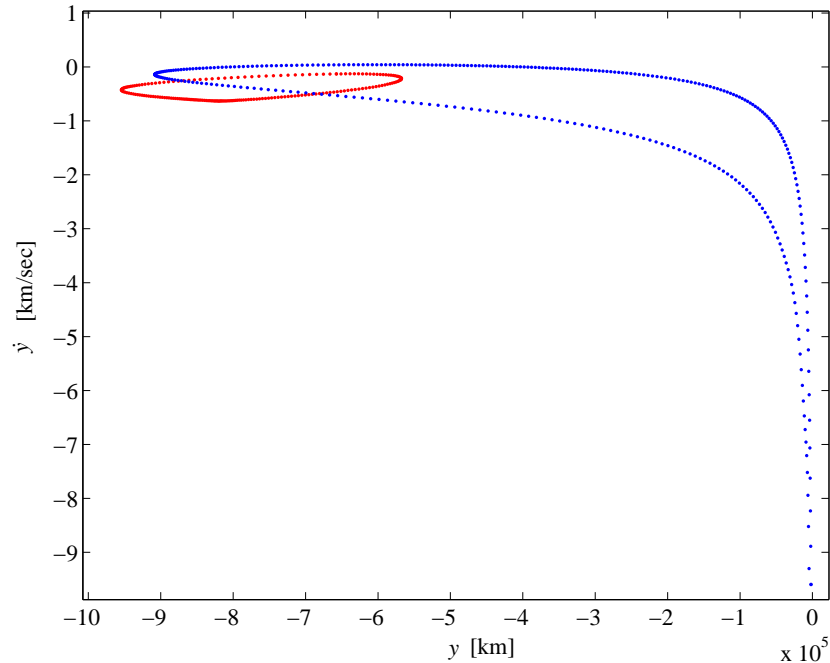
Figure 3.8. Projection of Poincaré Section onto y-$\dot{y}$ Plane; EM curve in red, SE curve in blue

Manifold-to-Transit Transfers

In Figure 3.8, a part of the red curve is inside the blue curve. If a point is selected from this part on the red curve, a free transit orbit that passes inside the Sun-Earth tube should be possible. The necessary condition for the existence of such an orbit is that the values of the Jacobi Constants are equal: the Jacobi Constant of the selected point on the red curve – on the Earth-Moon manifold – and the Jacobi Constant corresponding to the blue Sun-Earth tube. If they are indeed equal, a free transit orbit is possible. If they are not equal, the size of the Sun-Earth Lyapunov orbit must be modified to obtain the desired Jacobi Constant. Note that the value of Jacobi Constant that corresponds to an Earth-Moon manifold transformed into the Sun-Earth rotating frame is not constant because of the rotation of the Earth-Moon rotating frame. Thus, the value of Jacobi Constant varies along the red curve. If one of the values is the same as the value of the Sun-Earth tube, a free transit orbit is

possible. If none of them is the same, the size of the Sun-Earth Lyapunov orbit has to be changed to obtain the desired value of Jacobi Constant. The desired value can be selected from the Jacobi Constant value at any point on the red curve. Once the Sun-Earth tube is computed with the desired value of Jacobi Constant, again, it is necessary to examine the $\dot{y}$ vs y phase plot. The selected point has to be inside the closed curve computed from the new Sun-Earth tube. If the curve does not include the point, no cost-free transfer is possible. Then, it is necessary to change $\dot{y}$ to make the point inside the closed curve. Also, it is necessary to change $\dot{x}$ to adjust the value of Jacobi Constant. This indicates that a maneuver, i.e., $\delta\bar{V}$ is required. Again, the boundary condition for $\dot{y}$ along the transit orbit is defined by the blue curve in Figure 3.8. The $\dot{y}$ value has to be inside the blue curve when adjusted to satisfy the Jacobi Constant constraint. If the desired value cannot be achieved by changing $\dot{y}$, $\dot{x}$ is changed.

Even if no value of Jacobi Constant along the red curve is the same as the value of Jacobi Constant on the Sun-Earth tube, it it possible to construct a transit orbit inside the Sun-Earth tube by applying a maneuver. The $\dot{y}$ vs y phase plot is again used. An example of manifold-to-transit transfers appears in Figure 3.9. A transit orbit inside the Sun-Earth tube appears in black.

Transit-to-Manifold Transfers

One of the options for the transfers from the Earth-Moon system to the Sun-Earth system is a transit-to-manifold transfer. A transit orbit inside the Earth-Moon tube can be transferred to an intersecting Sun-Earth manifold. To compute such a transfer, the Sun-Earth manifold is selected first. Any Sun-Earth manifold can be selected such that – once propagated to the Earth-Moon system – it arrives inside the Earth-Moon tube. Then, the state of the Sun-Earth manifold at an intersection point is transformed into the Earth-Moon rotating frame to compute a transit orbit.
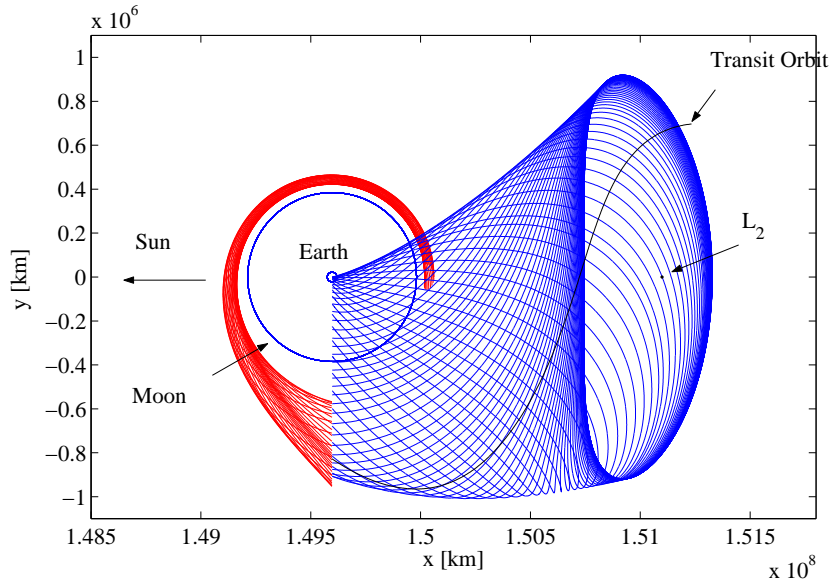
Figure 3.9. Manifold-to-Transit Transfer

To transform the state, the orientation of the Earth-Moon rotating frame relative to the Sun-Earth rotating frame is required. The orientation of the Earth-Moon rotating frame is dependent on the time at which the transit orbit arrives at the intersection. Determining the arrival time defines the orientation. Determination of the time can be accomplished in an iterative process. The appropriate time is then used to transform the point inside the Earth-Moon tube in the Earth-Moon rotating frame. A good initial guess for the appropriate time can be obtained from the time of intersection of nearby EM manifolds. Thus, after defining a PS plane in the Sun-Earth rotating frame, the time at which each Earth-Moon manifold intersects the PS plane is measured in the Earth-Moon rotating frame. Then, the intersecting time corresponding to each EM manifold appears in Figure 3.10. Note that characteristic quantities in the Earth-Moon system are used to dimensionalize the time. The value along the x-axis represents the tag numbers corresponding to the Earth-Moon manifolds. (Recall Figure 2.11) The first manifold is propagated from the point where the Lyapunov orbit crosses the x-axis perpendicularly on the far side of the Moon. Then, the point moves clockwise as the number increases. In the Earth-Moon rotating frame,

the transit orbit and Earth-Moon manifolds are under a similar gravitational influence, that is, the gravity of the Moon. Of course, the condition must be maintained in the Sun-Earth rotating frame. Also, the orientation of the Earth-Moon system determines the orientation of the Moon in the Sun-Earth rotating frame. Thus, the intersecting time of the transit orbit should be close to the intersecting time of the Earth-Moon manifolds. Therefore, the first guess can be selected from this range. However, an iterative process is still required to determine the precise time within this range.

After the transformation of the state into the Earth-Moon rotating frame, the next step is the computation of the conditions that define the transit orbit. However, the intersection in the Earth-Moon rotating frame is not a smooth vertical line, rather, it appears as is in Figure 3.11. In the figure, the blue circle indicates the Earth, and the magenta circle identifies the Moon. Each manifold leaves the Lyapunov orbit and terminates at a different point. In this case, the $\dot{y}$ vs y phase plot is not sufficient to determine the boundary conditions for a transit orbit. It is useful to re-define a Poincaré Section in the Earth-Moon rotating frame. The new Poincaré Section is determined by defining a new PS plane in the Earth-Moon rotating frame. The new PS plane such that it includes the desired transformed point, as it appears in Figure 3.12. Now the intersection is a smooth straight line. Also, a new reference frame is useful to determine the conditions for a transit orbit. As seen in the figure, the x_{ps}-axis is defined along the PS plane. Then, the y_{ps}-axis is perpendicular to the x_{ps}-axis so that it is parallel to the y-axis when the x_{ps} is parallel to the x-axis. Then, the velocity conditions for a transit orbit can be determined from the $\dot{x_{ps}}$ vs x_{ps} phase plot. Of course, $\dot{y_{ps}}$ can be modified, if necessary. An example of transit-to-manifold transfers appears in Figure 3.13.
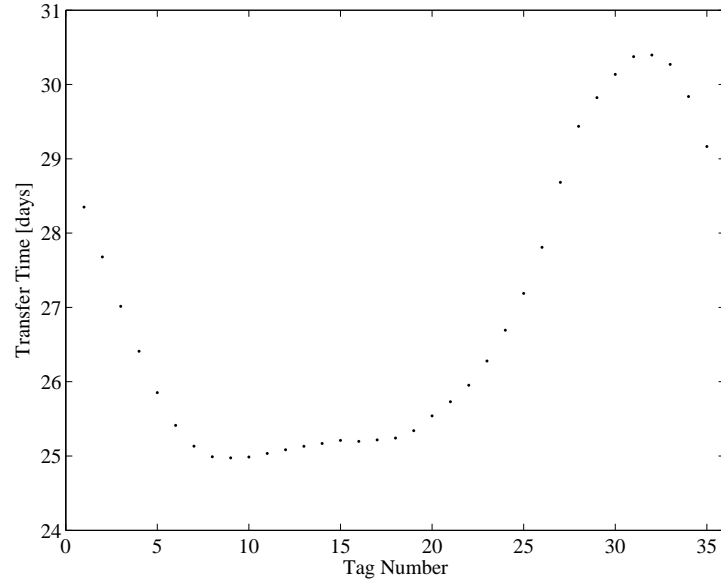
Figure 3.10. Nondimensional Time at a Poincaré Section for Each Manifold
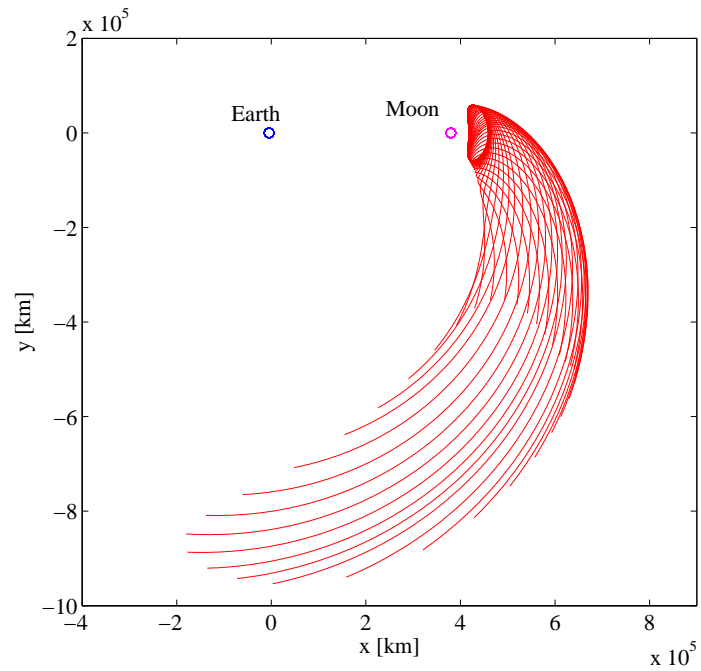
Figure 3.11. Unstable Earth-Moon Tube in Earth-Moon Frame; $Ay = 58,800$ km

Transit-to-Transit Transfers

A transit-to-transit transfer orbit can be computed applying a combination of the techniques from the previous two transfer types. First, a point is selected inside two
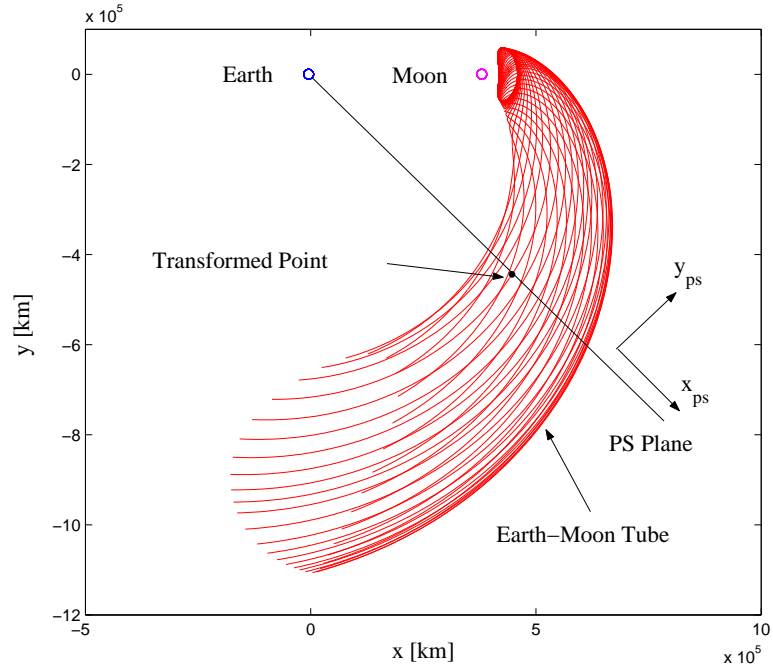
Figure 3.12. New PS Plane in Earth-Moon Rotating Frame
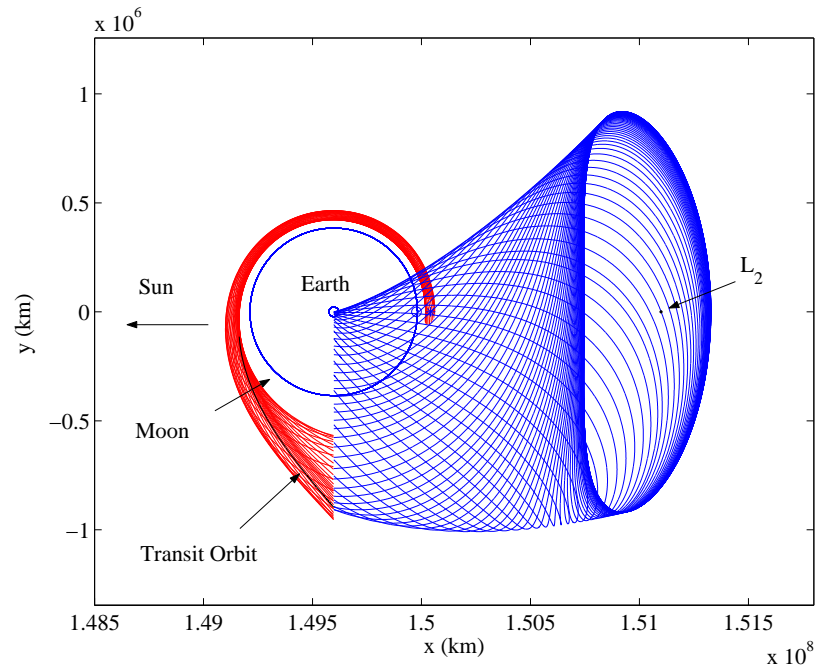
Figure 3.13. Transit-to-Manifold Transfer

intersecting tubes in Figure 3.7. To compute a transit orbit inside the Sun-Earth tube, the boundary condition corresponding to $\dot{y}$ is obtained from the $\dot{y}$ vs y phase plot on the Poincaré Section in a figure similar to Figure 3.8. The value of Jacobi Constant associated with the Sun-Earth tube is achieved by modifying both $\dot{y}$ and $\dot{x}$. Once the state of the Sun-Earth transit orbit is determined in the Sun-Earth rotating frame, it is transformed to the Earth-Moon rotating frame to obtain an Earth-Moon transit orbit. Of course, it is necessary to determine the transfer time. Then, again, a Poincaré Section is defined in the Earth-Moon rotating frame to obtain the velocity conditions for the transit orbit. The $\dot{x}_{ps}$ vs x_{ps} phase plot and the value of Jacobi Constant of the Earth-Moon tube are used to determine $\dot{x}_{ps}$ and $\dot{y}_{ps}$. An example of transit-to-transit transfers appears in Figure 3.14.
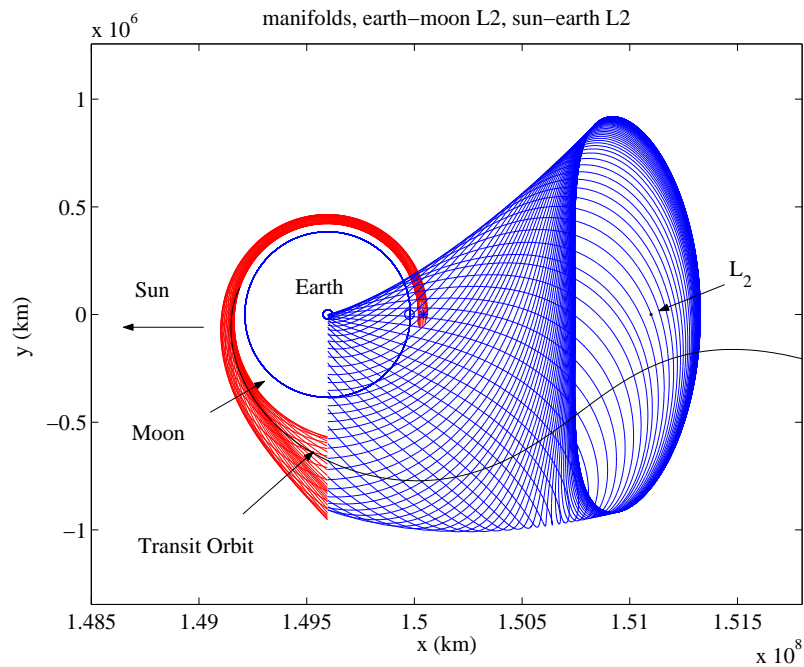
Figure 3.14. Transit-to-Transit Transfer

3.3.4 Example

Koon et al. [16] suggest that a transfer from the EM system to the SE system can be achieved with 34 m/sec. To verify the technique determined previously, a similar transfer is sought. However, the details of the transfer are not provided in the reference by Koon et al. The sizes of the EM and SE Lyapunov orbits are unknown. Only the location of the ΔV is available from the reference. This information determines the location of a Poincaré Section, however. The location of the Poincaré Section appears in Figure 3.15. The EM unstable manifold tube is in red. The endpoints of the trajectories in Figure 3.15 in the EM rotating frame correspond to the trajectories that terminate at the vertical Poincaré Section in the SE rotating frame. In this case, an arbitrary vertical PS plane is defined as seen in the figure. The circular lunar orbit appears in blue.

In this example, no cost-free transfer is possible because good intersection cannot be obtained under the Jacobi Constant condition. Instead of searching for a SE Lyapunov orbit with the desired value of Jacobi Constant, a more arbitrary SE Lyapunov orbit is selected first. The desired transfer can be modelled as a manifold-to-transit transfer in this case. So, secondly, it is necessary to compute a transit orbit inside the Sun-Earth tube. Since a low cost transfer is sought, it is necessary to compare the value of Jacobi Constant associated with each EM manifold in the Sun-Earth rotating frame with the desired Jacobi Constant value. Then, the small difference between the values indicates a relatively low cost maneuver. Thus, possible manifolds for the transfer are selected. The change in the value of the Jacobi Constant appears in Figure 3.16. The values along the x-axis represent the tag numbers corresponding to EM manifolds. Recall that the first manifold is computed at the point where the EM Lyapunov orbit crosses its x-axis vertically on the far side of the Moon. Then, the point moves clockwise as the manifold number increases. This figure identifies the location of a potential transit orbit. For example, a SE Lyapunov orbit with the Jacobi constant value of 3.000825429642264 is selected. The Ay amplitude is 650,000

km. This desired value is indicated by a black line in Figure 3.16. In this case, the 5th, 6th, 33rd, and 34th manifolds are desirable for the transit orbit because their values are close to the desired value. The $\dot{y}$ vs y phase plot at the Poincaré Section appears in Figure 3.17. The red dots are points from the Earth-Moon manifolds. The points from the desired manifolds are identified by black. The blue curve represents the points on the Sun-Earth tube. In the figure, all desired points are outside the blue curve. Also, it is obvious that a big change in $\dot{y}$ is required to move each point into the blue curve. Thus, a low cost transfer is not possible in this case.

There are several possible options when there is no good intersection. One possibility is a change in the size of the EM and SE Lyapunov orbits. The second option is to change the orientation of the EM manifold tube. Another alternative is to change the location of the Poincaré Section. These three options are attempted visually. Sometimes it may require the combination. One of the results appears in Figure 3.18. The Ay amplitudes of the EM and SE Lyapunov orbits are $88,000$ km and $650,000$ km, respectively. The EM manifolds are in red, and SE manifolds are in blue. An EM manifold that possesses a value of Jacobi Constant that is close to the one corresponding to the the SE Lyapunov orbit is selected as the location for application of a ΔV at the Poincaré Section. This result requires 31.8 m/sec of ΔV and is very close to the expected value. The transit orbit appears in black.
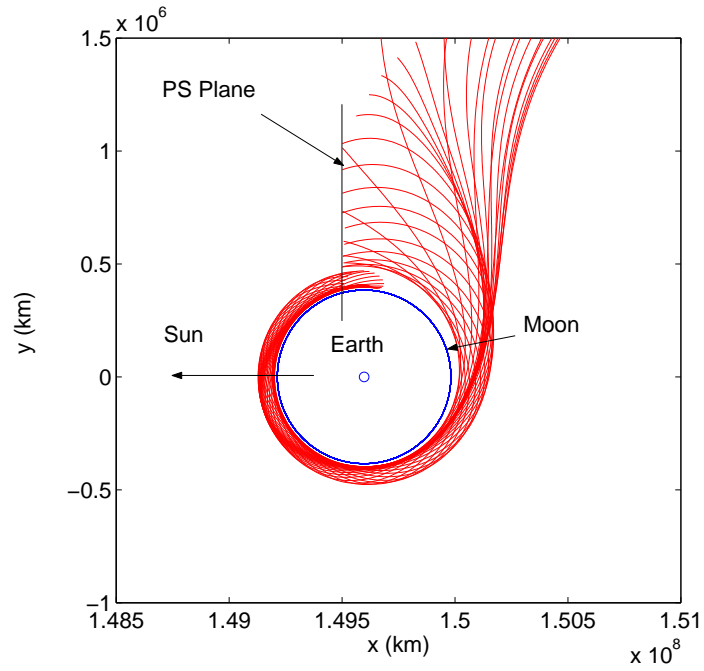
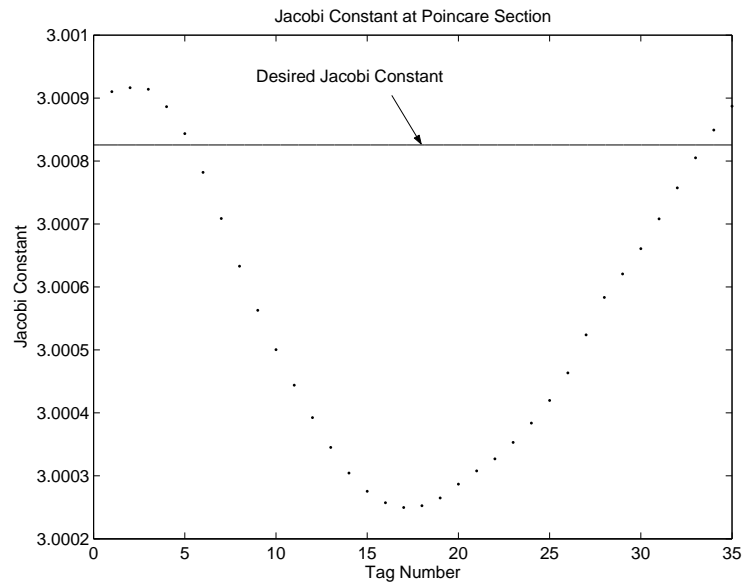Figure 3.15. Earth-Moon Manifold Tube Terminated at the Poincaré Section in Sun-Earth Frame

Figure 3.16. Jacobi Constant of Earth-Moon Tube Computed in Sun-Earth Frame
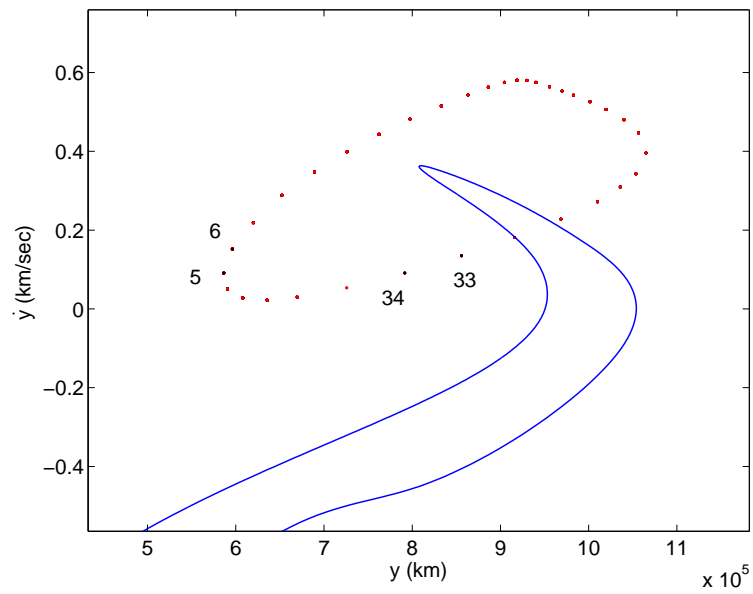
Figure 3.17. $\dot{y}$ vs y at Poincaré Section
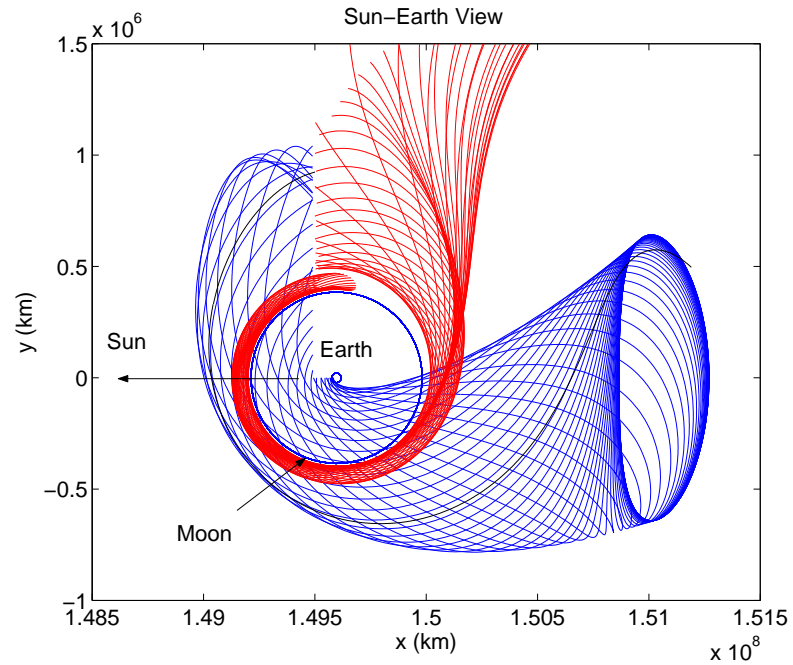
Figure 3.18. Transit Orbit From Earth-Moon Tube to Sun-Earth Tube

4. Three-Dimensional System-to-System Transfers

A collection of manifolds associated with a halo orbit creates a closed surface in three-dimensional space [14]. In this case, the closed surface forms a tube. It is also possible to compute transit orbits inside the three-dimensional tubes. However, the technique varies slightly from that described in the previous chapter. The difference is due to the complexity of the system by the out-of-plane motion of the Moon.

An addition of one dimension to the two-dimensional case causes additional complexity in the transfer problem. Thus, it is necessary to modify the procedures applied in the two-dimensional case to adjust to more complicated transfers. All the techiques established previously involve visual inspection. In the three-dimensional case, the visual inspection is more complicated because one projection is not sufficient to obtain the necessary information. Moreover, a visual decision process is not available when the design process is automated.

4.1 Model of Three-Dimensional System-to-System Transfers

In the two-dimensional model, the Earth-Moon system and the Sun-Earth system are assumed to be in the same plane. Thus, the orientation of the Earth-Moon system can be defined simply by one angle. However, this model is far from the reality. The Moon orbit is not actually in the same plane as the Earth orbit. Thus, the results from the two-dimensional model cannot be applied to the ephemeris model that includes actual information concerning the planetary ephemerides. However, a more accurate model is available in the three-dimensional model by including the inclination of the Moon. Some definitions associated with the three-dimensional model appear in Figure 4.1. The Earth-Moon and Sun-Earth rotating frames are defined by $[\hat{a}_1, \hat{a}_2, \hat{a}_3]^T$ and $[\hat{b}_1, \hat{b}_2, \hat{b}_3]^T$, respectively. The orientation of the Earth-Moon system is represented by

the angle sequence, Body-two 3-1-3. The first angle α defines the lunar line of nodes with respect to $\hat{b}_1$. The second angle is i, the inclination angle, and is fixed to be 5 degrees in this model. The third angle, β, positions the Moon in its orbit with respect to the line of nodes.
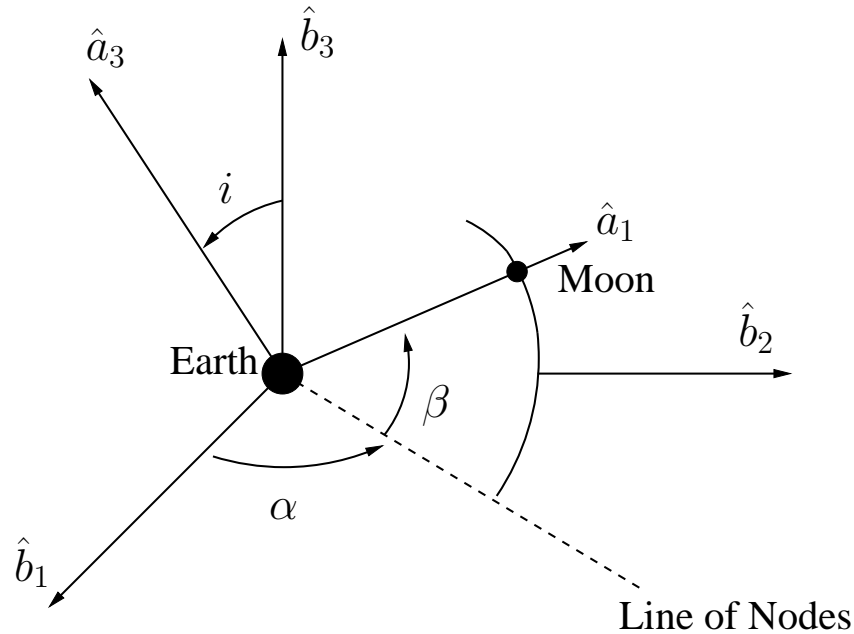
Figure 4.1. Angle Definitions in the Three-Dimensional Model

4.2 Correction of Jacobi Constant

Computing transit orbits requires correction of the value of Jacobi Constant. In the two-dimensional case, two variables, $\dot{x}$ and $\dot{y}$, are available to correct the Jacobi Constant. However, another variable, $\dot{z}$, is added in the three-dimensional case. Once a hyperplane is defined, a Poincaré Section can be computed. However, it is four-dimensional. For application to this problem, this Poincaré Section can be projected to subspaces that yields two-dimensional plots. Then, plots of the velocity component as a function of position components in each direction can be examined to identify the velocity constraints of interest for a transit orbit. Changing only one variable can occasionally achieve the desired value of Jacobi Constant in the two-dimensional

case. However, it is often necessary to change more than one variable in the three-dimensional case.

4.3 Four-Section Method

In the three-dimensional case, a task as simple as identifying an intersection between manifold tubes is nontrivial. Determining a Poincaré Section simplifies the task by reducing the system by one dimension. Then, a new frame can be defined relative to the Sun-Earth rotating frame at the location of the Poincaré Section such that the Z_{ref}-axis is parallel to the $\hat{b}_3$-axis and the X_{ref}-axis is along the Poincaré Section. In this way, the position components in the direction of the Y_{ref}-axis are zero. The plane defined by the X_{ref}-axis and the Z_{ref}-axis is still denoted as the PS plane. Even though it is easy to identify an intersection visually, visual inspection is not available in an automated process. Thus, the logic to identify an intersection is necessary for automation.

Consider the transfer from the Sun-Earth to the Earth-Moon system. Each Sun-Earth manifold is examined if it is inside the Earth-Moon tube. This condition is required to compute a transit orbit inside the Earth-Moon tube. The logic to examine this condition is fairly simple. The conceptual illustration appears in Figure 4.2. Blue dots and one red dot represent the Earth-Moon manifolds and a selected Sun-Earth manifold, respectively. Only position components are considered in this case. First, the Z_{ref} component of the Sun-Earth manifold is compared with the Z_{ref} components of the all Earth-Moon manifolds. This separates the Earth-Moon manifolds into two groups. One is the upper group with a higher Z_{ref} component. Another one is the lower group with a relatively lower Z_{ref} component. Then, the X_{ref} component of the Sun-Earth manifold is compared with X_{ref} components of the Earth-Moon manifolds in each group. Thus, the upper group is separated into subgroups 1 and 2. Also, the lower group is separated into subgroups 3 and 4. If the Sun-Earth manifold is

surrounded by Earth-Moon manifolds, these four groups must exist. If one or more groups are missing, the Sun-Earth manifold is outside of the Earth-Moon tube.
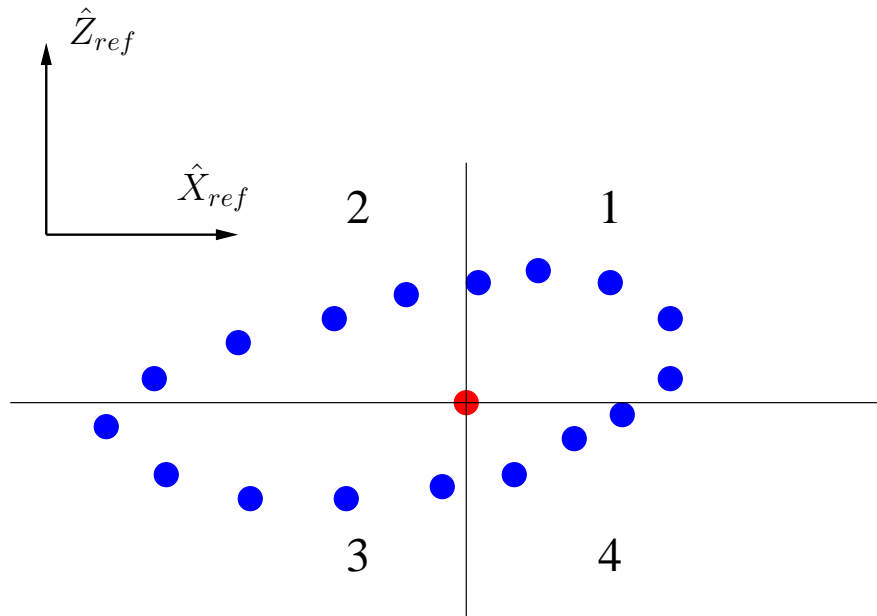
Figure 4.2. Schematics of the Four-Section Method

4.4   Design Technique for Low Cost System-to-System Transfers

The goal of this study is to establish a technique to efficiently design system-to-system transfers. The design of a low cost transfer in a four-body problem is extremely challenging. The three-dimensional model in Figure 4.1 simplifies the design process since characteristics of certain trajectory arcs in the CR3BP, such as halo orbits and invariant manifolds, can be exploited.

4.4.1   Sun-Earth and Earth-Moon Manifolds

It is possible to depart a Sun-Earth halo orbit from any point along the orbit using unstable manifolds for, essentially, no departure cost. However, globalization of the unstable manifolds reveals the unstable manifold tube and the limited regions

of space that can be accessed. The tube may deliver a vehicle to a wide variety of locations depending on the particular halo orbit with which the tube is associated and the specific trajectory that is exploited. Only certain manifolds might deliver a spacecraft to the desired location, and/or no manifolds may be available that reach the desired location in a reasonable time. The basis for a system-to-system transfer is a requirement that the Sun-Earth manifolds intersect the Earth-Moon manifolds. An example of a Sun-Earth unstable manifold tube appears in Figure 4.3. These manifolds are associated with a halo orbit defined by an in-plane excursion amplitude of $Ay = 699,000$ km and an out-of-plane amplitude $Az = 200,000$ km. It is obvious that some of the manifolds pass very close to the Earth. These manifolds do not generally yield productive intersections with the Earth-Moon manifolds, thus, it is not necessary to compute them for potential system-to-system transfers. To tag manifolds along the tube that may be useful, the halo orbit is decomposed into four regions, A, B, C, and D, as seen in Figure 4.4. In computation of manifolds by the integration of specific sets of initial conditions, manifolds departing from regions C and D are accessible to Earth-Moon manifolds. Thus, the search is focused on this part of a Sun-Earth tube.

Stable and unstable manifolds also exist in the Earth-Moon system since periodic orbits can be computed near all collinear libration points. For instance, once a stable manifold tube for a specified halo orbit is propagated backwards in the Earth-Moon coordinate frame, the position and velocity states along the tube can be transformed to another frame for visualization. In Figure 4.5, the relevant part of the Sun-Earth manifold is plotted in red. It is computed from regions C and D along the halo orbit. Also in the figure, the Earth-Moon stable manifold tube (blue) has been transformed to the Sun-Earth coordinate frame and plotted. The $\hat{a}_1$- and $\hat{a}_2$-axis appear in the figure to indicate the initial position of the Moon. The transformation in the figure assumes arbitrary values for the orientation of the Earth-Moon coordinate frame, that is, $\alpha = 60$ degrees and $\beta = -30$ degrees.
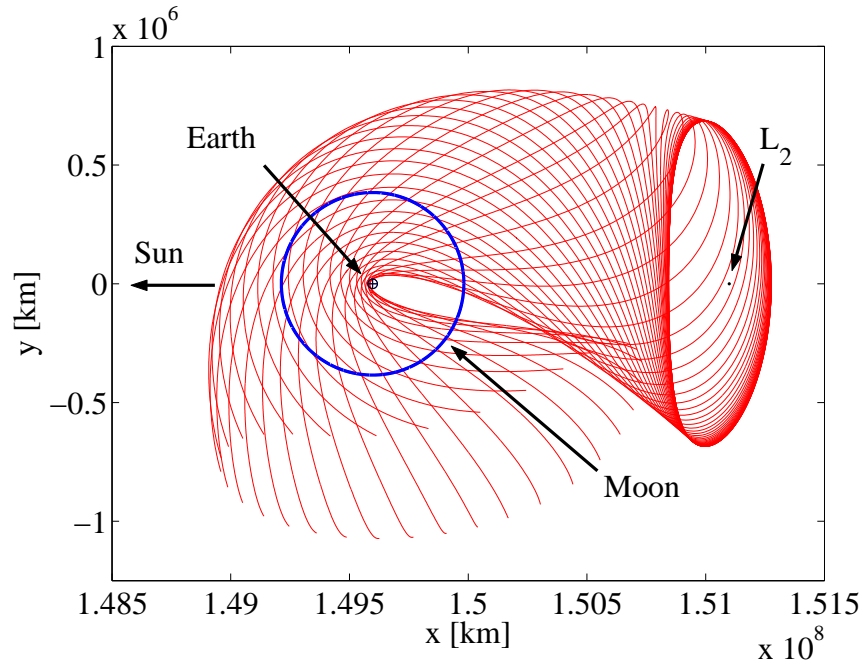
Figure 4.3. Sun-Earth unstable manifolds near L_2; $Ay = 699,000$ km, $Az = 200,000$ km
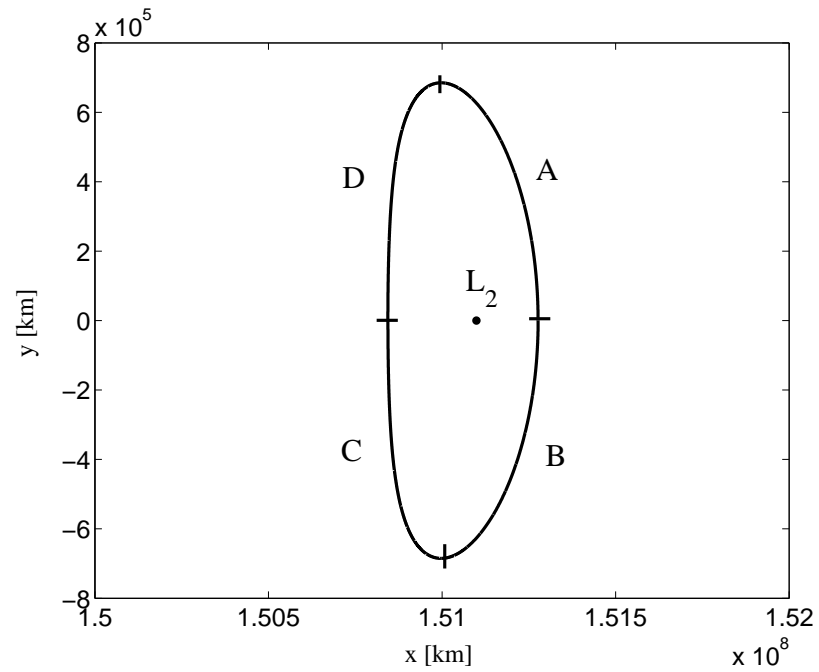
Figure 4.4. Sun-Earth Halo Orbit Near L_2; $Ay = 699,000$ km, $Az = 200,000$ km
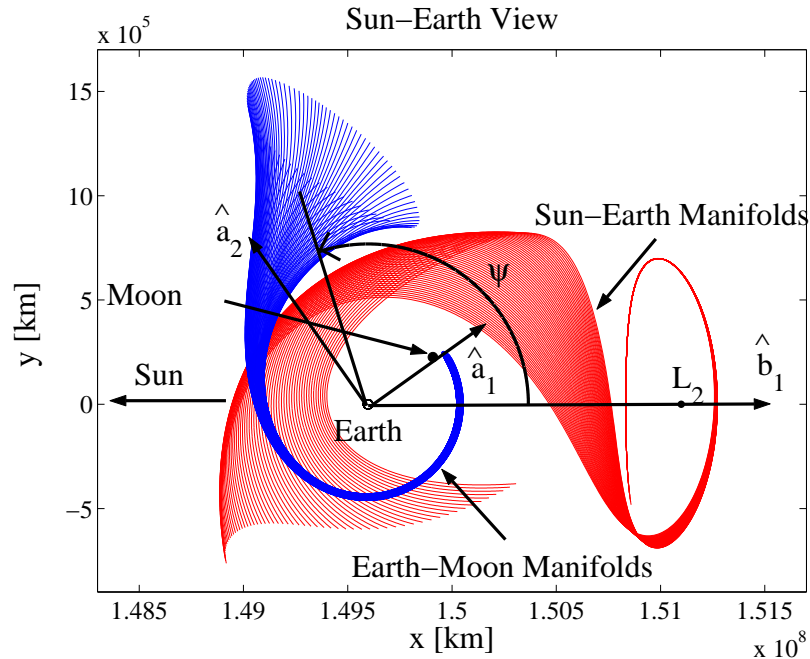
Figure 4.5. Earth-Moon and Sun-Earth Manifolds Corresponding to the Initial Conditions: $\text{EM}Ay = 41{,}100$ km, $\text{EM}Az = 30{,}000$ km, $\text{SE}Ay = 699{,}000$ km, $\text{SE}Az = 200{,}000$ km

4.4.2 Poincaré Sections

In this simplified model, the key concept in the design of system-to-system transfers is that the manifold tubes in the phase space provide the "pathways" from one system to another and, thus, this basic structure controls the trajectory. The intersection of the tubes allows motion from one system to the next. In the 3-D spatial CR3BP, the phase space is 6-D; the Jacobi Constant reduces it by one. Then, for some transversal slice, the Poincaré Section is an object in 4-D. The intersection of two such objects is not obvious. As discussed by Gómez et al. [17], however, projections of the objects onto lower dimensional planes can yield significant insight. Such projections originate with additional characteristics for the transfer that might be specified. For example, from the Sun-Earth halo orbit, integrate a tube associated with the unstable manifold forward in time until the trajectories cross the PS plane. This location

is identified by the angle ψ in Figure 4.6 that can be visualized in Figure 4.3. The angle is measured from the $\hat{b}_1$-axis and specifies a plane for intersection of the tubes. The angle is positive for rotation counter-clockwise about the $\hat{b}_3$-axis. Once the angle is specified, a stable manifold tube in the Earth-Moon system can be computed to also arrive at the same PS plane in negative time. It is noted again that, in the spatial problem, this plane is not actually a Poincaré Section, merely a projection given specified characteristics. It is denoted as a section for simplicity. Given that both manifold tubes are projected onto this plane and an intersection is determined, a transfer is defined by a search for essentially two possible types of state vectors. One type is a position state that is on both tubes (with a possible velocity discontinuity). A location on the tube (or, in reality, very near), ensures that the solution will pass from the Sun-Earth halo orbit to an Earth-Moon halo orbit. However, a transit orbit inside the tubes can also accomplish a shift from one system to the other. Transit orbits may or may not pass very close to the boundary. Since this study does not consider transitions from a stable to an unstable manifold corresponding to the same libration point orbit, non-transit orbits are not considered here.
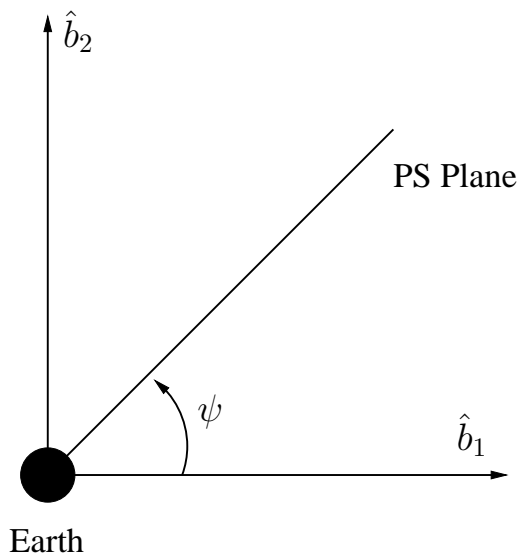

Figure 4.6. Definition of ψ

From the general concept, that is, defining a transfer via intersecting tubes, the lowest cost option is sought. But, the complexity of the system-to-system transfer problem between the Earth-Moon and the Sun-Earth systems increases further when the inclination of the lunar orbit is introduced. For efficient transfer design, the orientation of the Earth-Moon system, that is, the timing in the ephemeris model, is critical. The orientation of the Earth-Moon coordinate frame is determined by the three angles, α, i (fixed), and β. Of course, the location of the PS plane is another design parameter and unknown. Thus, the search for a low cost transfer is reduced to the three angles α, β, and ψ. It is necessary to search over the two angles α and β, as well as the PS plane orientation angle ψ.

4.4.3   Manifold Intersections

In the spatial problem, the intersection of two manifold tubes is nontrivial. In an automated process, it is especially difficult without the benefit of any visual inspection. To aid in this process, again, the PS plane and a new coordinate frame defined in the physical PS plane are exploited.

Even though Earth-Moon manifolds and Sun-Earth manifolds form a continuous surface, they are usually computed numerically from individual trajectories. An example of intersecting Earth-Moon and Sun-Earth manifolds appears in Figure 4.7, where discrete points are plotted in the PS plane. It is apparent that computation of the actual point of intersection, even in the physical plane of the figure, is nontrivial. Thus, an approximate method is required to determine the intersection in a short period of time. The intersection point is estimated in configuration space via splines. From the estimate, the full state vectors can be computed.

Although an intersection of the tubes in configuration space will yield a transfer, the velocity states are not generally equal and a maneuver is required. Most likely, the Earth-Moon and Sun-Earth manifolds actually intersect in, at least, two points in the PS plane. (See Figure 4.7.) It is simple to determine which of the two possesses
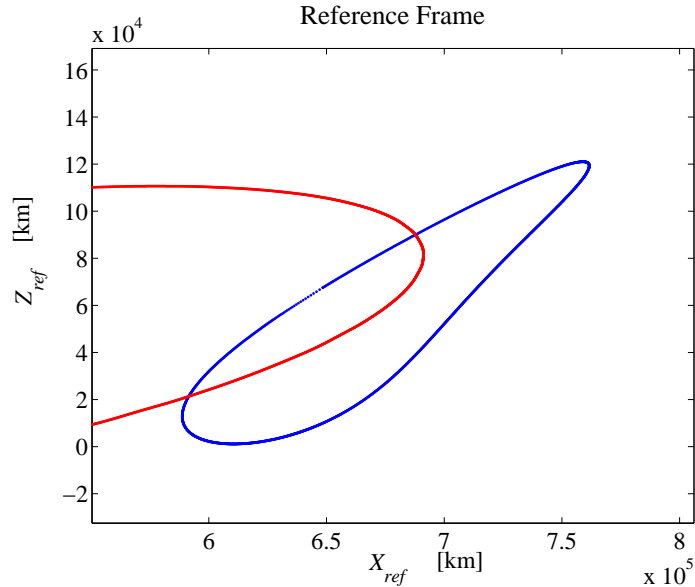
Figure 4.7. EM Manifolds (Blue) and SE Manifolds (Red) in the PS
Reference Frame

a smaller velocity discontinuity. The point of interest, however, is undoubtedly not at the best orientation. Thus, a modification of α and β will improve the result. To change the orientation, without affecting the intersecting point, it is necessary to change α and β at the same time. For example, when α is increased, β is decreased by the same angle. Strictly speaking, the intersecting point changes because the Earth-Moon manifolds are inclined. But, incorporating this assumption renders a preliminary estimate of the angles that results in a reasonably low maneuver cost.

4.4.4 Transit Orbits and Maneuvers

To complete a transfer between the Earth-Moon and Sun-Earth systems, one option is to shift between trajectories that lie on the manifold surfaces. Generally, the velocity states are not equal at the intersection point and the ΔV is computed as the norm of the vector defined by the differences in the velocity components. However, a transit orbit will also deliver a vehicle between the systems. To determine a transit orbit, velocity components must satisfy certain conditions [16]. Again, projections

onto the PS plane are useful in the form of phase plots of velocity components as functions of position components. Two phase plots for the Earth-Moon tube (blue) and Sun-Earth tube (red) appear in Figure 4.8. The X_{ref} components are plotted on the left, and on the right are curves representing the relationship for Z_{ref} components. For the selected Sun-Earth manifolds, note that the curves do intersect. The closed blue curves are boundary conditions for a transit orbit [16]. Thus, when a maneuver is applied, the new velocity components must be within the blue boundaries to approach the Moon. Another condition for a transit orbit is the Jacobi Constant. The value of the Jacobi Constant corresponding to a transit orbit must equal the value for trajectories on the Earth-Moon tube. However, because of the transformation, the value of the Jacobi Constant changes for points that lie on the blue Earth-Moon curve in Figure 4.8, i.e., in the PS coordinates and Sun-Earth rotating frame. Thus, it is most efficient to first transform the curves from Figure 4.8 into the Earth-Moon rotating frame. The value of the Jacobi Constant along the Earth-Moon manifolds is constant for representations in the Earth-Moon rotating frame. When points that intersect the PS plane of the Sun-Earth frame are transformed into the Earth-Moon rotating frame, they are no longer contained in a plane, however. In this case, two phase plots are no longer sufficient to determine the boundary conditions. It is useful to define a new local "Poincaré Section" and reference frame in the Earth-Moon rotating frame. The definition of the new reference frame in the Earth-Moon rotating frame appears in Figure 4.9. The x_{ref}-axis is directed from the barycenter of the system to the tube intersection point of interest from Figure 4.8. The z_{ref}-axis is parallel to the $\hat{a}_3$-axis, and the y_{ref}-axis is perpendicular to the x_{ref}-z_{ref} plane. Thus, this new projection of the Poincaré Section is defined by the x_{ref}-z_{ref} plane. The black solid line in Figure 4.9 represents the x-y projection of the new PS_{EM} plane. Phase plots of Earth-Moon manifolds on the PS_{EM} appear in Figure 4.10. These plots relate velocity as a function of position in both the x_{ref} and z_{ref} components. Now, the maneuver can be computed with these two phase plots and the value of the Jacobi Constant for the Earth-Moon tube.
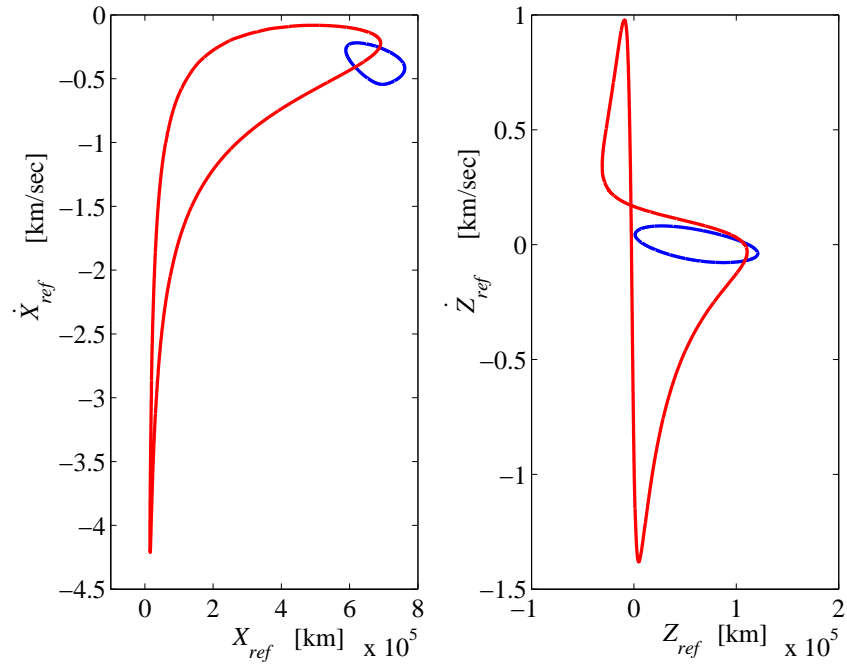
Figure 4.8. Velocity vs. Position at Poincaré Section; Earth-Moon manifolds (blue) and Sun-Earth manifolds (red)
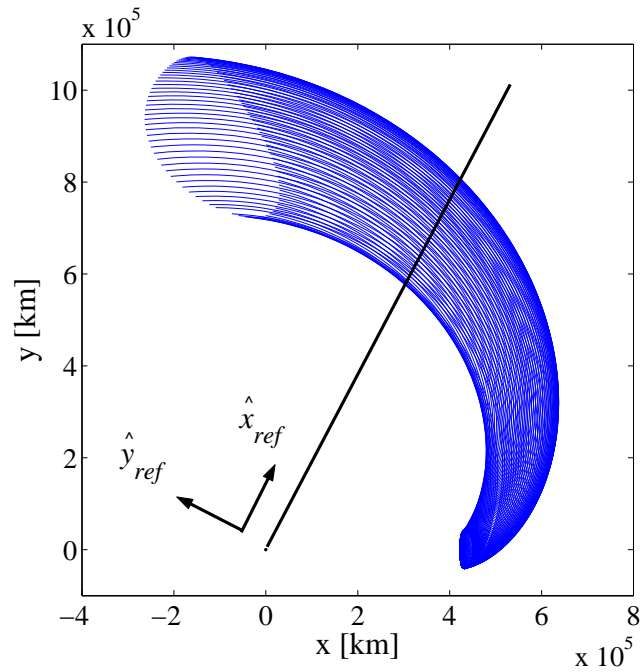

Figure 4.9. New Local PS$_{EM}$ Reference Frame in Earth-Moon Rotating Frame
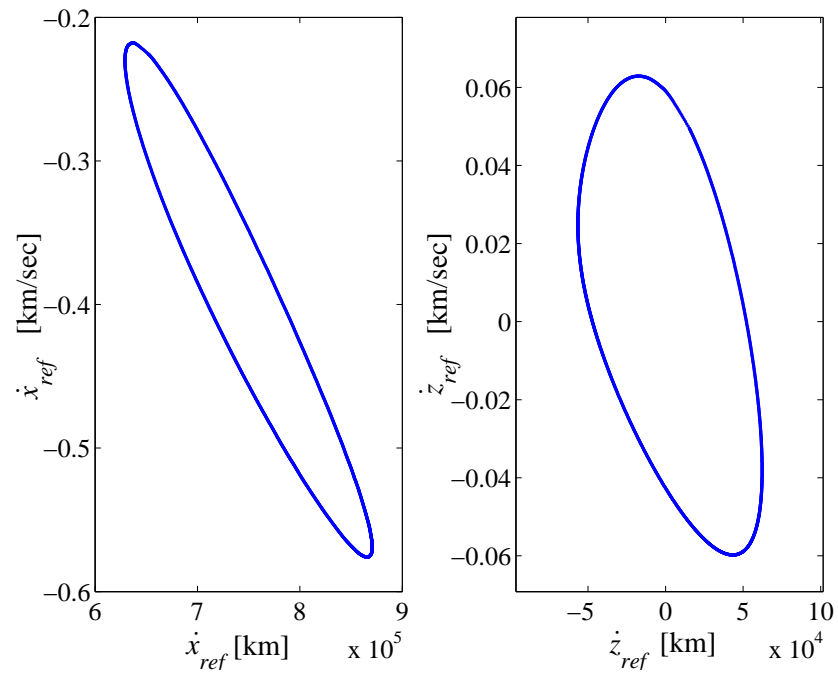
Figure 4.10. Velocity vs. Position in the PS$_{EM}$ Reference Frame in Earth-Moon Rotating Frame; Earth-Moon manifolds

4.4.5   Example: Halo-to-Halo Transfer

A transfer from a Sun-Earth halo orbit to an Earth-Moon halo orbit in the CR3BP is most simply achieved by connecting invariant manifolds. The velocity difference between the Earth-Moon and a Sun-Earth manifold at the intersection point becomes the ΔV for the transfer. For example, consider a Sun-Earth L_2 halo orbit with $Az = 200{,}000$ km and an Earth-Moon L_2 halo orbit with $Az = 30{,}000$ km. The computed ΔV from the previous methodology is 22.2 m/s when ψ is arbitrarily selected to be 95 degrees. To test the validity of this result, it is transitioned to the ephemeris model that uses the actual ephemerides for the locations of the of planets. The software package Generator, developed at Purdue University, is used to simulate the results in the ephemeris model. Generator uses JPLDE405 to simulate the ephemeris environment. The results appear in Figure 4.11. A complete halo-to-halo transfer in the ephemeris model appears in Figure 4.11. The figure is centered at the Earth and, in the Sun-Earth rotating frame, the Sun's direction is indicated. The ephemeris Moon location throughout the transfer appears in the figure in blue. A closeup of the transfer arriving in an Earth-Moon Lissajous orbit is plotted in Figure 4.12. This figure is centered at the Moon. The Earth is placed to the left of the Moon for a reference, but it shifts position in an ephemeris model. The ephemeris results appear in Table 4.1. In the ephemeris model, this transfer can be achieved with zero ΔV. The sizes of the Earth-Moon and Sun-Earth Lissajous orbits are slightly different from the sizes of original halo orbits, i.e., now Earth-Moon $Az = 30{,}300$ and Sun-Earth $Az = 195{,}000$ km. In Figure 4.11, the first x-axis crossing location in the SE rotating frame, after the departure from the SE Lissajous orbit, is indicated by $\times$. Also, in Figure 4.12, the x-axis crossing location in the EM rotating frame, before the arrival at the EM Lissajous orbit, is indicated by $\times$. The transfer time between these locations is defined to be the time of flight. This is because it is impossible to identify the exact location of the departure (arrival) along a Lissajous orbit. The time of flight for this transfer is approximately 50.6 days.
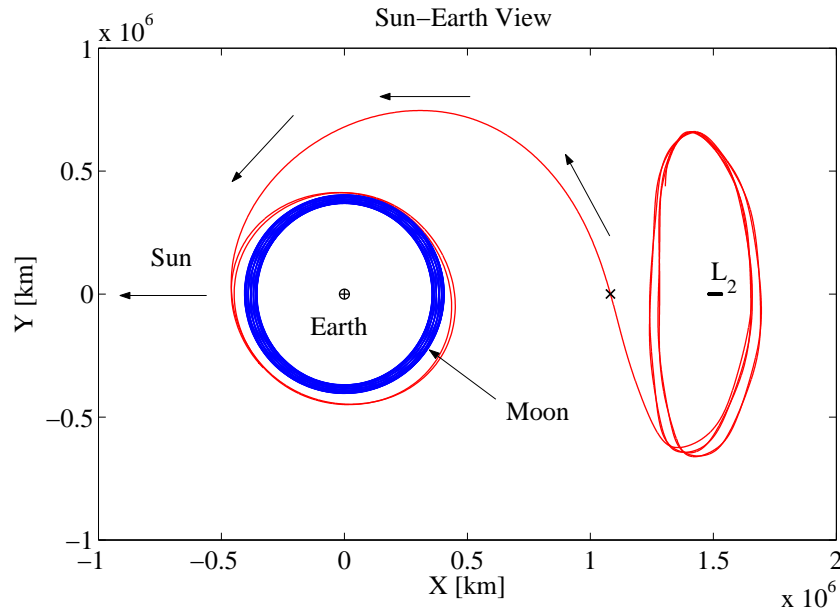
Figure 4.11. Halo-to-Halo Transfer in the Sun-Earth Rotating Frame; initial guess from CR3BP: EMAy = 41,100 km, EMAz = 30,000 km, SEAy = 699,000 km, SEAz = 200,000 km

Table 4.1 Transfer Results in the Ephemeris Model

Earth-Moon Az [km]	Sun-Earth Az [km]	ΔV [m/sec]	Time of Flight [days]
30,300	195,000	0	50.6
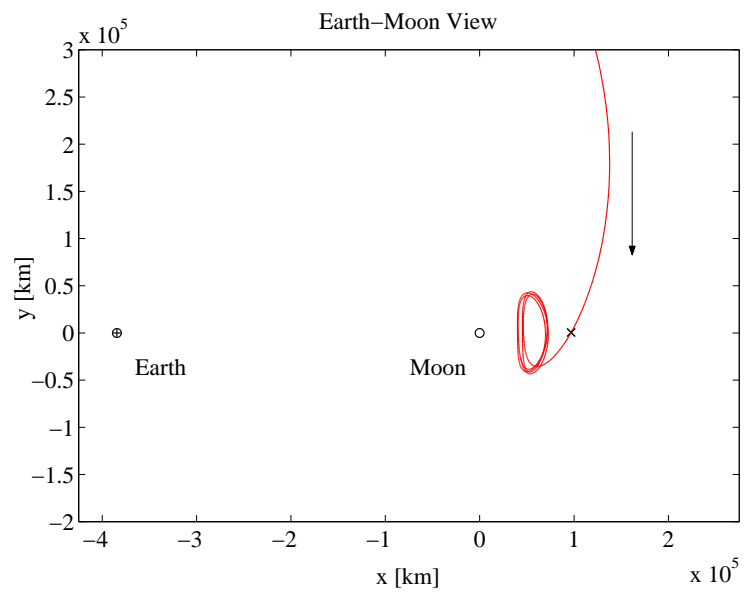
Figure 4.12. Earth-Moon Manifold Asymptotically Approaching an Earth-Moon Lissajous Orbit

5. Analysis

A large challenge in trajectory design in a multi-body regime is the sensitivity. Nevertheless, a large number of transfers can be determined using the previous design strategy. The results that emerge highlight some useful relationships, particularly the angle relationships that yield the results with the lowest cost. It was originally assumed that the key relationship to design transfers between the Earth-Moon and the Sun-Earth systems is the orientation of the Earth-Moon system in the Sun-Earth rotating frame. More information about the orientation of the Earth-Moon system reduces the computation time in the trajectory design process. Since the orientation is determined by α and β for a certain lunar phase angle ψ , any known relationship between these angles is useful.

5.1 Relationship Between θ and ψ

First, it is necessary to examine which combinations of angles are related in a simple or straightforward manner. Since the angles α and β are traded off in the design process, their sum is notable and this angle is defined to be θ, i.e., $\theta = \alpha + \beta$. An example of the relationship between θ and ψ appears in Figure 5.1. A particular Sun-Earth halo orbit with out-of-plane amplitude $Az = 200{,}000$ km is defined and transfers are computed to Earth-Moon halo orbits of various amplitudes. The range of the angle θ is selected from 80 degrees and 110 degrees. Usually, Earth-Moon and Sun-Earth manifolds intersect within this range. Fewer opportunities to obtain intersections exist beyond these values. The Earth-Moon orbits are sized from Az values of 16,000 km to 30,000 km. The plots are not smooth because the angle increment is fixed at one degree. To achieve smoother results, the increment could be reduced, for example, 0.1 degree. However, an increment of one degree is sufficient

to observe trends. The solid lines are linear fits of each data set. Thus, θ and ψ appear linearly related for different Earth-Moon halo orbits paired with a Sun-Earth periodic orbit of $Az = 200,000$ km. This result is also true if a search for transfers is expanded to include other Sun-Earth periodic orbits with Az amplitudes from 120,000 km to 200,000 km. Thus, it is possible to relate θ and ψ for each case by a linear equation i.e., $\theta = a\psi + b$. Moreover, these variables can be correlated in other ways. A linear relationship between the slope a and the Az amplitude of the Sun-Earth halo orbit appears in Figure 5.2; transfers to various Earth-Moon halo orbits are included. The relationship between b and various Sun-Earth halo orbits (represented through their Az amplitude) appears in Figure 5.3. Thus, these relationships allow an immediate estimate of θ for any lunar phase ψ and the correlation of these angles to the size of various Earth-Moon and Sun-Earth orbits. Although these relationships are very useful, the orientation of the Earth-Moon system is not immediately determined because θ is a combination of α and β. To determine a specific orientation, it is necessary to specify α or β. Once either angle is available, the other is obtained from θ.

5.2   Relationship Between α and β

Given the value of θ, if the relationship between α and β is identified, the angles can be determined. The relationship between α and β actually appears to be somewhat nonlinear. The relationship for transfers from a Sun-Earth halo orbit of $Az = 120,000$ km appears in Figure 5.4. The solid lines are quadratic fits of the data set. As the Az amplitude of the periodic Sun-Earth orbit is increased, the relationship becomes more complicated. Various transfers from a Sun-Earth halo orbit of $Az = 200,000$ km to a number of Earth-Moon orbits are plotted as points in Figure 5.5. The data points are not in any obvious relationship. However, the points are crowded into certain regions. Thus, the general trends are identified from crude linear rela-
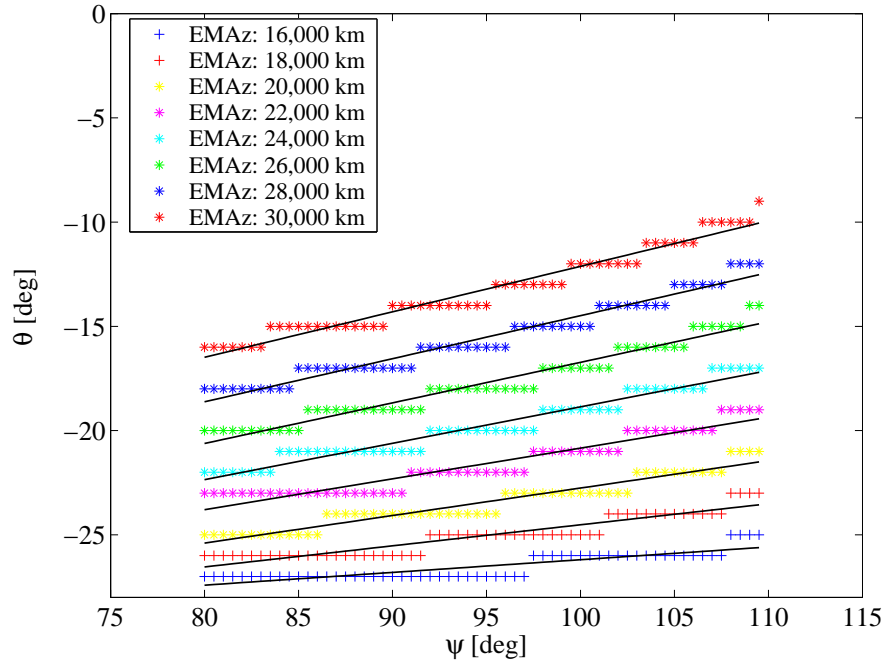
Figure 5.1. Relationship Between θ and ψ; SE$Az = 200{,}000$ km
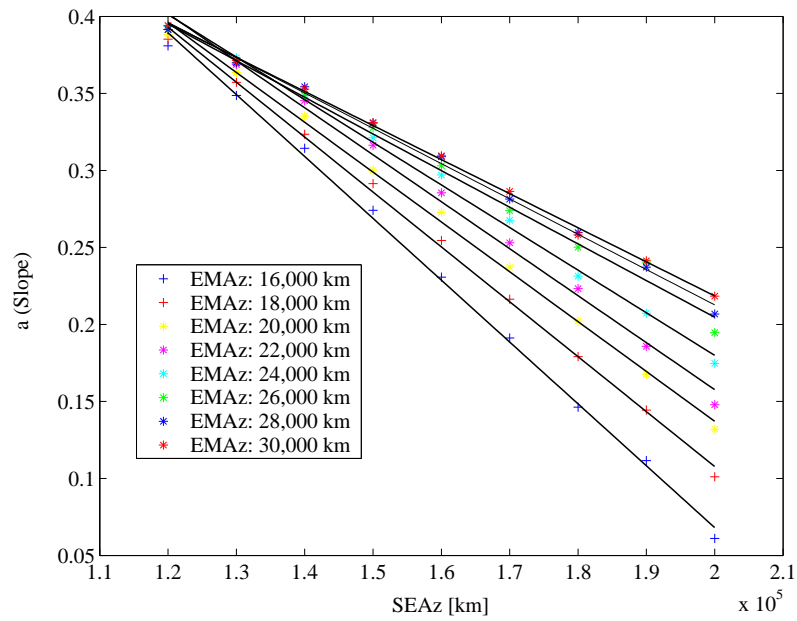
Figure 5.2. Relationship Between a and SEAz for Each EMAz
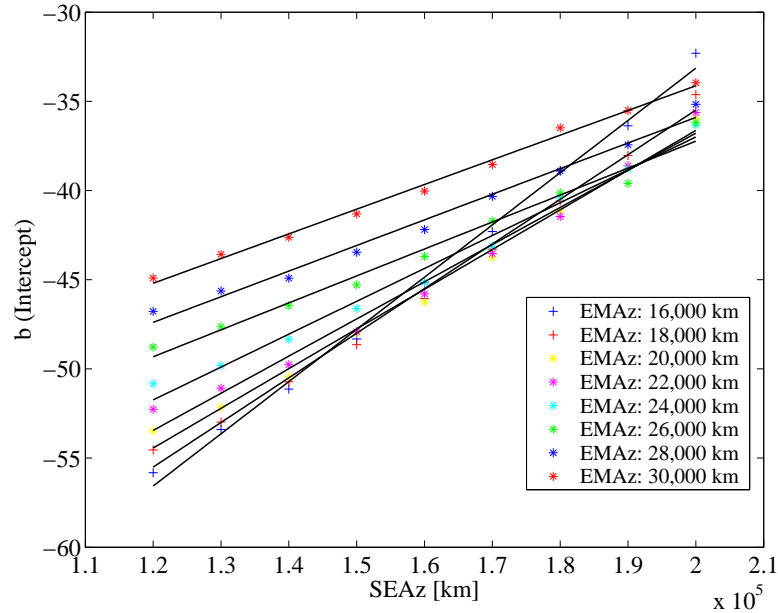
Figure 5.3. Relationship Between b and SEAz for Each EMAz

tionships. As seen in the figure, the solid lines do not pass through all the data points. But, the combinations that appear in the figure offer initial estimates.

5.3 Transfers: α-β Combinations

Even though the relationship between α and β is not known perfectly, it is now possible to estimate the values of α and β that will yield a successful system-to-system transfer for each combination of Earth-Moon and Sun-Earth halo orbits. Results using the α-β estimated relationship are compared with actual data in Table 5.1. For this case, the Earth-Moon orbit is defined such that $Az = 30{,}000$ km and the corresponding Sun-Earth halo possesses $Az = 200{,}000$ km. Also, note that ψ is selected to be 95 degrees. From such an initial transfer, the cost is investigated to determine: (a) whether the transfer can be transitioned to the ephemeris model; and, (b) whether a lower cost transfer can be computed from the estimate, if necessary. If the results are satisfactory, the estimate is useful. Some results are compared in Table 5.2. In the CR3BP, a transfer is constructed using the α-β estimated relationship to determine
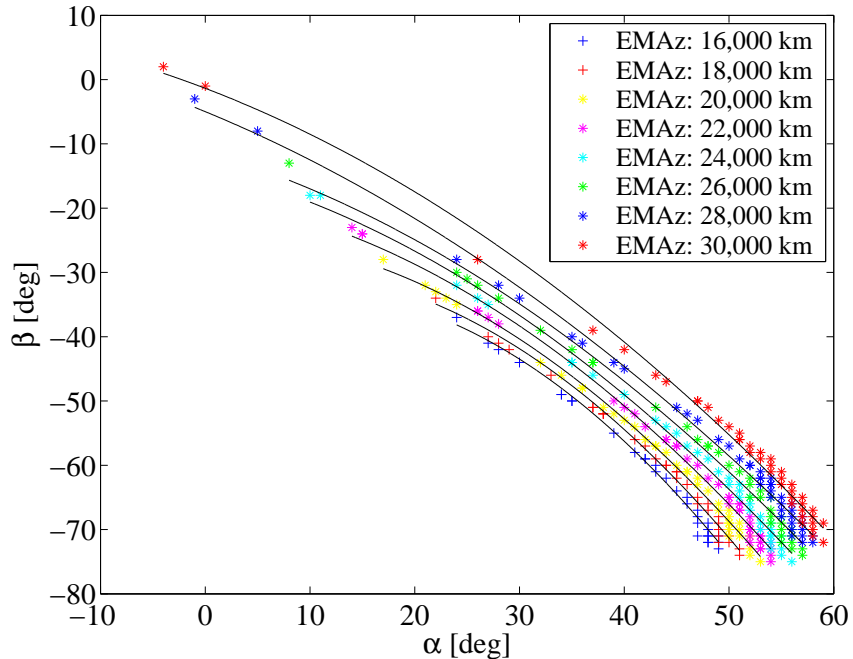
Figure 5.4. Relationship Between α and β for SE$Az = 120,000$ km; various EMAz orbits

the orientation of the Moon at initiation of the transfer. The resulting ΔV for a manifold-to-manifold transfer is 20.7 m/sec. This value is actually smaller than a nearby transfer computed as part of the initial sweep of solutions, a maneuver equal to 22.2 m/sec. More importantly, the final results in the ephemeris model are nearby solutions, and in both cases, the ΔV is reduced to zero. Thus, a slight difference in the α-β angles did not significantly affect the final result and the estimate is satisfactory. Other examples appear in Table 5.3. All cases share the same phase angle, $\psi = 95$ degrees, and the Earth-Moon halo orbit with $Az = 30,000$ km. The largest difference between the original data and the estimated angles is noted for the Sun-Earth orbit of $Az = 170,000$ km. The difference is 5 degrees for each angle. However, once the Az $= 170,000$ km case from Table 5.3 is transitioned to the ephemeris model, a zero cost solution still emerges from both CR3BP transfers. The comparison of the results in the ephemeris model appears in Table 5.4. Thus, even though the ΔV computed from the angle relationship is slightly larger in the CR3BP, the out-of-plane Az amplitude
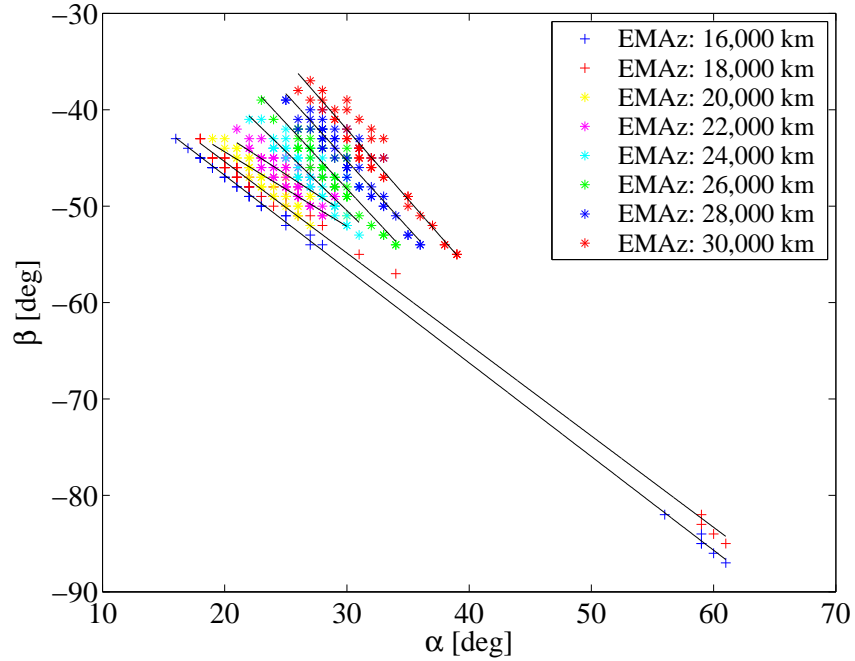
Figure 5.5. Relationship Between α and β for SEAz = 200,000 km; various EMAz orbits

in the final Lissajous orbits in the ephemeris model are still close to those specified in the CR3BP. Also, the difference in the time of flight is less than a day. Such results are useful in the design process. That is, nearby solutions are available for different α-β combinations.

Table 5.1 Angles α and β Computed from Actual Data and the Estimated Relationship; EMAz = 30,000 km, SEAz = 200,000 km, ψ = 95 degrees

	α [deg]	β [deg]
Actual Data	31	-45
Estimate	33	-46

Table 5.2 Comparison of Results from the Original Data and the Estimated Relationship; EMAz = 30,000 km, SEAz = 200,000 km

	Data	Estimate
CR3BP		
ΔV [m/sec]	22.2	20.7
Ephemeris		
EMAz [km]	30,300	30,900
SEAz [km]	195,000	197,000
ΔV [m/sec]	0	0

Table 5.3 Comparison of α and β from the Original Data and Estimated Relationship; EMAz = 30,000 km

	Data		Estimate	
Sun-Earth Az [km]	α [deg]	β [deg]	α [deg]	β [deg]
190,000	35	-48	35	-48
180,000	38	-50	37	-49
170,000	43	-55	38	-50
160,000	47	-58	44	-54
150,000	49	-59	47	-57
140,000	51	-60	50	-59

5.4 Transfers: Sun-Earth/Earth-Moon Halo Orbit Combination

The methodology allows for the computation of relatively low cost system-to-system transfers in a short time. Thus, it is possible to collect a large amount of data for a variety of cases. A comparison of interest is the combinations of Earth-Moon and Sun-Earth halo orbits that yield the lowest cost transfers. The halo orbits are always represented by their out-of-plane amplitude, Az. The range of the Az amplitude for the Earth-Moon halo orbits covers 16,000 km to 30,000 km. The Sun-Earth periodic

Table 5.4 Comparison of Results from Estimated Relationship and Original Data; EMAz = 30,000 km, SEAz = 170,000 km

	Data	Estimate
CR3BP		
ΔV [m/sec]	14.0	23.1
Ephemeris		
EMAz [km]	25.900	26,400
SEAz [km]	167,000	169,000
ΔV [m/sec]	0	0
Time of Flight [days]	52.7	53.2

orbits range over values of Az from 120,000 to 200,000 km. Also, the angle ψ varies from 80 degrees to 120 degrees. The best result for arrival into each Earth-Moon halo orbit appears in Table 5.5. From the results, good locations for maneuvers to achieve low cost transfers are apparently near $\psi = 110$ degrees, except in the last case. Also, for all Earth-Moon halo orbits, it appears possible to achieve a transfer with a relatively small ΔV.

To obtain complete information, it is necessary to examine the results in the ephemeris model. All results in Table 5.6 are transitioned to the ephemeris model, and the results appear in Table 5.7. The Earth-Moon halo orbits are fixed at the original values in terms of amplitude. Then, a Lissajous-to-Lissajous transfer is constructed by applying the same ΔV that is obtained in the CR3BP. If necessary, the Sun-Earth halo orbit is modified via a change in the amplitude Az. For each combination, a transfer is accomplished successfully with a change in the Sun-Earth orbit. The transfer to an Earth-Moon orbit with $Az = 18,000$ km requires a ΔV of 10.6 m/sec. This value is actually less than that computed in the CR3BP. Note that further reduction in the ΔV can be accomplished in the ephemeris model if there are no constraints. In fact, all can be reduced to zero for some change in the Sun-Earth Lissajous orbit.

Transfers with zero ΔV appear in Table 5.7. Note that the Earth-Moon orbit in the third case changes from $Az = 20{,}000$ km to 19,000 km. To accomplish this result is more challenging than any other example. A change in only the Sun-Earth orbit is not sufficient. If flexibility exists to modify the size of the Earth-Moon orbit via the out-of-plane component, the zero cost transfer is computed. If the size of the Sun-Earth orbits is fixed, a zero cost transfer can also be accomplished by modification of the size of the Earth-Moon orbit in all cases. Actually, this option is easier to accomplish in general. However, since the magnitude of the Earth-Moon Az amplitude is smaller than that of the Sun-Earth orbit, the same amount of change in the Earth-Moon Az amplitude causes a larger percentage error. Thus, this option might not be desirable for certain missions. In Table 5.6, the change in the time of flight is relatively small as the Earth-Moon Az altitude increases. The longest time of flight is 54.1 days for the sixth case in the table, i.e., the Earth-Moon Az is 26,000 km. The shortest time of flight is 49.6 days when the Earth-Moon Az is 30,000 km. Also, the cost reduction rarely affects the time of flight for all cases.

Table 5.5 Best Sun-Earth Az and ψ Combinations for Each EM Az; halo-to-halo transfer

Earth-Moon Az [km]	Sun-Earth Az [km]	ΔV [m/sec]	ψ [deg]
16,000	120,000	17.9	110.5
18,000	130,000	14.5	109
20,000	130,000	11.0	110
22,000	130,000	7.5	110.5
24,000	130,000	4.2	111
26,000	130,000	1.0	110
28,000	160,000	1.4	107.5
30,000	180,000	2.8	98

Table 5.6 Best Combinations Tested in the Ephemeris Model; Earth-Moon Az's fixed

Earth-Moon Az [km]	Sun-Earth Az [km]	ΔV [m/sec]	Time of Flight [days]
16,000	113,000	17.9	51.2
18,000	133,000	10.6	53.2
20,000	161,000	11.0	53.2
22,000	115,000	7.5	53.1
24,000	124,000	4.2	53.2
26,000	129,000	0.9	54.1
28,000	154,000	1.4	50.2
30,000	155,000	2.8	49.6

Table 5.7 Best Combinations with $\Delta V = 0$ m/sec in the Ephemeris Model

Earth-Moon Az [km]	Sun-Earth Az [km]	ΔV [m/sec]	Time of Flight [days]
16,000	111,000	0	51.3
18,000	142,000	0	53.7
19,000	140,000	0	53.7
22,000	126,000	0	53.3
24,000	130,000	0	53.2
26,000	131,000	0	54.1
28,000	155,000	0	50.1
30,000	157,000	0	49.4

5.5 System-to-System Transfers From Cells

System-to-system transfers computed using the previous design process rely on knowledge of the libration point orbits at each end of the transfer. The trajectory arcs are extracted directly from the invariant manifolds. However, that step is not

necessary. For example, the particular libration point orbit may not be constrained or, in the case of transit orbits, the trajectory arc is not from a manifold. An alternative technique to compute a transfer involves the use of cells to represent a volume of manifolds [1]. This technique allows storage of a large amount of estimated manifold information in the CR3BP. Thus, it avoids computation of manifolds numerically for a wide variety of different periodic halo orbits to search for intersections. The halo orbit is a design parameter and emerges as part of the procedure.

Given a number of Sun Earth L_2 periodic halo orbits, a set of cells can be created that approximates a continuous distribution of manifolds from the volume of halo orbits. Such a set of cells appears in Figure 5.6; they approximate the stable manifolds corresponding to a range of L_2 halo orbits. Assume that some trajectory enters the volume. The trajectory may be an Earth-Moon manifold, an Earth-Moon transit orbit, or some other trajectory from another region of space. In the figure, the unstable manifolds associated with an Earth-Moon L_1 halo orbit of amplitude $Az = $ 39,000 km are entering the volume. The goal is to deliver the trajectory to the region of the Sun-Earth L_2 libration point orbit with a minimum cost. For any trajectory that enters the volume, a cell can be identified that envelops the entering trajectory. Within the cell, approximate analytical relationships represent position and velocity states for manifolds that approach Sun-Earth L_2 halo orbits. A maneuver to bring the trajectory to a halo orbit can be approximated. Transitioned to the ephemeris model, an actual transfer can be determined and the cost reduced, frequently to zero [1]. In this example, only the manifolds in the Sun-Earth system have been approximated, but approximations for the Earth-Moon system are also possible.

For this investigation, the problem is focused on transfers from Sun-Earth L_2 halo orbits to the vicinity of the Moon. Let an Earth-Moon halo orbit be defined by an Az amplitude of 30,000 km. From the numerical study summarized in Table 5.5, the "best" Sun-Earth halo orbit for this transfer is $Az = 180,000$ km. Recall that the ΔV is equal to 2.8 m/sec at a phase angle $\psi = 98$ degrees. The orientation of the Earth-Moon tube is determined such that $\alpha = 31$ degrees and $\beta = -44$ degrees. Then,

this Earth-Moon tube is propagated to enter the cell volume. A search ensues for an intersecting Sun-Earth manifold that yields the lowest ΔV. For a single Earth-Moon manifold, all the intersecting Sun-Earth manifolds in the local volume are examined. The results from the cell estimation process in the CR3BP appear in Table 5.8. The Sun-Earth Az is reduced to 165,000 km. Also, the resulting value of ψ is 123.9 degrees. This is beyond of the range of the ψ angle that is typically examined (80-120 degrees) in this study. The manifold intersection process will still determine an intersection at this value of ψ using the same orientation angles. However, the ΔV values are usually larger with ψ beyond the typical range. Actually, in this case, the manifold intersection process yields $\Delta V = 60.6$ m/s at $\psi = 123.9$ degrees for the same orientation. However, the transfer estimation process using cells incorporates two ΔVs. The first, ΔV_1, is a maneuver to leave a Sun-Earth halo orbit. This maneuver is required because the cell estimation technique uses the estimation of manifolds, not actual, globalized manifolds. The second maneuver, ΔV_2, is the maneuver to transfer from a Sun-Earth manifold to an Earth-Moon manifold. Thus, the total ΔV is the sum, i.e., 22.0 m/sec. The approximation from the cell procedure is also shifted to the ephemeris model and can, once again, be reduced to a system-to-system transfer with zero cost. The results in the ephemeris model appear in Table 5.9. The final solution, based on an initial guess with two maneuvers, is different than that obtained from the angle approximations. A solution still exists, however.

Table 5.8 Results from the Cell Estimation Technique; CR3BP

Earth-Moon Az [km]	30,000
Sun-Earth Az [km]	165,000
ψ [deg]	123.9
ΔV_1 [m/sec]	14.4
ΔV_2 [m/sec]	7.6
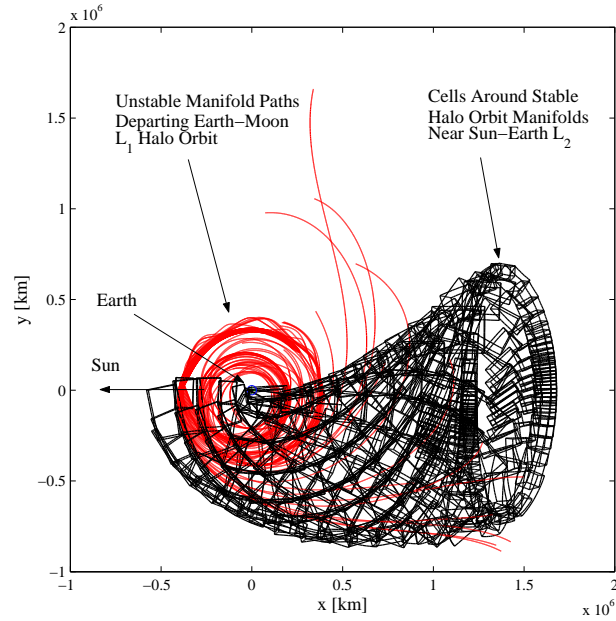
Figure 5.6. EM Manifolds Intersect Cells [1]

Table 5.9 Results with Zero Cost in the Ephemeris Model

Earth-Moon Az [km]	29,000
Sun-Earth Az [km]	160,000
ΔV_1 [m/sec]	0
ΔV_2 [m/sec]	0

5.6 Transfer From Sun-Earth Halo Orbit Near L_2 to The Moon

The accessibility of the Moon may also be critical in the system-to-system design problem. Computation of a transfer from a halo orbit in the Sun-Earth L_2 family to a lunar orbit is also possible by using this system-to-system transfer design strategy, i.e., halo-to-halo transfers and transfers incorporating transit orbits.

5.6.1   Halo-to-Halo Transfer

A straightforward option to reach the Moon from a halo orbit near the Sun-Earth L_2 libration point is a simple modification of a halo-to-halo transfer. Since a halo-to-halo transfer allows arrival in the vicinity of an L_2 halo orbit in the Earth-Moon system, the transfer to the Moon can be accomplished by exploiting an unstable Earth-Moon manifold after arrival in the Earth-Moon libration point orbit. One example in the ephemeris model appears in Figure 5.7. The original halo-to-halo transfer in the CR3BP between a Sun-Earth halo orbit of amplitude $Az = 130{,}000$ km and arrival in an Earth-Moon halo orbit with Az equal to 24,000 km is selected for this example. With this combination, the Earth-Moon Az amplitude and Sun-Earth out-of-plane Az do not change as the solution is shifted to the ephemeris model as is evident in Table 5.7. The Lissajous-to-Lissajous trajectory in Figure 5.7 is plotted in the Earth-Moon rotating frame. Departure from a halo or Lissajous along an unstable manifold incurs no cost. The trajectory includes at least one revolution of the Moon. A maneuver is necessary, of course, to maintain the lunar orbit. In this example, the altitudes at the periapsis and apoapsis of the new orbit are 2,090 km and 3,230 km. Also noted, the angle between the orbit plane and the Earth-Moon x-y plane is about 35 degrees. The end-to-end transfer from the Sun-Earth L_2 Lissajous orbit to a Moon orbit in the Sun-Earth rotating frame as computed in the ephemeris model appears in Figure 5.8. In this case, the time of flight is defined differently. It is still measured from the same location, as previous definition, where the trajectory crosses the Sun-Earth x-axis. However, the time is measured till the first closest approach to the Moon. Then, the time of flight is about 115.8 days. In this case, however, there are about four revolutions around the Earth-Moon Lissajous orbit, so it is possible to reduce the time by reducing the number of revolutions.
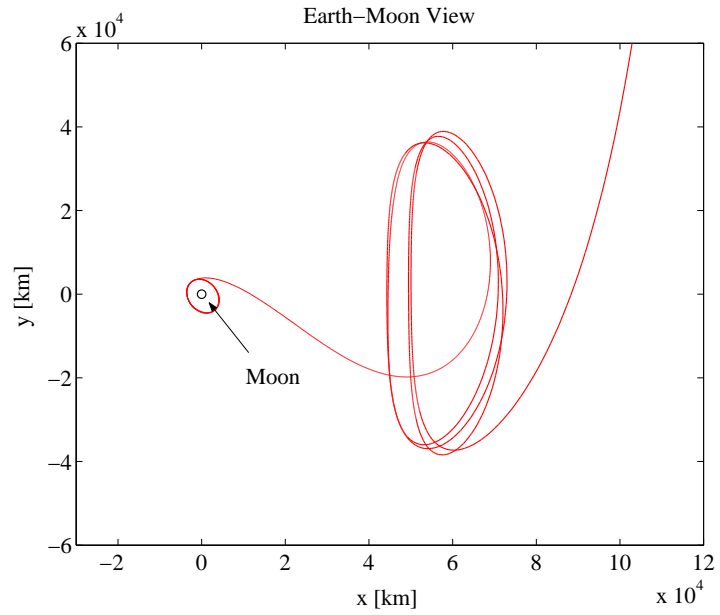
Figure 5.7. Arriving at the Moon via Halo-to-Moon Transfer; Earth-Moon rotating frame; Earth-Moon $Az = 24{,}000$ km; ephemeris model
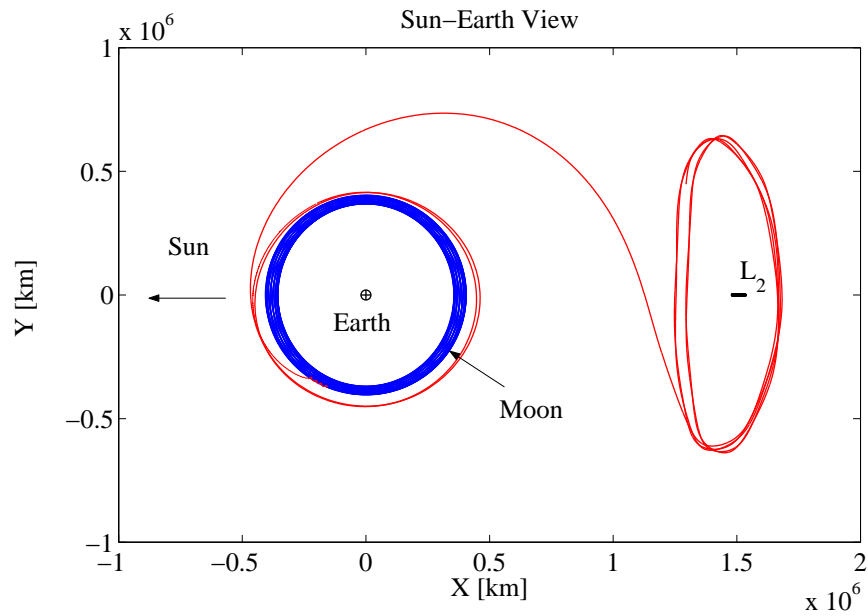

Figure 5.8. Lissajous-to-Moon Transfer in the Sun-Earth Rotating Frame; ephemeris model

5.6.2 Transit Orbit

A system-to-system transfer can also be accomplished by computing a transit orbit inside a stable Earth-Moon tube. Transit orbits allow a more direct delivery of the trajectory to the vicinity of the Moon. Thus, it is possible to apply transit orbits in developing transfers to the Moon. An example of such a transfer in the ephemeris model appears in Figures 5.9 and 5.10. The sizes of these orbits are the same as those in the previous example. The arrival orbit does not converge to the halo orbit, but rather approaches the Moon. Again, this transfer is cost-free to the vicinity of the Moon and the trajectory encircles the Moon at least once. Then, a ΔV is, of course, necessary to permanently insert into lunar orbit. In the figure, the periapsis and apoapsis of this new orbit are 6,980 km and 9,170 km, respectively. Also, in this example, the angle between the orbit plane and the Earth-Moon x-y plane is about 21 degrees. No constraint was applied to specify a particular inclination. A complete transfer in the Sun-Earth rotating frame appears in Figure 5.10. The time of flight is about 72.9 days. This transfer allows arriving at the Moon earlier than the previous transfer.
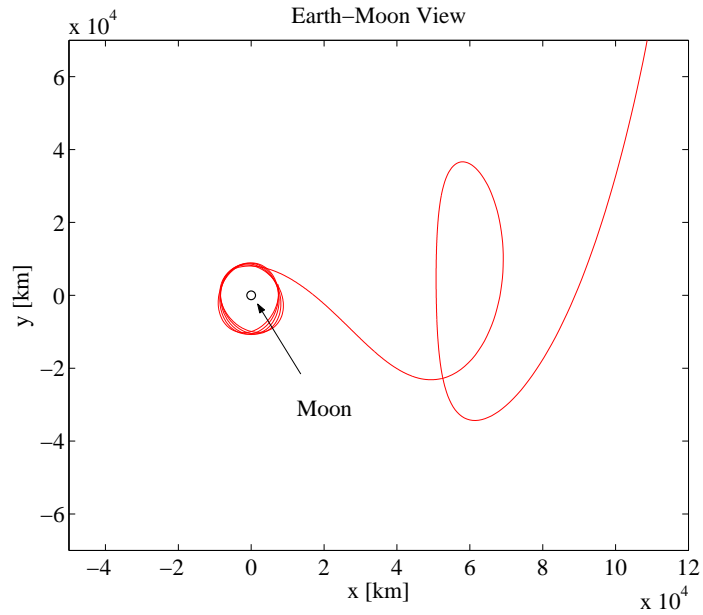
Figure 5.9. Transfer to the Moon via a Transit Orbit; Earth-Moon rotating frame; Earth-Moon $Az = 24{,}000$ km; ephemeris model
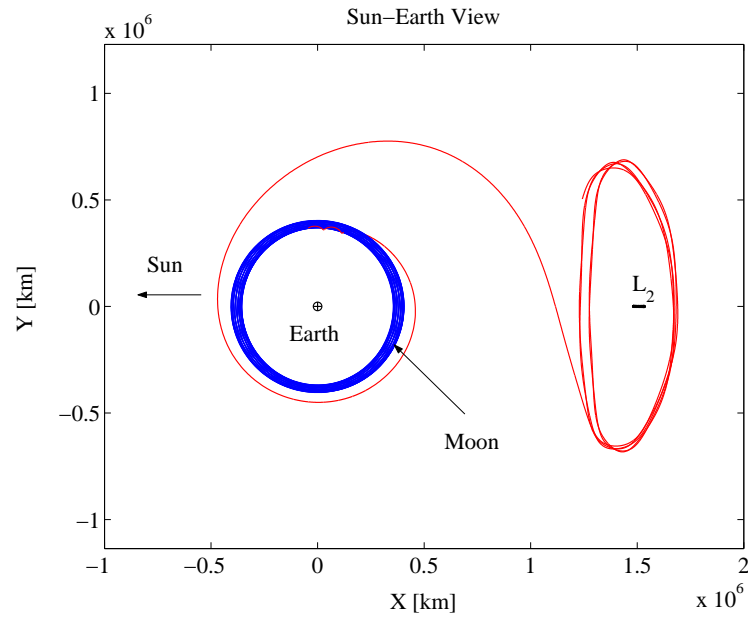

Figure 5.10. Lissajous-to-Moon Transfer in the Sun-Earth Rotating Frame; ephemeris model

6. Conclusions and Recommendations

The objective of this research effort is the development of a technique for the preliminary design of system-to-system transfers between the Sun-Earth and Earth-Moon systems. The technique is based on the application of the dynamical structure of the invariant manifold tubes associated with the periodic libration point orbits. This technique allows a search for low cost transfers in a relatively short time period by limiting the search space with the knowledge of the dynamics. The linear and quadratic angle relationships are introduced to determine desirable orientations of the Earth-Moon system for low cost transfers. These relationships can directly determine an orientation of the Earth-Moon system in the Sun-Earth rotating frame for orbit sizes and the lunar phase angle ψ, within certain error bounds. The relationships then represent timing constraints in the full model. All results are successfully reproduced in the ephemeris model for zero cost and meet all timing conditions. Examples of transfers to the Moon are introduced by application of the process to construct a halo-to-Moon transfer via a Lissajous or transit trajectory. These transfers allow a relatively quick design process for transferring from a Sun-Earth Lissajous orbit near L_2 to the vicinity of the Moon for zero cost.

In this study, certain ranges of ψ and Az amplitudes are selected. It would be interesting to analyze the data from wider ranges. It may be possible to identify a new relationship between α and β by studying wider ranges. Also, it would be very convenient if the relationship between angles, α and β, and Az altitudes can be identified. It may be necessary to define new parameters to identify new relationships. Although the transfers summarized here are only one-way, i.e., the Sun-Earth system to the Earth-Moon system, this technique can be modified for various types of transfers between two systems.

LIST OF REFERENCES

LIST OF REFERENCES

[1] K. Howell, M. Beckman, C. Patterson, and D. Folta. Representations of invariant manifolds for applications in three-body systems. Paper No. AAS 04-287, Maui, Howaii, February 2004. AAS/AIAA.

[2] June Barrow-Green. *Poincaré and the Three Body Problem*. American Mathematical Society/London Mathematical Society, 1997.

[3] Victor G. Szebehely. *Theory of orbits, the restricted problem of three bodies*. Academic Press, New York, 1967.

[4] Gregory L. Baker and Jerry P. Gollub. *Chaotic Dynamics*. Cambridge University Press, New York, second edition, 1996.

[5] Thomas S. Parker and Leon O. Chua. *Practical numerical algorithms for chaotic systems*. Springer Verlag, New York, third edition, 1989.

[6] Lawrence Perko. *Differential equations and dynamical systems*. Springer-Verlag, New York, 1991.

[7] K. C. Howell and R. W. Farquhar. John Breakwell, the restricted problem, and halo orbits. *Acta Astronautica*, 29(6):485–488, 1993.

[8] J. V. Breakwell and J. V. Brown. The 'halo' family of 3-dimensional periodic orbits in the earth-moon restricted 3-body problem. *Celestial Mechanics*, 20:389–404, 1979.

[9] R. W. Farquhar and A. A. Kamel. Quasi-periodic orbits about the translunar libration point. *Celestial Mechanics*, 7:458–473, 1973.

[10] K. C. Howell. Three dimensional, periodic, halo orbits. *Celestial Mechanics*, 32(1):53–71, 1984.

[11] R. W. Farquhar, D. P. Muhonen, C. R. Newman, and H. S. Heuberger. Trajectories and orbital maneuvers for the first libration-point satellite. *Journal of Guidance and Control*, 3(6):549–554, 1980.

[12] R. W. Farquhar, D. P. Muhonen, and D. L. Richardson. Mission design for a halo orbiter of the earth. Paper No. AIAA 76-810, AIAA/AAS Astrodynamics Conference, San Diego, California, August 18-20 1976.

[13] D. Folta and K. Richon. Libration orbit mission design at l2: A map and ngst perspective. Paper No. AIAA 98-4469, AIAA/AAS Astrodynamics Specialist Conference, Boston, MA, August 10-12 1998.

[14] K. C. Howell, B. T. Barden, and M. W. Lo. Application of dynamical systems theory to trajectory design for a libration point mission. *The Journal of the Astronautical Sciences*, 45(2):161–178, April-June 1997.

[15] K. C. Howell and J. P. Anderson. *Generator User's Guide.* 2001.

[16] W. S. Koon, M. W. Lo, J. E. Marsden, and S. D. Ross. Shoot the moon. Paper No. AAS 00-166, AAS/AIAA Space Flight Mechanics Meeting, Florida, January 2000.

[17] G. Gómez, W. S. Koon, M. W. Lo, J. E. Marsden, J. Masdemont, and S. D. Ross. Invariant manifolds, the spatial three-body problem and space mission design. AAS Paper No. 01-301, AAS/AIAA Astrodynamcis Specialist Conference, Quebec City, Canada, August 2001.

[18] F. Topputo, M. Vasile, and A. E. Finzi. An approach to the design of low energy interplanetary transfers exploiting invariant manifolds of the restricted three-body problem. Paper No. AAS 04-245, AAS/AIAA Space Flight Mechanics Conference,Manui, Hawaii, February 2004.

[19] Archie E. Roy. *Orbital Motion.* Adam Hilger Ltd, Bristol, 1982.

[20] John Guckenheimer. *Nonlinear oscillations, dynamical systems, and bifurcations of vector fields.* Springer-Verlag, New York, 1983.

[21] K. C. Howell. Families of orbits in the vicinity of the collinear libration points. *The Journal of the Astronautical Sciences*, 49(1):107–125, January-March 2001.

[22] B. Marchand. Temporary satellite capture of short-period jupiter family comets from the perspecitve of dynamical systems. M.S. Thesis, School of Aeronautics and Astronautics, Purdue University, West Lafayette, Indiana, December, 2000.

[23] V. A. Yakubovich and V. M. Starzhinskii. *Linear Differential Equations with Periodic Coefficients.* Halsted Press, New York, 1975.

[24] S. Wiggins. *Introduction to Applied Nonlinear Dynamical Systems and Chaos.* Springer-Verlag, New York, 1990.

[25] B. T. Barden. Using stable manifolds to generate transfers in the circular restriced problem of three bodies. M.S. Thesis, School of Aeronautics and Astronautics, Purdue University, West Lafayette, Indiana, December, 1994.

[26] G. Strang. *Linear Algebra and Its Applications.* Thomson Learning, third edition edition, 1988.